ISSN 2221-6413 (Print), ISSN 2223-2559 (Online)
Coden: PJSIB5 56(2) 59-124 (2013)

Pakistan Journal of Scientific and Industrial Research

Series A: Physical Sciences

Vol. 56, No.2, May-June, 2013

(for on-line access please visit web-site http://www.pjsir.org)

Published by
Scientific Information Centre
Pakistan Council of Scientific and Industrial Research
Karachi, Pakistan

Pakistan Journal of Scientific and Industrial Research
Series A: Physical Sciences

Pakistan Journal of Scientific and Industrial Research started in 1958, has been bifurcated in 2011 into:

Series A: Physical Sciences [**ISSN 2221-6413 (Print); ISSN 2223-2559 (online)]** (appearing as issues of January-February, May-June and September-October) and
Series B: Biological Sciences [**ISSN 2221-6421 (Print); ISSN 2223-2567 (online)]** (appearing as issues of March-April, July-August and November-December).
Each Series will appear three times in a year.

This Journal is indexed/abstracted in Biological Abstracts and Biological Abstracts Reports, Chemical Abstracts, Geo Abstracts, CAB International, BioSciences Information Service, Zoological Record, BIOSIS, NISC, NSDP, Current Contents, CCAB, Rapra Polymer Database, Reviews and Meetings and their CD-ROM counterparts etc.
Subscription rates (including handling and Air Mail postage): ***Local:*** Rs. 2000 per volume, single issue Rs. 350; ***Foreign:*** US$ 400 per volume, single issue US$ 70.
Electronic format of this journal is available with: Bell & Howell Information and Learning, 300, North Zeeb Road, P.O. 1346, Ann Arbor, Michigan 48106, U.S.A; Fax.No.313-677-0108; http://www.proquest.com
Photocopies of back issues can be obtained through submission of complete reference to the Executive Editor against the payment of Rs. 25 per page per copy (by Registered Mail) and Rs. 115 per copy (by Courier Service), within Pakistan; US$ 10 per page per copy (by Registered Mail) and US$25 per page per copy (by Courier Service), for all other countries.

Printed and Published by: PCSIR Scientific Information Centre, PCSIR Laboratories Campus, Shahrah-e-Dr. Salimuzzaman Siddiqui, Karachi-75280, Pakistan.

Editorial Address

Executive Editor
Pakistan Journal of Scientific and Industrial Research, PCSIR Scientific Information Centre
PCSIR Laboratories Campus, Shahrah-e-Dr. Salimuzzaman Siddiqui, Karachi-75280, Pakistan
Tel: 92-21-34651739-40, 34651741-43; Fax: 92-21-34651738; Web: http://www.pjsir.org, E-mail: info@pjsir.org

Pakistan Journal of Scientific and Industrial Research
Series A: Physical Sciences
Vol. 56, No.2, May-June, 2013

Contents

Short Communication

Pak. j. sci. ind. res. Ser. A: phys. sci. 2013 **56** (2) 59-69

Cyclic Voltammetric Studies of Thymoquinone with Iron (III)

Farah Kishwar* and Qamar-ul-Haq
Department of Chemistry, Federal Urdu University of Arts, Science and Technology,
Gulshan-e-Iqbal Campus, Karachi-75300, Pakistan

(received November 28, 2012; revised February 11, 2013; accepted March 6, 2013)

Abstract. Complexation of thymoquinone an active ingredient of *Nigella sativa*, with Fe(III) has been analyzed using cyclic voltammetry. This electrochemical study was performed at glassy carbon as working electrode, platinum as auxiliary and saturated calomel as reference electrode. Whole work was performed at 25±1 °C in aqueous medium using NaCl as supporting electrolyte. Present study reflects effects of scan rates, concentrations, ratios and successive cyclic scans on Fe(III)-thymoquinone complex. Results revealed that the complex shows quasi-reversible electron transfer process. E° of complex was found to be 0.271± 0.030 V whereas diffusion coefficient was 9.178×10^{-5} cm^2s^{-1}. The values of transfer coefficients, α and β were also determined. The value of α was found to be 0.786±0.01-0.923±0.02 whereas value of β was found in the range of 0.813±0.01-1.021±0.01. Calibration curve method with linear regression line confirms that cyclic voltammetry can be used for quantification of Fe(III)-thymoquinone complex for pharmaceutical assay.

Keywords: thymoquinone, iron (III), cyclic voltammetry, Quasi-reversible behaviour, Randles-Sevick equation

Introduction

Thymoquinone (2-methyl-5-isopropyl-1,4-benzoquinone) (TQ) is the major component of the essential oil of *Nigella sativa*, but it is also present in the fixed oil of the seed (Ali and Blunden, 2003) and it is an active principle responsible for many of the seed's beneficial effects (Mehta *et al*., 2009; Xin *et al*., 2008). Among various bioactivities, examined for TQ, one of the most important is its antioxidant activity (Badary *et al*., 2003; Mansour *et al*., 2002). The compound has been observed to decrease cellular oxidative stress (Mohamed *et al*., 2003) and has a potent chemo-preventive potential of inhibiting the process of carcinogenesis (Badary *et al*., 2007; Badary *et al*., 1999). In addition, several research studies have shown its other pharmacological activities such as anti-inflammatory (Syed, 2008; Gazzar *et al*., 2007), anti-tumor (Gali-Muhtasib *et al*., 2008; Shoieb *et al*., 2003), antidiabatic (Abdelmeguid *et al*., 2010; Fararh *et al*., 2005), antitussive (Hosseinzadeh *et al*., 2008), antimicrobial (Mouhajir *et al*., 1999), apoptosis induction (El-Mahdy *et al*., 2005) and neuro-protective (Al-Shabanah *et al*., 1998) activities.

Structurally, TQ (Fig. 1) belongs to 2,5-di-substituted benzoquinone class of compounds having methyl and isopropyl groups at carbon-2 and carbon-5, respectively (Padhye *et al*., 2008). TQ can be prepared by oxidation of thymol (Dockal *et al*., 1955). The crystal structure of TQ has been determined using high-resolution X-ray powder diffraction, which showed that TQ belongs to the triclinic system. Weak Vander Walls forces have been found in the molecules by thermal analysis (Pagola *et al*., 2004).

Iron is the second most abundant metal after aluminium and the fourth most abundant element in the earth's crust. The earth's core is believed to consist mainly of iron and nickel (Cotton and Wilkinson, 1988). Iron has a key role in our life also, as it is an essential component of several proteins and enzymes. Iron can serve different functions because of the fact that it can exist in two different ionic states, ferrous and ferric iron, e.g., it can

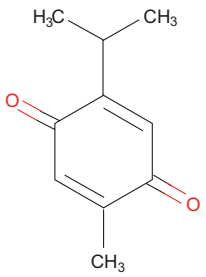

Fig. 1. Structure of thymoquinone.

*Author for correspondence; E-mail: farahkishwar@yahoo.com

serve as a cofactor to enzymes involved in oxidation-reduction reactions. Iron forms a part of the electron carriers that participate in the electron transport chain. In the final step, these carrier transport hydrogen and electrons form energy-yielding nutrients to oxygen, forming water, and in the process make ATP. Most of the body's iron is found in two proteins: hemoglobin in the red blood cells and myoglobin in the muscle cells. In both iron helps to accept, carry and then release oxygen. Iron is also required by enzymes, which are involved in the making of amino acids, collagen, hormones and neurotransmitters (Eleanor and Sharon, 2002).

Iron (III) forms complexes with a number of ligands such as; chloride, fluoride, cyanide, amines etc., but oxygen containing ligands have high affinity for it. Iron (III) also forms complexes with oxalate and phosphate ion, glycerol and sugars etc. Formation of oxo and/or hydroxo bridges is one of its characteristic features (House croft and Sharpe, 2005). Iron (III) in aqueous solution has tendency to hydrolyze and form complexes such as $[Fe(H_2O)_6]^{3+}$(Cotton and Wilkinson, 1988). Regarding stability, iron (II) and iron (III) lie much closer together as compared to (II) and (III) oxidation states of other transition elements. This is the reason that ferrous (Fe^{2+}) and ferric (Fe^{3+}) ions are readily inter-convertible by the use of mild oxidizing or reducing agents. The standard electrode potential of Fe^{2+}/Fe^{3+} ($E°=0.77$) shows that iron (III) is a good oxidizing agent (House croft and Sharpe, 2005).

Since most of the biological activities of TQ are due to its antioxidant behaviour, its electrochemical study is very important. Although polarographic behaviour of TQ has been examined (Michelitsch and Rittmannsberger, 2003), which shows a single reversible peak, not much work is done on electrochemical study of complexes of TQ. Keeping this point in view electrochemical study of complex of TQ with iron has been performed.

Materials and Methods

Reagents and glassware. All reagents used were of analytical grade, purchased from Merck, and MP Biochemicals LLC. All glassware used were of standard quality, properly cleaned and rinsed with distilled-deionized water before use. For cyclic voltammetric studies ferric chloride (hexa hydrate), thymoquinone (TQ) and sodium chloride were used.

Instrumentation. ***Cyclic voltammeter.*** CHI-760 D Electrochemical work station, cyclic voltammeter was used for electrochemical studies. The instrument consists of a computer under Windows environment, a potentiostat and a cell assembly. The cell assembly consisted of a cell stand and a cyclic voltammetric (CV) glass cell. There were three electrodes, a glassy carbon electrode as working electrode, a saturated calomel electrode as reference electrode and a platinum wire electrode as an auxiliary or counter electrode. Repolishing and resurfacing of working electrode was done time to time, especially when supporting electrolyte or analyte was changed. Alumina polishing compound was used to polish working electrode. Then the electrode was thoroughly washed with distilled water in order to remove alumina compound from its surface. Finally, nitrogen purging was checked for the system, but its presence or absence was found to produce no change in voltammograms, so all experimental work was performed without nitrogen.

Sample preparation. ***Supporting electrolyte solution.*** In a 500 mL volumetric flask 2.9220 g of NaCl was taken then dissolved in distilled deinoized water to prepare 0.1 M solution of NaCl.

Analyte solutions. 0.005M solution of TQ and equimolar solution of ferric chloride were prepared as analyte by taking sodium chloride (0.1 M) as electrolyte solution.

Cyclic voltammetric studies. Fresh solutions of analyte and supporting electrolyte were prepared every time. The cell assembly was rinsed thrice with the analyte every time and the working electrode was repolished time to time throughout the experiment. First of all, the base-line of the supporting electrolyte was taken and then 15.0 mL of analyte was run to get overlay of NaCl (0.1 M), Fe(III) solution (5×10^{-4} M), TQ (5×10^{-4} M) and Fe(III) – TQ (5×10^{-4} M). The scan rate was 0.1 V and current sensitivity was 1×10^{-4} A/V. The potential range was set from -0.20 V to + 0.80 V and then reversed back to -0.20 V. The complexation of Fe(III) and TQ was studied in the light of effects of several parameters such as, effect of metal ligand ratio, effect of scan rate, effect of concentration and effect of repeated scan.

To check effect of metal-ligand ratio on complexation, complex solutions having metal ligand ratios 1:1 to 1:4 were prepared. To study the effect of concentration, complex solutions having concentrations 0.02×10^{-3}, 0.1×10^{-3}, 0.2×10^{-3}, 0.4×10^{-3}, 0.6×10^{-3}, 0.8×10^{-3}, 1.0×10^{-3} and 1.2×10^{-3} M were prepared. In order to examine effect of scan rate Fe(III)-TQ complex was analyzed at different scan rates ranging 0.05-200 V by keeping all parameters constant. Repeated scan of the complex of Fe(III) and TQ was also recorded up to 14 sweep segments. The metal-ligand ratio of the complex solution for the effect of concentration, scan rate and repeated scan was 1:3.

Results and Discussion

Cyclic voltammetric study of Fe(III)-thymoquinone complex revealed valuable information which is as follows:

Confirmation of complex formation. Complex formation was checked by comparing voltammograms of supporting electrolyte NaCl (0.1M), Fe(III) (5×10^{-4} M), thymoquinone (5×10^{-4} M) and Fe(III)-thymoquinone complex(1:1) (5×10^{-4} M) (Table 1, Fig. 2a-d). Analysis was performed at 0.1 V/sec at current sensitivity 1×10^{-4} A/V. Linearity in baseline confirms absence of impurity and cleanliness of working electrode (Fig. 2a). Fe(III)-thymoquinone complex showed anodic and

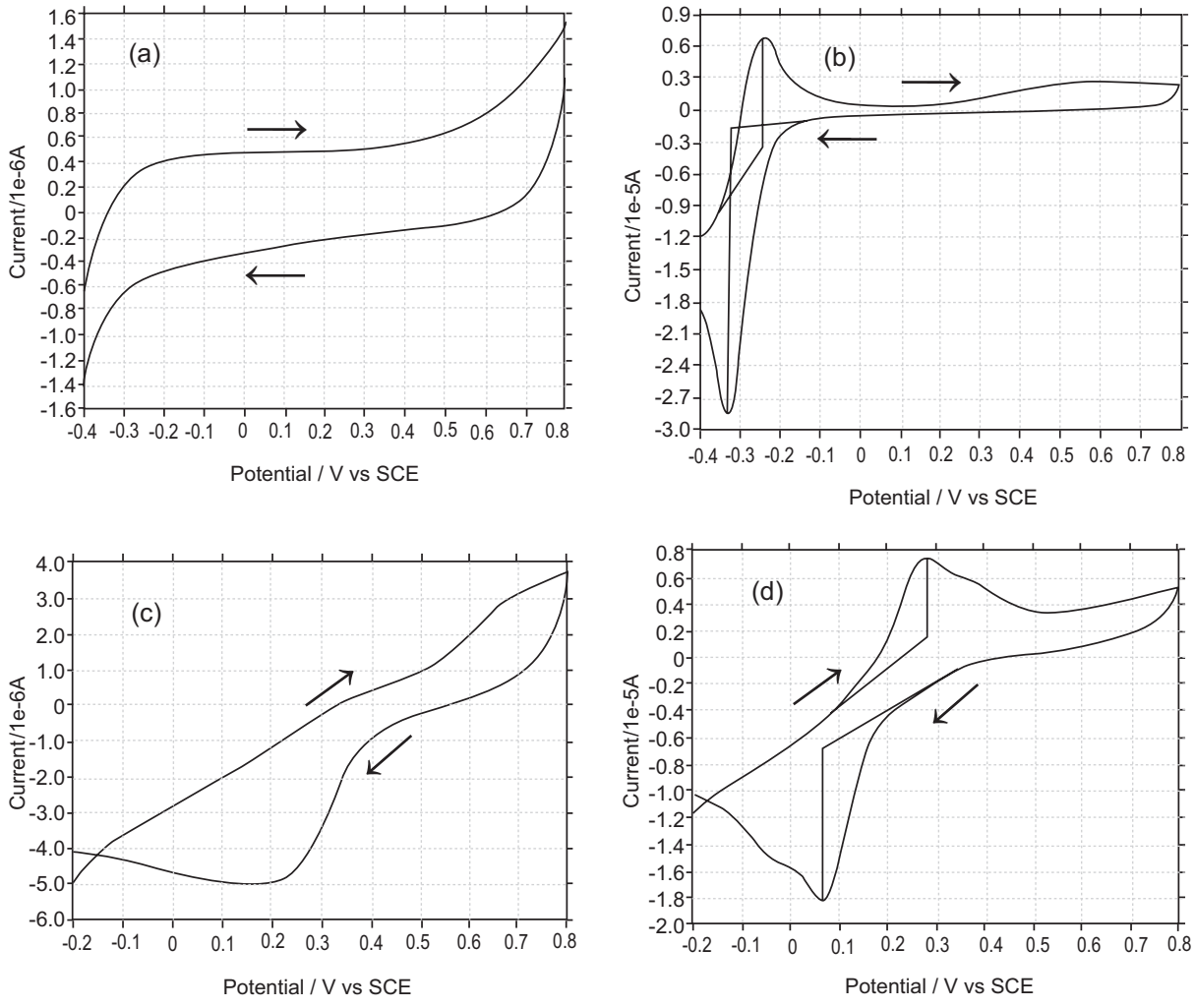

Fig. 2a-d. Cyclic voltammograms of (a) NaCl (0.1 M), (b) thymoquinone (5×10^{-4} M), (c) Fe(III) (5×10^{-4} M) and (d) Fe(III)-thymoquinone complex (5×10^{-4} M) at 0.1 V/s.

cathodic peaks at 0.282 V and 0.066 V, respectively. Neither Fe(III) nor thymoquinone showed peaks within this potential range which clearly indicates that complex formation has occurred in aqueous medium (Table 1, Fig. 2a-d).

Effect of scan rate on voltammograms of Fe(III)-thymoquinone complex. Effect of scan rate from 0.05 V/s to 0.2 V/s was analyzed on Fe(III)-thymoquinone complex (1:3) (5×10^{-4} M) and different electrochemical parameters E_{pa}, E_{pc}, I_{pa}, I_{pc} etc. were determined (Table 2, Fig. 3). Voltammograms fulfill the criteria of quasi-reversible behaviour (Table 3) because by increasing scan rates anodic peak potential shifts from 0.298 V to 0.326 V. Similarly cathodic peak shifted from 0.049 V to 0.018 V. Another quasi-reversible behaviour found was that I_{pa}/I_{pc} was not equal to 1. Furthermore, E_{pa}-E_{pc} was observed greater than 59/n mV and it increased with the increase in ν. I_p was also found to increase with $\nu^{1/2}$ (Fig. 4). Negative shift of E_{pc} with increase of ν further favours the quasi-reversible behaviour (Table 2 and 3). Plot of the peak potential against log of scan rates gave very good R^2 values (Fig.5). The values of α and β were also determined using the relation $0.048/(E_p-E_{p/2})$. Values of α and β at

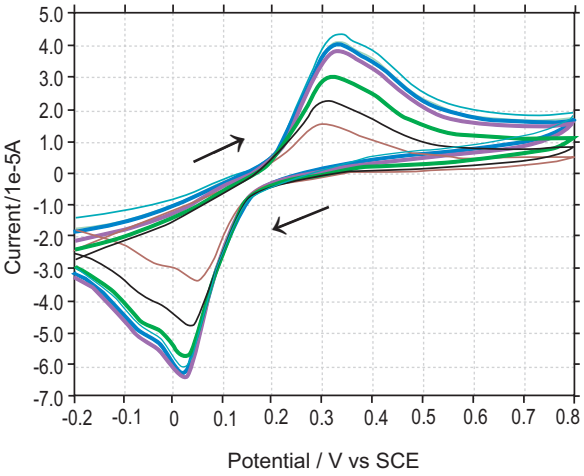

Fig. 3. Cyclic voltammograms of Fe(III)-thymoquinone complex at different scan rates (0.05 V, 0.1 V, 0.15 V, 0.2 V).

Table 1. Electrochemical parameters of cyclic voltammograms of thymoquinone, Fe(III), and Fe(III)-thymoquinone complex

Component/Complex	I_{pa} (A)	I_{pc} (A)	E_{pa} (V)	E_{pc} (V)
Thymoquinone	$1.017\times10^{-5}\pm0.01$	$2.717\times10^{-5}\pm0.01$	-0.242±0.01	-0.326±0.01
Fe(III)	-	-	-	-
Fe(III)-thymoquinone complex	$5.875\times10^{-6}\pm0.01$	$1.149\times10^{-5}\pm0.01$	0.282±0.01	0.066±0.01

Table 2. The values of E_p, $E_{p/2}$, E_p-$E_{p/2}$, E_{pa}-E_{pc} and I_p from cyclic voltammograms of Fe(III)-thymoquinone complex with different scan rates

Scan rate (V/s)	E_{pa} (V)	$E_{pa/2}$ (V)	E_{pa}-$E_{pa/2}$ (V)	I_{pa} $\times10^{-5}$(A)	I_{pa}/I_{pc}	βn_b $=0.048/E_{pa}$-$E_{pa/2}$
0.05	0.298 ± 0.01	0.25 ± 0.01	0.048 ± 0.011	0.798 ± 0.01	0.274 ± 0.01	1.00 ± 0.01
0.10	0.309 ± 0.01	0.26 ± 0.01	0.049 ± 0.011	1.035 ± 0.01	0.253 ± 0.01	1.021 ± 0.01
0.15	0.318 ± 0.01	0.266 ± 0.01	0.052 ± 0.011	1.743 ± 0.01	0.355 ± 0.01	0.923 ± 0.01
0.20	0.326 ± 0.01	0.269 ± 0.01	0.057 ± 0.011	2.541 ± 0.01	0.463 ± 0.01	0.842 ± 0.01

Scan rate (V/s)	E_{pc} (V)	$E_{pc/2}$ (V)	E_{pc}-$E_{pc/2}$ (V)	E_{pa}-E_{pc} (V)	I_{pc} $\times10^{-5}$(A)	αn_a $=0.048/E_{pc}$-$E_{pc/2}$
0.05	0.049 ± 0.01	0.11 ± 0.01	-0.061 ± 0.011	0.249 ± 0.01	2.917 ± 0.01	0.786 ± 0.01
0.10	0.034 ± 0.01	0.09 ± 0.01	-0.056 ± 0.011	0.275 ± 0.01	4.084 ± 0.01	0.857 ± 0.01
0.15	0.024 ± 0.01	0.082 ± 0.01	-0.058 ± 0.011	0.294 ± 0.01	4.912 ± 0.01	0.828 ± 0.01
0.20	0.018 ± 0.01	0.076 ± 0.01	-0.058 ± 0.012	0.308 ± 0.01	5.488 ± 0.01	0.828 ± 0.01

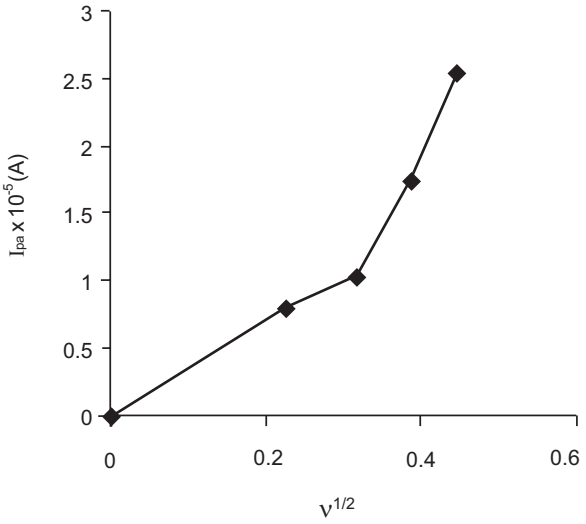

Fig. 4. Variations of anodic and cathodic peak current with square root of sweep rate from the cyclic voltammograms of Fe(III)-thymoquinone complex.

different scan rates were found 0.786 ± 0.01-0.923 ± 0.02 and 0.813 ± 0.01-1.021 ± 0.01, respectively.

Effect of concentration on voltammograms of Fe(III)-thymoquinone complex. Effect of concentration was judged by calibration curve method. To understand the effect of concentration for current study Randles-Sevcik equation is helpful as given below:

$$I_p = 0.4463\ nFACo^*\ (nF\nu D^\circ/RT)^{1/2}$$

Where:

I_p = peak current (A)
ν = scan rate (V/s)
n = Number of electron transfer
F = Faraday's constant
A = Area of electrode (cm^2)
Co* = Concentration of Fe(III)-thymoquinone complex (moles/cm^3)
D^0 = Diffusion coefficient of Fe(III)-thymoquinone complex ($cm^2\ s^{-1}$)
T = 25 ± 2 °C
R = Rate constant

More precisely this equation can be written as follows:

$$I_p = (2.69\times10^5)\ D^{1/2}(n)^{3/2}\ AC\ (\nu)^{1/2}$$

Effect of concentration (0.02×10^{-3} M to 1.2×10^{-3} M) followed Randles-Sevcik equation, because current was directly proportional to concentration (Fig. 6). Calibration curve along with least square fit line showed no major deviation from zero. So no adsorption occurred on electrode surface. These results indicate that calibration curve method can be used for quantification of Fe(III)-thymoquinone complex

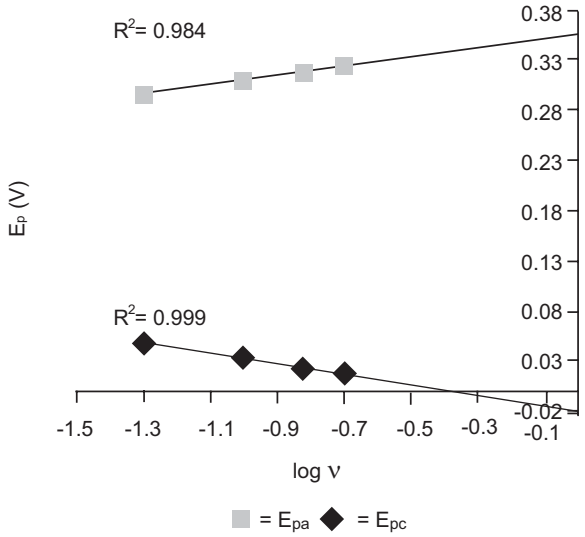

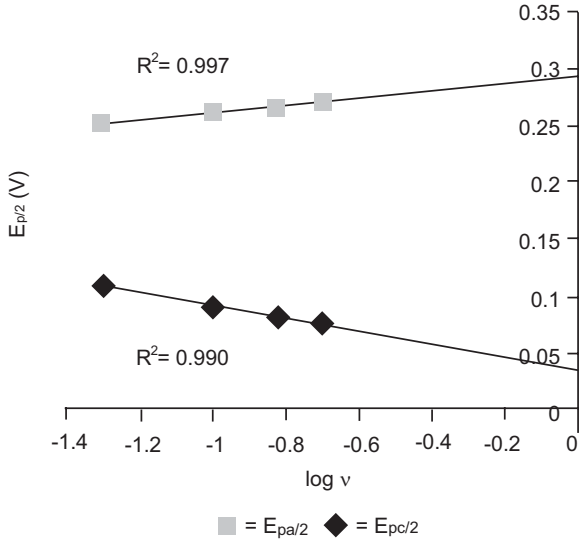

Fig. 5. Variation of anodic and cathodic peak potentials with sweep rate from cyclic voltammograms of Fe(III)-thymoquinone complex.

Table 3. Comparison of diagnostic criteria for reversible, irreversible and quasi-reversible systems at 25±1 °C and results obtained from Fe(III)- thymoquinone complex

S.No.	Comparison of diagnostic criteria	Results obtained from Fe(III)-thymoquinone complex
	Criteria for reversible system*	
1	$\|I_p\| \alpha \nu^{1/2}$	$\|I_p\|$ is not proportional to $\nu^{1/2}$
2	$\|I_{pa} / I_{pc}\| = 1$	$\|I_{pa} / I_{pc}\| \neq 1$
3	$\Delta E_p = E_{pa}-E_{pc} = 59/n$ mV	$\Delta E_p = E_{pa}-E_{pc} > 59/n$ mV and increases as ν increases
4	E_p is independent of ν	E_p is dependent of ν
5	$\|E_p-E_{p/2}\| = 59/n$ mV	$\|E_p-E_{p/2}\| \neq 59/n$ mV
	Criteria for irreversible system*	
1	$\|I_{pc}\| \alpha \nu^{1/2}$	$\|I_{pc}\| \alpha \nu^{1/2}$
2	No reverse peak	Reverse peak is present
3	E_{pc} shifts $-30/\alpha_c n_\alpha$ mV for each decade increase in ν	E_{pc} shift $\neq -30/\alpha_c n_\alpha$ mV for each decade increase in ν
4	$\|E_p-E_{p/2}\| = 48/\alpha_c n_\alpha$ mV	$\|E_p-E_{p/2}\| \neq 48/\alpha_c n_\alpha$ mV
	Criteria for Quasi-reversible system**	
1	$\|I_p\|$ is not proportional to $\nu^{1/2}$, but increases with increase in $\nu^{1/2}$	$\|I_p\|$ increases with increase in $\nu^{1/2}$
2	$\|I_{pa}/I_{pc}\| = 1$, provided $\alpha_c = \alpha_a = 0.5$	$\|I_{pa}/I_{pc}\| \neq 1$
3	$E_{pa}-E_{pc} > 59/n$ mV and increases with increase in ν	$E_{pa}-E_{pc} > 59/n$ mV and increases with increase in ν
4	E_{pc} shifts negatively as ν increases	As ν increases E_{pc} shifts negatively

References* = (Greef *et al*., 1985); References** = (Bard and Faulkner, 2004; Greef *et al*., 1985; Nicholson, 1965).

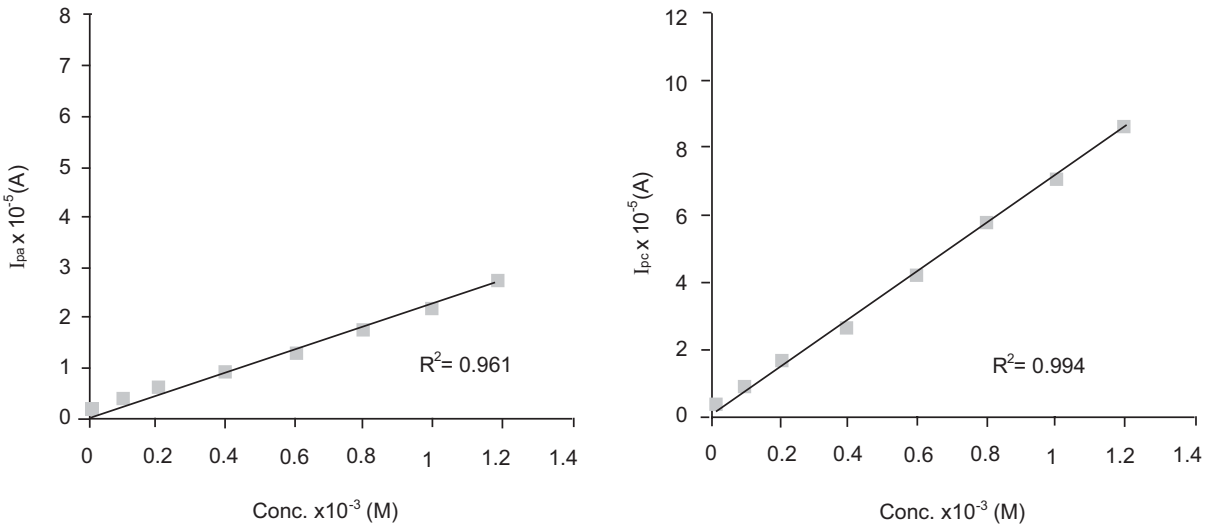

Fig. 6. Plot of anodic and cathodic peak current against concentration of Fe(III)-thymoquinone complex.

within a wide range i.e. (0.02×10^{-3} M to 1.2×10^{-3} M).

Effect of concentration on peak potential (E_{pa}) gives a straight line similarly $E_{pc/2}$ against log of concentration also shows a straight line with good R^2 value (Fig. 7).

Effect of ratio. Here as well, cyclic voltammograms followed the criteria for quasi-reversible reactions because I_{pa}/I_{pc} was not equal to one and $E_{pa}-E_{pc}$ showed values greater than 59/n mV and it increased with the increase in ν. The values of α and β were found in the range of 0.827 ± 0.01 to 0.923 ± 0.02 and 0.842 ±

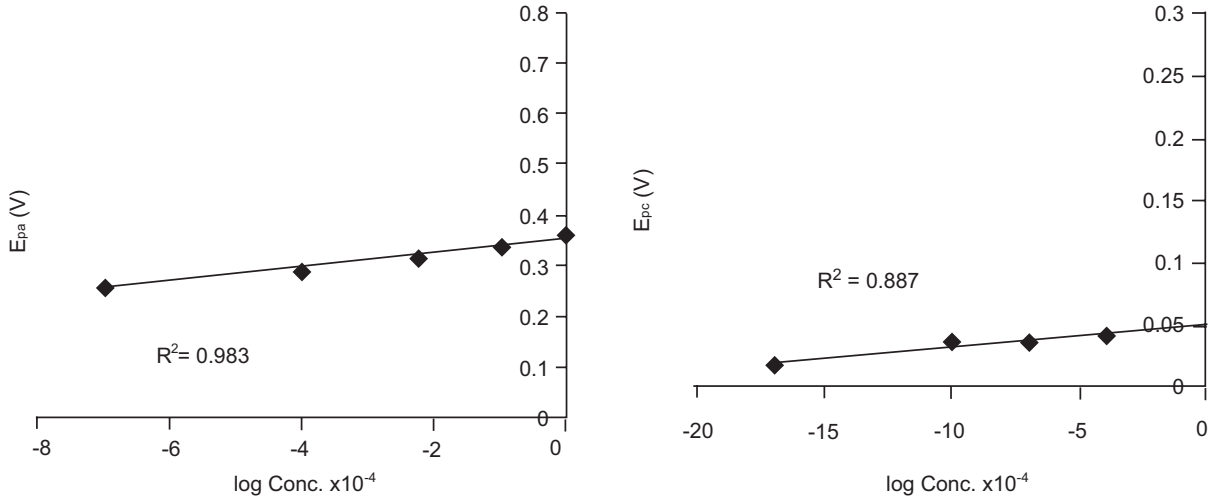

Fig. 7. Variation of anodic and cathodic peak potential with log of concentration on cyclic voltammogram of Fe(III)-thymoquinone complex.

0.01 to 0.979 ± 0.01, respectively (Table 4). Effect of metal ligand ratio on peak potential (E_{pa} and E_{pc}) gave a straight line, similarly the plot of $E_{p/2}$ against M: L ratio also gave a straight line with good R^2 value (Fig. 8).

It was found that by increasing the ratio I_{pa} become approximately constant at 1:3 metal to ligand ratio which may be due to maximum complexation at this ratio (Table 4, Fig. 9).

Effect of repeated scan. Effect of repeated scan on Fe(III)-thymoquinone complex was analyzed up to 14 repeated scans in aqueous medium (NaCl) (Fig. 10). Results revealed that the shape of the cyclic voltammograms of complex remain unchanged in terms of peak potentials (E_{pa} and E_{pc}) but a little bit change in anodic and cathodic peak heights was noticed in these cycles, however, only up to 3rd to 4th cycle limiting values were achieved. The shape of single and multiple scan was similar which confirms neither adsorption nor deposition of complex on electrode surface.

Analysis of diffusion coefficient for Fe(III)-thymoquinone complex. Cyclic voltammetry is a cheap and easy technique for the determination of diffusion coefficient of different complexes and compounds (Anwer, 2006; Ali, 1995). So present study has used cyclic voltammetry for calculation of diffusion coefficient of Fe(III)-thymoquinone complex. For this

Table 4. The values of E_p, $E_{p/2}$, E_{pa}-E_{pc}, I_p and αn_a and βn_b from cyclic voltammograms of Fe(III)-thymoquinone complex with different metal-ligand ratios

Ratio L/M	$E_{pa/2}$ (V)	E_{pa}-$E_{pa/2}$ (V)	I_{pa}/I_{pc}	β_{nb} = 0.048/ E_{pa}-$E_{pa/2}$
1	0.23 ± 0.03	0.052 ± 0.03	0.511	0.923 ± 0.01
2	0.241± 0.01	0.057 ± 0.01	0.343	0.842 ± 0.01
3	0.26 ± 0.01	0.049 ± 0.01	0.253	0.979 ± 0.01
~~4~~	~~0.27 ± 0.02~~	~~0.051 ± 0.02~~	~~0.237~~	~~0.941 ± 0.02~~
Ratio L/M	$E_{pc/2}$ (V)	E_{pc}-$E_{pc/2}$ (V)	E_{pa}-E_{pc} (V)	α_{na} = 0.048/ E_{pa}-$E_{pa/2}$
1	0.12 ± 0.01	-0.054 ± 0.01	0.216 ± 0.01	0.889 ± 0.01
2	0.1 ± 0.01	-0.052 ± 0.02	0.25 ± 0.02	0.923 ± 0.02
3	0.09 ± 0.01	-0.056 ± 0.01	0.275 ± 0.01	0.857 ± 0.01
4	0.08 ± 0.02	-0.058 ± 0.02	0.299 ± 0.02	0.827 ± 0.01

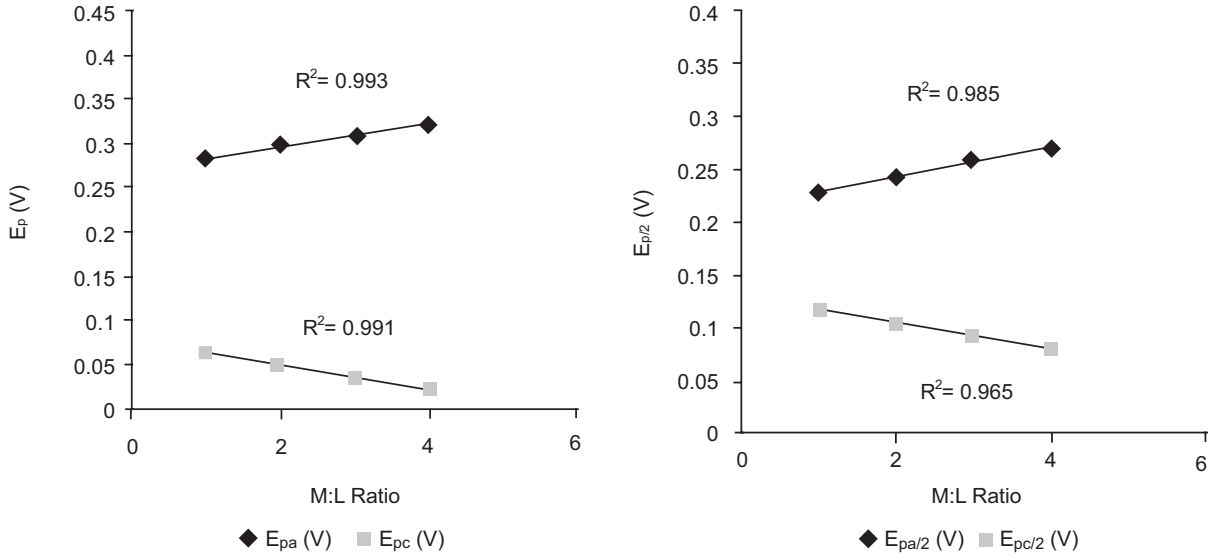

Fig. 8. Variation of anodic and cathodic peak potential with change of metal-ligand ratio in cyclic voltammograms of Fe(III)-thymoquinone complex.

purpose diffusion coefficient of the complex was determined using Randles- Sevcik (Greef *et al*., 1985) equation by varying scan rates, concentrations and metal-ligand ratios (Table 5a-c). Its value was found to be approximately same and no reasonable effect of varying scan rates, concentration or metal-ligand ratio was observed. Area of electrode (A) was 0.0706 cm^2 whereas number of electron transfer (n) was 1.

Analysis of E°, a characteristic property. E° (the potential corresponding to 85% of the peak current) is a characteristic property and is constant for a particular system. Effects of scan rate, concentration and ratio were observed on E° and it was found to be constant at all scan rates, concentration and ratios (Table 6).

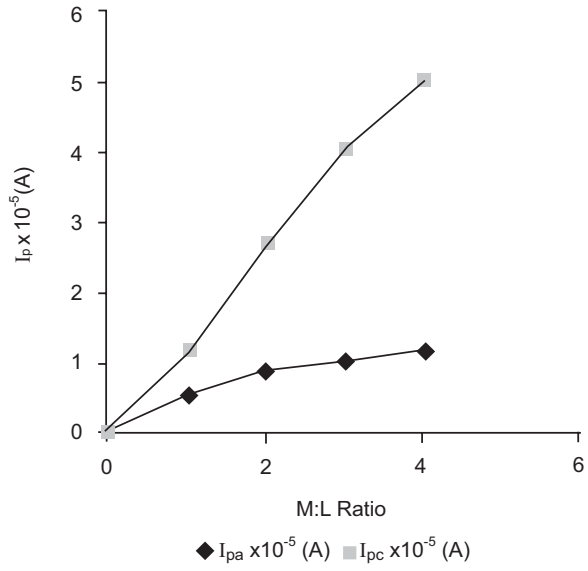

Fig. 9. Variation of anodic and cathodic peak currents with change of metal-ligand ratio in cyclic voltammograms of Fe(III)-thymoquinone complex.

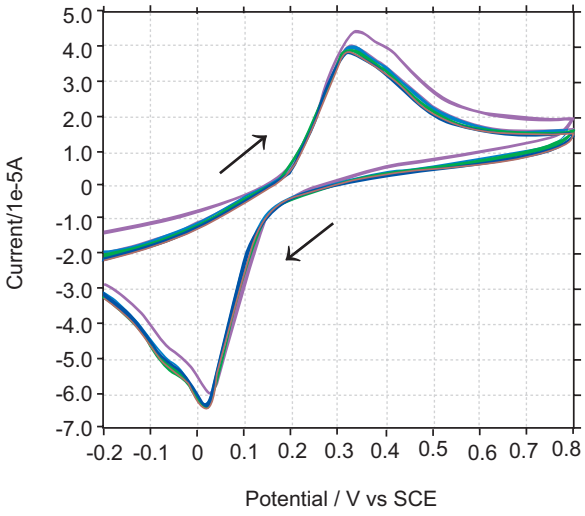

Fig. 10. Repeated scan cyclic voltammograms of Fe(III)-thymoquinone (1:3) complex at 0.1 V.

Table 5a. Diffusion coefficients of the Fe(III)-thymoquinone complex at different scan rates $D^{1/2} = I_p/(2.69\times10^5)(n)^{3/2}\ AC\ (\nu)^{1/2}$

ν (V/s)	$\nu^{1/2}$	I_{pa} $\times10^{-5}$(A)	$D^{1/2}$	D ($cm^2\ s^{-1}$)
0.05	0.224	0.798 ± 0.01	3.572×10^{-3}	1.408×10^{-5}
0.10	0.316	1.035 ± 0.01	3.449×10^{-3}	1.189×10^{-5}
0.15	0.387	1.743 ± 0.01	4.743×10^{-3}	2.25×10^{-5}
0.20	0.447	2.541 ± 0.01	5.986×10^{-3}	3.583×10^{-5}
ν (V/s)	$\nu^{1/2}$	I_{pc} $\times10^{-5}$ (A)	$D^{1/2}$	D ($cm^2\ s^{-1}$)
0.05	0.224	2.917 ± 0.01	1.371×10^{-2}	1.880×10^{-4}
0.10	0.316	4.084 ± 0.01	1.361×10^{-2}	1.852×10^{-4}
0.15	0.387	4.912 ± 0.01	1.34×10^{-2}	1.796×10^{-4}
0.20	0.447	5.488 ± 0.01	1.292×10^{-2}	1.669×10^{-4}

Table 5b. Diffusion coefficients of Fe(III)-thymoquinone complex at different concentrations

Conc. (M)	I_{pa} $\times10^{-5}$ (A)	$D^{1/2}$	D ($cm^2\ s^{-1}$)
0.1×10^{-3}	0.4839 ± 0.01	8.064×10^{-3}	6.503×10^{-5}
0.2×10^{-3}	0.7272 ± 0.01	6.06×10^{-3}	3.672×10^{-5}
0.4×10^{-3}	0.9398 ± 0.01	3.916×10^{-3}	1.533×10^{-5}
0.6×10^{-3}	1.188 ± 0.01	3.299×10^{-3}	1.088×10^{-5}
0.8×10^{-3}	1.735 ± 0.01	3.614×10^{-3}	1.306×10^{-5}
1.0×10^{-3}	2.199 ± 0.01	3.664×10^{-3}	1.342×10^{-5}
1.2×10^{-3}	2.788 ± 0.02	3.871×10^{-3}	1.498×10^{-5}
Conc. (M)	I_{pc} $\times10^{-5}$ (A)	$D^{1/2}$	D ($cm^2\ s^{-1}$)
0.1×10^{-3}	1.007 ± 0.01	1.678×10^{-2}	2.816×10^{-4}
0.2×10^{-3}	1.738 ± 0.01	1.448×10^{-2}	2.097×10^{-4}
0.4×10^{-3}	2.582 ± 0.01	1.076×10^{-2}	1.158×10^{-4}
0.6×10^{-3}	4.236 ± 0.01	1.176×10^{-2}	1.383×10^{-4}
0.8×10^{-3}	5.87 ± 0.01	1.223×10^{-2}	1.496×10^{-4}
1.0×10^{-3}	7.088 ± 0.02	1.181×10^{-2}	1.395×10^{-4}
1.2×10^{-3}	8.73 ± 0.01	1.212×10^{-2}	1.469×10^{-4}

Table 5c. Diffusion coefficients of Fe(III)-thymoquinone complex at different metal-ligand ratios

L/M Ratio	$I_{pa}\times10^{-5}$ (A)	$D^{1/2}$	D ($cm^2\ s^{-1}$)
1	0.588 ± 0.02	1.96×10^{-3}	3.84×10^{-6}
2	0.919 ± 0.01	3.063×10^{-3}	9.38×10^{-6}
3	1.035 ± 0.01	3.449×10^{-3}	1.19×10^{-5}
4	1.187 ± 0.03	3.956×10^{-3}	1.565×10^{-5}
L/M Ratio	$I_{pc}\times10^{-5}$ (A)	$D^{1/2}$	D ($cm^2\ s^{-1}$)
1	1.149 ± 0.01	3.829×10^{-3}	1.466×10^{-5}
2	2.683 ± 0.02	8.941×10^{-3}	7.995×10^{-5}
3	4.084 ± 0.01	1.36×10^{-2}	1.852×10^{-4}
4	5.002 ± 0.02	1.67×10^{-2}	2.779×10^{-4}

Cyclic voltammetric study of Fe(III)-thymoquinone complex was performed at glassy carbon elelctrode against Standard calomel electrode. Horizontal base line (NaCl) indicates the purity of system. The qualitative and quantitative analyses were performed for this complex. Qualitative analysis clearly showed the formation of complex on mixing of Fe(III) and thymoquinone. Quantitative analyses included determination of E°, D, α and β. Effects on complexation were observed at different parameters. Present research reveals that calibration curve method by cyclic voltammetry can be used for quantification of this complex. Effect of repeated scanning on cyclic voltammograms showed no pre or post peak indicating no adsorption of the complex on electrode surface. E° being a characteristic property is constant for a particular system. In present study, effects of scan rate, concentration and ratio were observed on E° and it was found to be constant in all above mentioned cases. Diffusion coefficient was calculated using Randles- Sevick equation. The values of transfer coefficients, α and β were also determined by varying scan rates and metal ligand ratios.

Table 6. Half wave potential ($E^\circ = E_{1/2}$) for Fe(III)-thymoquinone complex

Scan rates (ν) V/s	$(E^\circ)_a$ (V)	Conc. $\times10^{-3}$ M	$(E^\circ)_a$ (V)	Ratio LM	$(E^\circ)_a$ (V)
0.05	0.274 ± 0.01	0.1	0.195 ± 0.01	1	0.256 ± 0.01
0.10	0.286 ± 0.01	0.2	0.237 ± 0.01	2	0.27 ± 0.01
0.15	0.292 ± 0.01	0.4	0.266 ± 0.01	3	0.285 ± 0.01
0.20	0.297 ± 0.01	0.6	0.295 ± 0.01	4	0.296 ± 0.02

Electrochemical study revealed quasi-reversible behaviour for Fe(III)-thymoquinone complex. It was supported by diagnostic criteria for a quasi-reversible reaction (Table 3).

References

Abdelmeguid, E.N., Fakhoury, R., Kamal, S.M., Al Wafai, R.J. 2010. Effect of *Nigella sativa* and thymoquinone on biochemical and subcellular changes in pancreatic β-cells of streptozotocin induced diabetic rats. *Journal of Diabetes*, **2:** 256-266.

Ali, B.H., Blunden, G. 2003. Pharmacological and toxicological properties of *Nigella sativa*. *Phytotherapy Research*, **17:** 299-305.

Ali, S.A. 1995. Electrochemical Studies of Some Biologically Active Compounds using Graphite Paste Electrode, *Ph.D. Thesis*, pp. 223-240, University of Karachi, Karachi, Pakistan.

Al-Shabanah, O.A., Badary, O.A., Nagi, M.N., Al-Gharably, N.M., Al-Rikabi, A.C., Al-Bekairi, A.M. 1998. Thymoquinone protects against doxorubicin-induced cardio-toxicity without compromising its antitumor activity. *Journal of Experimental Clinical Cancer Research*, **17:** 193-198.

Anwer, H. 2006. Complexation of Vanadyl Compounds with Maltol, *Ph.D. Thesis*, pp. 235-240, University of Karachi, Karachi, Pakistan.

Badary, O.A., Abd-Ellah, M.F., El-Mahdy, M.A., Salama, S.A. Hamada, F.M. 2007. Anticlastogenic activity of thymoquinone against benzo (a) pyrene in mice. *Food and Chemical Toxicology*, **45:** 88-92.

Badary, O.A., Taha, R.A., Gamal el-Din, A.M., Abdel-Wahab, M.H. 2003. Thymoquinone is a potent superoxide anion scavenger. *Drug and Chemical Toxicology*, **26:** 87-98.

Badary, O.A., Al-Shabanah, O.A., Nagi, M.N., Al-Rikabi, A.C. Elmazar, M.M. 1999. Inhibition of benzo (a) pyrene- induced forestomach carcinogenesis in mice by thymoquinone. *European Journal of Cancer Prevention*, **8:** 435-440.

Bard, A.J., Faulkner, L.R. 2001. *Electrochemical Methods: Fundamentals and Applications*, pp. 239-243, 2nd edition, John Wiley and Sons (Asia), Singapore, NY, USA.

Cotton, F.A., Wilkinson, G. 1988. *Advanced Inorganic Chemistry*, pp. 710-713, 5th edition, John Wiley & Sons, New York, USA.

Dockal, E.R., Cass, Q.B., Brocksom, T.J., Brocksom, U., Correa, A.G. 1955. A simple and efficient synthesis of thymoquinone and methyl-p-benzoquinone. *Synthetic Communications*, **15:** 1033-1036.

Eleanor, N.W., Sharon, R.R. 2002. *Understanding Nutrition*, 430 pp., 9th edition, Wadsworth, Belmont, USA.

El-Mahdy, M.A., Zhu, Q., Wang, Q.E., Wani, G., Wani, A.A. 2005. Thymoquinone induces apoptosis through activation of caspase-8 and mitochondrial events in p53-null myeloblastic leukemia HL-60 cells. *International Journal of Cancer*, **117:** 409-417.

Fararh, K.M., Shimizu, Y., Shiina, T., Nikami, H., Ghanem, M.M., Takewaki, T. 2005. Thymoquinone reduces hepatic glucose production in diabetic hamsters. *Research in Vaterinary Science*, **79:** 219-223.

Gali-Muhtasib, H., Ocker, M., Kuester, D., Krueger, S., El-Hajj, Z., Diestel, A., Evert, M., El-Najjar, N., Peter, B., Jurjus, A., Roessner, A., Schneider-Stock, R. 2008. Thymoquinone reduces mouse colon tumor cell invasion and inhibits tumor growth in murine colon cancer models. *Journal of Cellular and Molecular Medicine*, **12:** 330-342.

Gazzar, M.A., El Mezayen, R., Nicolls, M.R., Dreskin, S.C. 2007. Thymoquinone attenuates proinflammatory responses in lipolysaccharide-activated mast cells by modulating NF-kappa B nuclear transactivation. *Biochimica et Biophysica Acta*, **1770:** 556-564.

Greef, R., Peat, R., Peter, L.M., Pletcher, D., Robinson, J. 1985. *Instrumental Methods in Electrochemistry*, pp. 183-188, 1st edition, John Wiley and Sons, New York, USA.

Hosseinzadeh, H., Eskandari, M., Ziaee, T. 2008. Antitussive effect of thymoquinone, a constituent of *Nigella sativa* seeds, in guinea pigs. *Pharmacology online*, **2:** 480-484.

Housecroft, C.E., Sharpe, A.G. 2005. *Inorganic Chemistry*, pp. 590-594, 2nd edition, Longman Singapore Publishers (Pvt) Ltd, Singapore, Pearson Prentice Hall, England, UK.

Mansour, M.A., Nagi, M.N., El-Khatib, A.S., Al-Bekairi, A.M. 2002. Effects of thymoquinones on antioxidant enzyme activities, lipid peroxidation and DT-diaphorase in different tissues of mice: a possible mechanism of action. *Cell Biochemistry and Function*, **20:** 143-151.

Mehta, B.K., Pandit, V., Gupta, M. 2009. New principles from seeds of *Nigella sativa*. *Natural Product Research*, Part A, **23:** 138-148.

Michelitsch, A., Rittmannsberger, A., 2003. A simple differential pulse polarographic method for the determination of thymoquinone in black seed oil. *Phytochemical Analysis*, **14:** 224-227.

Mohamed, A., Shoker, A., Bendjelloul, F., Mare, A., Alzrigh, M., Benghuzzi, H., Desin, T. 2003. Improvement of experimental allergic encephalomyelitis (EAE) by thymoquinone; an oxidative stress inhibitor. *Biomedical Sciences Instrumentation*, **39:** 440-445.

Mouhajir, F., Pedersen, J.A., Rejdali, M., Towers, G.H.N. 1999. Antimicrobial thymohydroquinones of Moroccan *Nigella sativa* seeds detected by electron spin resonance. *Pharmaceutical Biology*, **37:** 391-395.

Nicholson, R.S. 1965. Theory and application of cyclic voltammetry for measurement of electrode reaction kinetics, *Analytical Chemistry*, **37:** 1351-1355.

Padhye, S., Banerjee, S., Ahmed, A., Mohammad, R., Sarkar, F.H. 2008. From here to eternity- the secret of pharaohs: therapeutic potential of black seeds and beyond. *Cancer Therapy*, **6:** 495-510.

Pagola, S., Benavente, A., Raschi, A., Romano, E., Molina, M.A.A., Stephens, P.W. 2004. Crystal structure determination of thymoquinone by high-resolution X-ray powder diffraction. AAPS. *Pharmaceutical Science and Technology*, **5:** 24-31.

Shoieb, A.M., Elgayyar, M., Dudrick, P.S., Bell, J.L., Tithof, P.K. 2003. *In vitro* inhibition of growth and induction of apoptosis in cancer cell lines by thymoquinone. *International Journal of Oncology*, **22:** 107-113.

Syed, A.A. 2008. Thymoquinone protects renal tubular cells against tubular injury. *Cell Biochemistry and Function*, **26:** 374-380.

Xin, X., Xue, H., Ajiaikebaier, A., Wang, H. 2008. Research advances of *Nigella* spp. plants. *Schizhen Guoyi Guoyao*, **19:** 1514-1517.

Pak. j. sci. ind. res. Ser. A: phys. sci. 2013 **56** (2) 70-85

Kinetic and Equilibrium Study of Adsorption of Di-Azo Dyes on Commercial Activated Carbon

Emad Abdulilah Saleh Al-Hyali* and Ra´ed Tariq Ghanim Al-Abady
Chemistry Department, College of Education, University of Mosul, Mosul, Iraq

(received June 13, 2011; revised May 1, 2012; accepted July 16, 2012)

Abstract. This research work is concerned with studying the adsorption of a number of di-azo dyes on commercial activated carbon (CAC).The synthesized dyes vary in their structures by the central parts, which are either ortho, meta or para phenylene diamine. This variation affects the linearity of molecules, their spatial arrangement and electron movement throughout the molecule by resonance. Factors affecting adsorption process, such as the effect of contact time, initial concentration, pH of the adsorption medium, adsorbent dose, effect of solvent and temperature were studied. The results indicated that, the adsorption process is fast in the first 10 min, then gradually decreased with time and approaches maximum within 70-80 min for all the studied dyes. The increase of initial concentration and temperature decreased the adsorption efficiency. The results also shows that, the adsorption is found to be more efficient at low pH value. The increase of the adsorbent dose increases the adsorption efficiency and decreases its capacity. The variation of solvent (ethanol-water ratio) indicates that the decrease of dielectric constant lowers the adsorption efficiency. The study included application of three adsorption isotherms; Freundlich, Langmuir and Tempkin on the experimental data of the studied systems. The results indicated that, Freundlich isotherm fits better the adsorption data. Kinetic analysis of the adsorption data was also conducted by employing 4 kinetic models; pseudo first order and pseudo second order, Elovich and intra particle diffusion equations. The results obtained conclude that, the studied systems follow the Pseudo second order model.

Keywords: kinetic study, equilibrium of adsorption, di-azo dyes, activated carbon

Introduction

Dyes are organic compounds; usually have a complex aromatic molecular structure making them stable and resistant to biodegradation (Mohorcic *et al*., 2004).

Azo dyes represent the largest class of commercially produced dyes, in which the chromophores are the azo group (Sutherland, 2004; Wallace, 2001). Synthetically, they were produced in a huge amounts, exceeding (500,000) tons annually (Lewis, 1999), and were used in various industrial fields including the textile industry. The high stability and distinguishing colour of azo dyes, especially those with di and multiple azo groups attracted the attention of many manufactures and become valuable for such industry. The excess of dye remains in the effluent after dyeing process is commonly forms a wastewater with concentration ranging (from 10 to 200 g/L) of dyestuffs (Van der Zee, 2002).

Since some azo dyes and their degradation products are toxic and carcinogenic, their disposal into wastewater without advanced treatment creates a dramatic source of pollution and damages the aquatic life. For this reason, a proper treatment is needed and dyes removal from wastewater became essential.

Intensive research work was carried out concerning treatment of such problems and aiming for providing a suitable technology for environmental protection. Various physiochemical and biological methods are described in the literature which can be employed for removing dyes from wastewater including; filtration (Dushankov *et al*., 1995), chemical precipitation, flocculation (Vandevivere *et al*., 1998; Smith *et al*., 1993), ion exchange (Annadurai *et al*., 2002; Slokar and Marechal, 1998), membrane separation, flotation (Dushankov *et al*., 1995) and adsorption (Suteu and Bilba, 2005). Each of these techniques has its advantages and limitations regarding the environmental conditions. Its technical and economic feasibility is determined by different measures related to the dye type, wastewater composition, and cost. Sometimes, the use of one individual technique is not sufficient for achieving complete decolourization; therefore, the dye removal strategy may involve more than one technique (Suteu and Bilba, 2005).

*Author for correspondence; E-mail: emadabd2006@yahoo.com

Adsorption seems to be the most potential technique for dye removal from wastewater because of its simple design, initial cost, ease of operation and insensitivity to toxic substances (Eren and Acar, 2006). The use of various low cost materials as adsorbents for the removal of dyes from wastewater such as, chitin (McKay *et al*., 1982), natural clay (El-Geundi, 1991), rice husk (Malik, 2003) etc. have been investigated. Activate carbon remains the most effective and widely used adsorbent for the dye uptake from aqueous solutions because of its large surface area, dye binding capacity and regeneration properties (Yasin *et al*., 2007).

The rate of adsorbate uptake from solution onto the adsorbent solid surface after surmounting all the molecular forces, those trying to preclude the adsorption process is termed as adsorption kinetic. The kinetic data are valuable for determining the period required to reach equilibrium and assessing the adsorbent efficiency for adsorbate removal from effluents (Hameed, 2009; Ahmed *et al*., 2007). Such data can also provide a clue for understanding the mechanism of adsorption, which is essential for improving the efficiency of such process and optimization of various parameters in dye recovery (Eren and Acar, 2006) for this reason, several research groups have focused their efforts on developing such studies (Hameed, 2009; AL-Hyali and Al-Jarjari, 2008; Ahmed *et al*., 2007; Yasin *et al*., 2007; Ho, 2006; Malik, 2003).

Kinetic models. The significance of the kinetic analysis of adsorption data lies in that, it provides a valuable insight into the adsorption pathways and mechanism of the attachment of adsorbate onto solid surfaces of adsorbents, which involve mass transfer and chemical reactions, those important for determining the efficiency of adsorption process.

The kinetic data of the adsorption of diazo dyes considered in this study onto a commercial activated carbon (CAC) were analyzed using four different kinetic models, namely; Pseudo first order and Pseudo second order, Elovich equation and intra particle diffusion model rate equation.

Pseudo first order model. It was suggested by Lagergren (Lagergren, 1898), which can be represented as in equation (1):

$$\frac{dq_t}{dt} = k_1(q_e - q_t) \quad \text{.....(1)}$$

Where, (k_1/min) is the Pseudo first order rate constant, q_e and q_t (mg/g) represent the adsorption capacities (amount of adsorbed dye on unit mass of carbon) at equilibrium and time (t), respectively. The integrating rate law by applying the initial condition of t=0 to t=t and q_t=0 to q_t=q_t, equation (1) becomes:

$$\log (q_e - q_t) = \log q_e - \frac{k_1}{2.0303} t \quad \text{.....(2)}$$

The adsorption data of the considered system fits this model, if the plot of log(q_e-q_t) versus time gave a linear relationship with correlation coefficient (R^2) close to unity, and the experimental (q_e) value was consistent with the value calculated from the intercept of the plot.

Pseudo second order model. This model is first applied by Ho *et al*. (1996), to assess the kinetic of adsorption data of heavy metal adsorption. It showed that, the rate depends on the adsorption capacity on the solid and not on the concentration of the adsorbate (Eren and Acar, 2006; Ho, 2006).

The Pseudo second order kinetic model can be represented as in equation (3); (Ho *et al*., 1996):

$$\frac{dq_t}{dt} = k_2(q_e - q_t)^2 \quad \text{.....(3)}$$

Where, k_2 is the rate constant of Pseudo second order adsorption (g/mg/min). The integrated linear from of equation (3) is (McKay and Ho, 1999):

$$\frac{t}{q_t} = \frac{1}{k_2 q_e^{\,2}} + \frac{1}{q_t} t \quad \text{.....(4)}$$

This model is applicable only when the value of t/q_t is linearly correlated with time and the value of calculated q_e is well fit the experimental data.

Elovich kinetic model. The Elovich as modified by Chien and Clayton (1980), is the rate equation based on the adsorption capacity commonly expressed as in equation (5); (Chien and Clayton, 1980):

$$\frac{dq_t}{dt} = \alpha \exp(-\beta q_t) \quad \text{.....(5)}$$

Where, α (mg/g/min) is the initial rate of adsorption, β(g/mg) the adsorption constant during any experiment related to extent of surface coverage and activation energy of chemisorptions.

The Elovich equation can be simplified by assuming $\alpha\beta t >> t$ by applying the boundary conditions $q_t=0$ at t=0 and $q_t = q_t$ at t=t, equation (5) becomes:

$$q_t = \frac{1}{\beta} \ln = (\alpha\beta) + \frac{1}{\beta} \ln t \quad \text{.....(6)}$$

The plot of q_t versus ln(t) gives a linear relationship. The value of α and β can be calculated from the intercept and slope, respectively.

Intra particle diffusion model. This model was first developed by Weber and Morris (1963) and used to explore the possibility of intra-particle diffusion resistance affecting the adsorption. It can be represented by the relation between q_t and the square root of time ($t^{1/2}$), as in equation (7):

$$q_t = K_{diff}\, t^{1/2} + C \quad \text{.....(7)}$$

Where, K_{diff} (mg/g/min) is the diffusion rate constant and C (mg/g) is a value proportional to boundary layer thickness (Kannan and Sundaram, 2001).

According to this model, if the plot of adsorption capacity (q_t) versus $t^{1/2}$ is linear, the Intra particle diffusion is involved and if the line passes through the origin, diffusion into the adsorbent pores is the only controlling step.

Materials and Methods

All the experiments in this study were performed as batch method.

Adsorbent. The adsorbent used in this study for removing dyes from their aqueous solutions is a commercial powdered activated carbon with particle size of 50 µl and ash ratio less than 2%. The CAC was dried at 100 °C for 24 h before used and kept in a sealed bottle for further use.

Adsorbate. Five di-azo dyes were used as adsorbate in this study. These dyes vary in structure by their central parts, which are either ortho, meta or para phenylene diamine. They were synthesized from the reaction of phenylene diamine with the resorcinol or *m*-amino phenol with (1:2) mole ratio, via dizonium salts, respectively (AL-Abady, 2010; Volgel, 1964), as in the following equation:

The chemical compositions and other physical properties of the synthesized dyes are listed in Table 1.

The starting materials used for the preparation of these dyes and other chemicals such as *o*, *m*, and *p*-phenylene diamine, *m*-amino phenol, ethanol, $NaNO_2$, HCl and NaOH are of analytical grade and supplied by BDH and Fluka chemical companies.

Analytical method. The dye concentrations were monitored by measuring the absorbance of the filtrate of each dye at its λ_{max}(indicated in Table 1). By employing a single beam, UV-Vis spectrophotometer (Cecil-CE.1021) after separation of the adsorbent from dye solution by filtration. A calibration curve for each dye was constructed prior to the measurement by using various solution of known concentrations and within the detection limit of the dye according to Beers Law ($A = \varepsilon\, b\, C$).

The amount of dye bound on the unit volume of adsorbent was estimated from the difference between the initial concentration of dye and free (unbound) dye concentration left in the solution.

Equilibrium study. As batch mode experiments, samples of 2 g of CAC were equilibrated with 1L of solutions containing various concentrations of each dye (35-245 mg/L) under continuous stirring.

The initial pH of the solution was adjusted by employing diluted solutions of NaOH or HCl and pH meter of the (pH 720 WTW 82362 Weilheim) type.

The study is conducted at various temperatures (20, 30, 40, 50 and 60 °C). The temperature was controlled by thermostatic water bath shaker (Julabo SW23). Constant rate of shaker (90 rpm) was used throughout the study. The samples were filtered to isolate the carbon particles. The residual dye concentration was determined spectrophotometrically at the maximum wave length corresponding to each dye.

The amount of adsorbed dye is evaluated in terms of the adsorption capacity (q_e, mg of dye per gram

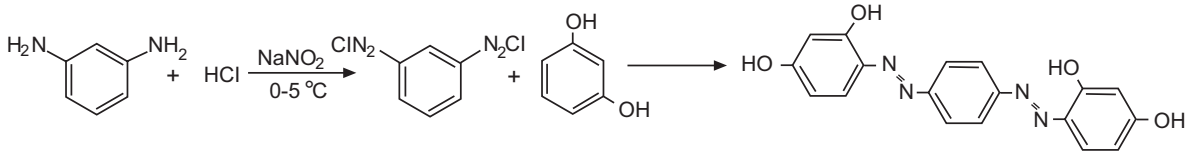

of adsorbent), which can be calculated by equation (8):

$$q_e = \frac{C_i - C_e}{M} \times \frac{V}{1000} \quad \text{.....(8)}$$

And by the percent of adsorbed dye (Ads. %) as,

$$\text{Ads. \%} = \frac{C_i - C_e}{C_i} \times 100 \quad \text{.....(9)}$$

Where, C_i and C_e, are the initial and equilibrium concentrations (mg/L) of the dye solutions. M is the amount of adsorbent (g) and V is the volume of the agitated dye solution (mL).

Kinetic study. The effect of contact time was determined by carrying out series of experiments. In each of them, dye solution with initial concentration 87 mg/L was agitated with CAC (dose 2 g/L) at different time intervals. The temperature of solution was held constant (20 °C) by using thermostatic bath shaker at constant rate of stirring (90 rpm). The samples were filtered and the residual dye concentrations were determined spectrophotometrically at the λ_{max} of the dye under study.

The effect of contact time experiments were repeated at various initial concentrations of dye (60, 87,100 and 120 mg/L) and the data were tested to fit the kinetic models selected for achieving this study.

Results and Discussion

Effect of adsorption dose. Two dyes, 1,3DHAB and 1,4HAAB, with initial concentrations 87 and 192 mg/L, respectively were selected for this study. The investigation was carried out at different doses of adsorbent (0.8 - 6 g of CAC per liter of dye solution), 20 °C and pH=7. The results obtained are shown in Fig. 1a-b. It indicates that, the increase of adsorbent dose increases the adsorption efficiency (%Ads), but decreases the adsorption capacity (q_e, mg/g). This can be readily

Table 1. Chemical composition, physical properties and molar absorbtivity (ε_{max}) of the synthesized dyes

Dye (Abbreviation)	Structure	Colour	M.P. (°C)	λ_{max} (nm)	ε_{max} L/mol/cm
1,4-di(2,4-dihydroxy phenyl azo) benzene (1,4DHAB)	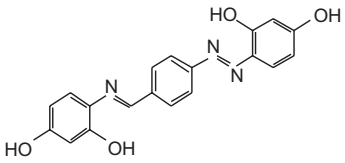	Dark grey	165-167	421	29460
1,3-di(2,4-dihydroxy phenyl azo) benzene (1,3DHAB)	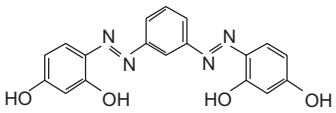	Black	207-208	390	25590
1,4-di(2-amino 4-hydroxy phenyl azo) benzene (1,4HAAB)	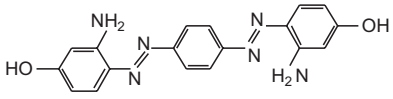	Dark red	256-258	449	19750
1,2-di(2-amino 4-hydroxy phenyl azo) benzene (1,2HAAB)	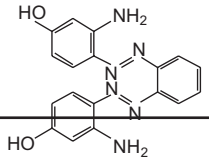	Dark grey	103-105	440	17760
1,3-di(2-amino 4-hydroxy phenyl azo) benzene (1,3HAAB)	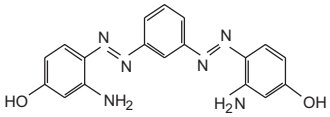	Dark grey	101-103	455	17760

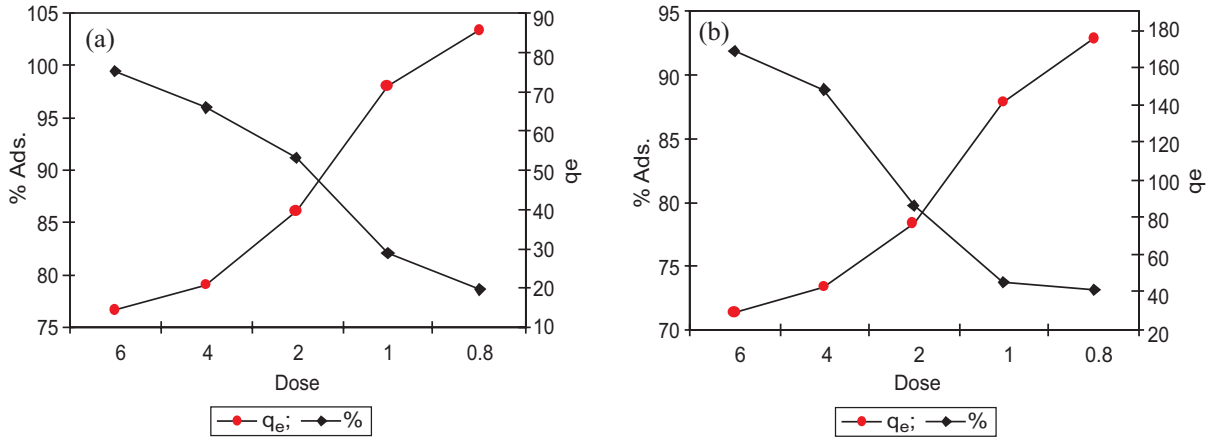

Fig. 1a-b. Relation between adsorption capacity (mg/g), adsorption efficiency and adsorbent dose (mg/g) of two azo dyes; (a) 1,3DHAB; (b) 1,4-HAAB.

illustrated; the increase of adsorbent dose increases the active sites available for adsorption on the carbon surface which in turn increases the percentage of dye adsorbed.

The decrease in adsorption capacity with the increase of adsorbent dose is apparently because of the instauration of the additional adsorption sites through adsorption process (Eren and Acar, 2006; Yu *et al*., 2003; Shukla *et al*., 2002).

Effect of contact time. The effect of contact time was investigated at initial concentration of 87 mg/L, neutral medium (pH=7), carbon dose 2 g/L and 20 °C. The variations of adsorption efficiency with time for the studied dyes are shown in Fig. 2.

The variation of the adsorption efficiency with time portrayed in Fig. 2 shows that the adsorption process proceeded in two stages; an initial rapid stage represented by the first 10 min being very sharp. In this stage 70-80% of the dyes were removed from solution by CAC. This stage is followed by a slower one in which the uptake rate is gradually decreased with time and reaches equilibrium with in 70-80 min. The time 80 min is used for further studies.

The curve representing the variation of adsorption ratio of the dye 1,3HAAB with time shows different adsorption pattern. This could be attributed to the non linear shape of the molecule, in addition to that, the electronic distribution through the resonance effect is restricted on two rings only in contrast to the other molecules in which the mesomeric effect is distributed over all the three rings.

Effect of initial concentration. The importance of initial concentration lies in that, it may provide an important driving force to overcome all the mass transfer resistances of the dye between the aqueous and solid phases.

The effect of varying initial concentrations of the dye on adsorption efficiency is tested in the range of 35 to 245 (mg/L), while keeping all other parameters constant. The results obtained are listed in Table 2. The adsorption capacity and efficiency are calculated as in equations (8) and (9), respectively.

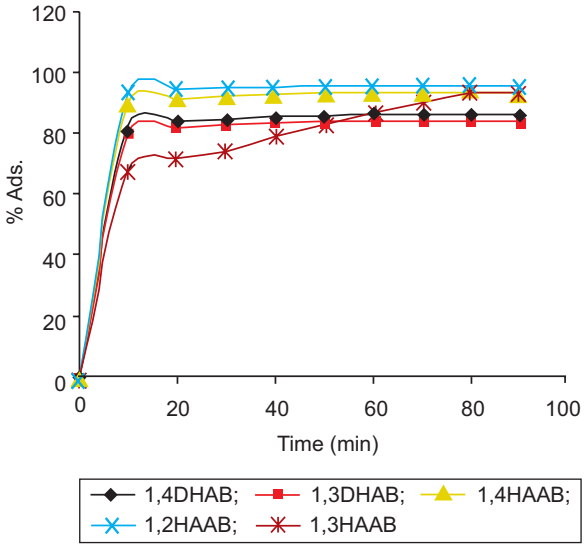

Fig. 2. Variation of adsorption efficiency with time for the considered dyes.

The results of Table 2 show that, the removal of the studied dyes showed the same trend of variation. The adsorption efficiency of dye on activated carbon is highly dependent on the initial concentration. The amount of adsorbed dye is increased with the increase of initial concentration, while the adsorption efficiency is decreased. This could be attributed to the increase of competition among dye molecules to be adsorbed on a constant number of active sites available for adsorption on a certain amount of adsorbent. This competition decreases the binding energy between the dye and the solid surface, and preclude the adsorption process as a result (Shah *et al*., 2009; Sharma and Goyal *et al*., 2009). This result indicates that, the adsorption of such dyes on CAC is more efficient at low concentration.

Effect of initial pH. The pH of an aqueous medium is an important factor that could affect the uptake efficiency of a dye by activated carbon, since the chemical characteristics of functional groups of both dye structures and carbon surface can be affected by the variation of pH.

Table 2. Effect of initial concentration on adsorption capacity and efficiency

Dye	C_i (mg/L)	C_e (mg/L)	q_e (mg/g)	%Ads.
1,4DHAB	35	4.131	15.435	88.20
	87	11.960	37.520	86.25
	140	21.595	59.203	84.58
	192	31.993	80.004	83.34
	245	-	-	-
1,3DHAB	35	4.128	15.436	88.21
	87	12.517	37.242	85.61
	140	23.986	58.007	82.87
	192	37.430	77.285	80.51
	245	-	-	-
1,4HAAB	35	1.057	16.972	96.98
	87	5.413	40.794	93.78
	140	12.654	63.673	90.96
	192	25.659	83.171	86.64
	245	42.847	101.077	82.51
1,2HAAB	35	0.460	17.270	98.69
	87	3.301	41.850	96.21
	140	9.728	65.136	93.05
	192	18.505	86.748	90.36
	245	30.408	107.296	87.59
1,3HAAB	35	1.402	16.799	96.00
	87	5.377	40.812	93.82
	140	14.754	62.623	89.46
	192	29.524	81.238	84.62
	245	45.901	99.550	81.26

This investigation is carried out by varying the initial pH from 4 to 11, under a constant initial dye concentration of 87 mg/L, carbon dosage of 2 g/L and constant temperature (20 °C). The dependence of the removal capacity of CAC to adsorb the dyes considered in this study on pH is presented in Table 3.

Table 3. Effect of pH medium of dye on adsorption capacity and efficiency, initial concentration of dye is 87 mg/L, CAC dose 2 g/L and 20 °C

Dye	pH	C_e (mg/L)	q_e (mg/g)	%Ads.
1,4DHAB	4	4.418	41.541	94.95
	6	9.412	41.291	89.18
	7	11.894	37.803	86.41
	9.4	14.507	36.496	83.42
	11	19.449	33.776	61.17
1,3DHAB	4	1.318	43.091	98.49
	6	9.860	38.57	88.67
	7	13.981	36.759	84.45
	9.4	22.343	32.578	74.46
	11	27.910	29.545	67.92
1,4HAAB	4	1.986	42.507	97.72
	6	4.371	41.315	95.04
	7	5.413	40.793	93.78
	9.4	11.336	37.832	86.97
	11	16.136	35.432	81.45
1,2HAAB	4	1.553	42.723	98.21
	6	2.593	42.204	97.02
	7	3.262	41.869	96.25
	9.4	4.582	41.209	94.73
	11	6.022	40.489	93.08
1,3HAAB	4	2.656	42.172	96.95
	6	4.336	41.332	95.02
	7	5.311	40.844	93.89
	9.4	11.656	37.672	86.60
	11	17.913	34.544	79.4

According to the results of Table 3, both adsorption efficiency and capacity estimated at equilibrium decreased with increasing the pH value of dye solution. The maximum removal of the tested dyes by CAC is observed at pH=4, which may due to reduce of the negative charges on the carbon surface as a result of the excess of portions present in solution (Shukla *et al*., 2002). On the other hand, the basic medium increases the repulsion between the dye molecules and the negatively charged surface of carbon. This result is consistent with the results of other studies reported in the literature (EL-Ashtoukhy, 2009; Arami *et al*., 2005).

Effect of solvent. One of the main problem encountered this study is the weak solubility of the investigated dye

in water. Ethanol was selected for this purpose because it is cheap, available and commonly used in various industries. Preliminary tests proved that, few milliliters of ethanol can dissolve the dye and dilution with water (to a certain limit) dose not affects the dye solubility in ethanol. Therefore, mixtures of ethanol-water were tested as dye solvent with varying ethanol ratio from 10-90%. The effect of solvent with different ethanol ratio was estimated. The investigation was carried out using initial concentration 87 mg/L of dye solution at neutral medium (pH=7) and 20 °C, the results of this study are listed in Table (4).

Table 4. Effect of ethanol ratio on the adsorption efficiency, C_i=87 mg/L, temperature = 20 °C and pH=7

Dye	% Ethanol	C_e (mg/L)	q_e (mg/g)	% Ads.
1,4 DHAB	10	9.757	38.622	88.79
	30	10.576	38.212	87.84
	50	11.960	37.520	86.25
	70	13.488	36.756	84.50
	90	14.939	36.031	82.83
1,3 DHAB	10	10.080	38.460	88.41
	30	10.945	38.028	87.42
	50	12.517	37.242	85.61
	70	14.115	36.443	83.78
	90	15.752	35.624	81.89
1,4 HAAB	10	4.482	41.259	94.85
	30	5.026	40.987	94.22
	50	5.413	40.794	93.78
	70	5.729	40.636	93.41
	90	6.415	40.293	92.63
1,2 HAAB	10	2.660	42.170	96.94
	30	2.990	42.005	96.56
	50	3.301	41.850	96.21
	70	3.748	41.626	95.69
	90	4.233	41.384	95.13
1,3 HAAB	10	3.623	41.689	95.84
	30	4.541	41.230	94.78
	50	5.377	40.812	93.82
	70	6.639	40.181	92.73
	90	8.082	39.459	90.71

The results of Table 4 showed that, the decrease of dielectric constant of the solvent (increase of ethanol ratio) decreases the adsorption efficiency and adsorption capacity. A solvent of 50% ethanol was used for achieving this study in order to ensure clear dye solution that stand for sufficient period without precipitation.

Effect of temperature. The Effect of temperature on adsorption is important for providing information regarding the nature of the studied system and the kind of forces controlling the adsorption process.

In this work, the effect of varying temperature on the adsorption of di-azo dyes on CAC is investigated in the range of 20-60 °C and at concentration of 87 mg/L. The obtained results are listed in Table 5.

Table 5. Effect of temperature on adsorption efficiency of the tested dyes Ci=87 mg/L, pH=7

Dye	% Adsorption				
	20 °C	30 °C	40 °C	50 °C	60 °C
1,4 DHAB	86.25	86.04	85.83	85.57	85.46
1,3 DHAB	85.61	85.40	85.08	84.82	84.60
1,4 HAAB	93.78	93.27	92.73	92.28	91.84
1,2 HAAB	96.21	85.58	95.11	94.44	93.95
3 HAAB	93.82	93.50	93.22	92.84	92.63

The results of Table 5 indicate the adsorption efficiency decreased with increasing the temperature in all of the studied dyes regardless of their straps. This observation is naturally acceptable since rising the temperature increases the desorption process.

Adsorption isotherms. Adsorption isotherms are usually used for describing the relationship between adsorbent and adsorbate at equilibrium. This relationship is expressed in terms of the ratio between the quantity of the adsorbed and remained solute in the solution at certain temperature at equilibrium.

Several models have been observed in the literature, applied to fit experimental data of adsorption in various systems.

In this work, the experimental data of the tested dyes were fitted to Freundlich, Langmuir and Tempkin isotherm equations.

Freundlich isotherm (Freundlich, 1906) is an empirical equation that can be applied to non-ideal adsorption systems involving heterogeneous adsorbent surface. It can be represented by the following linear form:

$$\log q_e = \log K_f + \frac{1}{n} \log C_e \quad \text{.....(10)}$$

Where, K_f (L/g) and n are constant related to adsorption capacity and adsorption intensity, respectively.

Their values can be calculated from the intercept and slope of the line plotted between log q_e versus log C_e, respectively. The obtained values of K_f and n are shown in Table 6.

The Langmuir isotherm (Woodard, 2001) can be expressed as in equation (El-Geundi, 1991). It suggests mono layer coverage of dye on adsorbent.

$$\frac{C_e}{q_e} = \frac{1}{K_L . Q_{max}} + \frac{1}{Q_{max}} C_e \quad \text{.....(11)}$$

Where, C_e is the concentration of dye in the solution at equilibrium, Q_{max} (mg/g) and K_L(L/mg) are Langmuir constants related the maximum adsorption capacity and energy of adsorption, respectively.

The values of Q_{max} and K_L are estimated from the slope and intercept of the straight line plotted between C_e/q_e against C_e, respectively. The values obtained are given in Table 6.

A dimensionless constant termed as separation factor (R_L) can be deduced from the Langmuir isotherm data describing the essential under investigation. It can be defined by equation (12):

$$R_L = \frac{1}{1 + K_L . C_O} \quad \text{.....(12)}$$

Where, C_o is the initial dye concentration, K_L is the Langmuir constant which is related to the affinity of binding sites and is calculated by equation (13) shown below (Aksu, 2003).

$$K_L = Q_{max} \times b \quad \text{.....(13)}$$

According to McKay *et al*., (1982) R_L value refers to irreversible adsorption process when (R_L=0), favourable (0< R_L<1), linear (R_L=1) or unfavourable (R_L>1). The values of K_L obtained are shown in Table 7.

The Tempkin isotherm (Thambavani and Sabitha, 2012) is presented as in equation (14):

$$q_e = B_T \ln K_T + B_T \ln C_e \quad \text{.....(14)}$$

Where,

$$B_T = RT / b_T \quad \text{.....(15)}$$

T is the absolute temperature, R is the gas constant (8.314 J/mol/K), b_T (J/mol) is a constant related to the heat of adsorption and K_T (L/mg) is the equilibrium binding constant, and representing an indication on to the maximum binding energy.

The plot of q_e against ln C_e can help for the determination of Tempkin constants, K_T and B_T. The later enables the calculation of b_T. The results obtained from the application of Tempkin isotherm on the adsorption of the tested dye on CAC are presented in Table 6.

Looking at the results of Table 6, the following conclusion can be driven; the high correlation coefficient (R) values (0.992-0.999) obtained from the application of Freundlich model show that, it fits the experimental data better than the other isotherms. Good fit is also observed from applying Langmuir equation on the adsorption data of the studied dyes on CAC indicated by the values of R which are in range (0.982-0.995).

Table 6. Isotherms constants obtained from adsorption data of dyes on CAC at 20 °C

Isotherm	1,4 DHAB	1,3 DHAB	1,4 HAAB	1,2 HAAB	1,3 HAAB
Freundlich					
n_f	1.243	1.364	2.057	2.298	2.001
K_f	4.990	5.591	17.282	24.400	15.513
R	0.999	0.998	0.997	0.999	0.992
Langmuir					
b(L/mg)	0.018	0.026	0.107	0.173	0.0940
Q_{max}(mg/g)	212.766	153.846	11.047	121.951	117.647
R	0.989	0.995	0.991	0.982	0.991
Tempkin					
B_T	30.526	27.388	22.553	20.713	23.037
K_T(L/mg)	0.354	0.379	1.574	3.555	1.257
R	0.979	0.984	0.984	0.969	0.989
b_T(J/mol)	79.800	88.944	108.012	117.607	105.743

Although weaker values of correlation coefficients are obtained from the application of Tempkin isotherm on the adsorption data, its parameters can still provide valuable information since it dose not oppose the chemical intuition. Figs. 3-5 show the relations obtained from the fit of Freundlich, Langmuir and Tempkin isotherms, respectively.

The values of n_f are higher than unity ($1< n_f <10$), referring that, the adsorption of the investigated dyes on CAC is a favourable process (Khaled *et al*., 2009; Crini *et al*., 2007).

The values of maximum adsorption obtained from the fitting of Langmuir isotherm on the adsorption data lie in the range (119-212, mg/g), which are in agreement with the results reported in the literature for similar studies (Khaled *et al*., 2009; Crini *et al*., 2007; Reddy *et al*., 2006).

The results listed in Table 7, explain that, all R_L values calculated by employing equation (12), are greater than zero and less than unity, showing favourable adsorption of dye on CAC.

According to the results of applying Tempkin isotherm on the adsorption data on CAC, the values of the heat of adsorption (b_T) decrease and the binding energies (K_T) fall with surface coverage of the adsorbent due to the increase of adsorbate-adsorbate-interactions (Khaled *et al*., 2009).

Kinetic study. In this work, four models are employed for examining the controlling mechanism of adsorption process such as mass transfer and chemical reaction. The experimental data were analyzed by using the pseudo first order, pseudo second order, Elovich, and intraparticle diffusion kinetic models. The study is conducted at various initial dye concentrations (16-120 mg/L), adsorbent dose (2 g/L) and constant temperature (20 °C), as follow:

Pseudo first order model. According to this model (eq. 2), the value of k_1 and q_e are determined from the plot of log (q_e-q_t) versus time. Their values, the value of correlation coefficient and experimental q_e are given in Table 8.

The results of Table 8 indicated that, this model cannot be applied for the entire adsorption process. This may

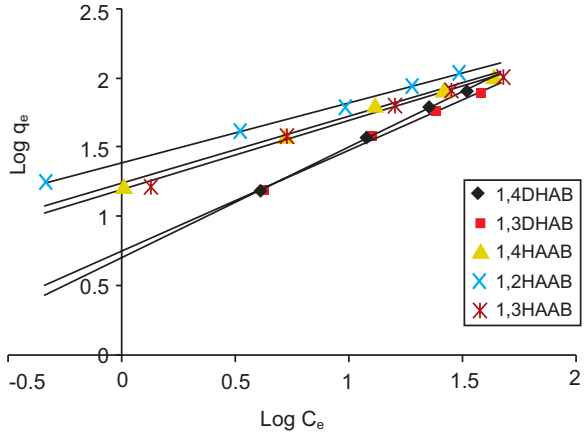

Fig. 3. Application of Freundlich isotherm on the adsorption data at 20 °C.

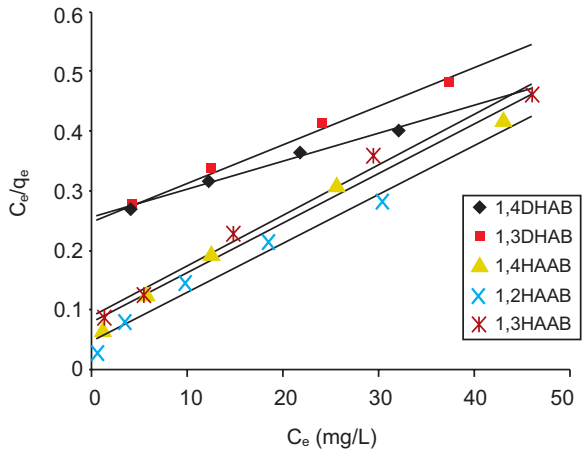

Fig. 4. Application of Langmuir isotherm on the adsorption data at 20 °C.

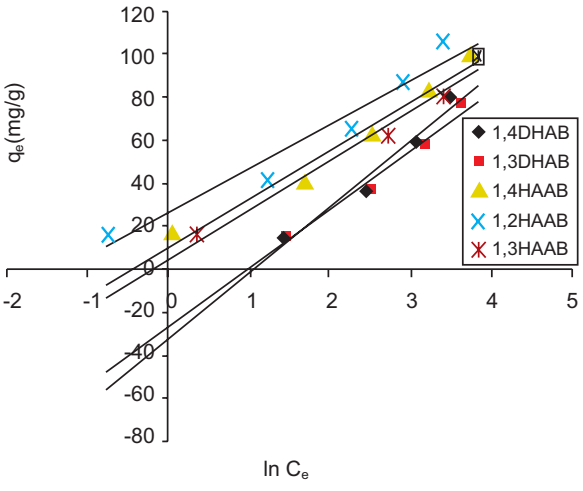

Fig. 5. Application of Tempkin isotherm on the adsorption data at 20 °C.

Table 7. Values of R_L and b obtained from the application of Langmuir isotherm at 20 °C

Dye	B (L/mg)	C_i (mg/L)	R_L
1,4 DHAB	0.0184	35	0.6083
		87	0.3845
		140	0.2796
		192	0.2206
		245	0.1816
1,3 DHAB	0.0261	35	0.5226
		87	0.3057
		140	0.2149
		192	0.1664
		245	0.1352
1,4 HAAB	0.1074	35	0.2101
		87	0.0967
		140	0.0624
		192	0.0463
		245	0.0366
1,2 HAAB	0.1734	35	0.1415
		87	0.0622
		140	0.0396
		192	0.0292
		245	0.023
1,3 HAAB	0.0944	35	0.2323
		87	0.1085
		140	0.0703
		192	0.0523
		245	0.0414

be attributed to the decrease in the adsorption rate (which is initially fast) due to pore diffusion (Eren and Acar, 2006; Ozacar and Sengil, 2003). For this reason, the calculated q_e values are quite low if compared to the experimental q_e. Furthermore, the values of R for all of the plotted lines are far less than unity denoting that, the adsorption of the studied dyes on to CAC is not first order reaction.

Pseudo second order model. The experimental data of the adsorption of the diazo dyes on activated carbon are fitted to the Pseudo second order model (eq. 4). The values of k_2 (g/mg/min) and q_e (mg/g) are calculated from the slope and intercept of the straight lines obtained by plotting t/q_e against time (Fig. 6a-e), respectively. The initial rate of adsorption (h, mg/g/min), is evaluated using equation (12):

$$h = k_2 q_e^2 \quad \text{.....(12)}$$

The results obtained from the application of this kinetic model are portrayed in Table 9.

The results of Table 9 indicated that, contrary to the first order equation, this model fit the adsorption data well for the whole range of contact time. Excellent linear relationships obtained (Fig. 7) indicated by the values of correlation coefficients which found to be in

Table 8. Results of the fitting of the pseudo first order model on adsorption data, pH=7 and T= 20 °C

Dye	C_i (mg/L)	q_e calc (mg/g)	k_1(min)	q_e exp (mg/g)	R
1,4DHAB	60	-0.447	0.0378	25.847	0.6074
	87	-	0.0113	37.737	0.2480
	100	-0.853	0.0412	42.304	0.5116
	120	-	0.0299	50.720	0.4572
1,3DHAB	60	-0.306	0.0292	25.340	0.7549
	87	-0.560	0.0472	36.786	0.5361
	100	-0.944	0.0302	41.159	0.5208
	120	-	0.0184	49.548	0.4399
1,4HAAB	60	-0.482	0.0327	28.400	0.6181
	87	-0.377	0.0523	40.793	0.7232
	100	-1.241	0.0316	46.116	0.4641
	120	-	0.0249	54.851	0.3939
1,2HAAB	60	-	0.027636	28.835	0.4954
	87	-0.440	0.036618	41.862	0.5093
	100	-	0.025103	47.088	0.4706
	120	-	-4.6E-05	56.010	0.0008
1,3HAAB	60	0.134	0.0359	28.295	0.9654
	87	0.124	0.0355	40.828	0.9670
	100	0.120	0.0359	45.574	0.9707
	120	0.114	0.0366	53.861	0.9768

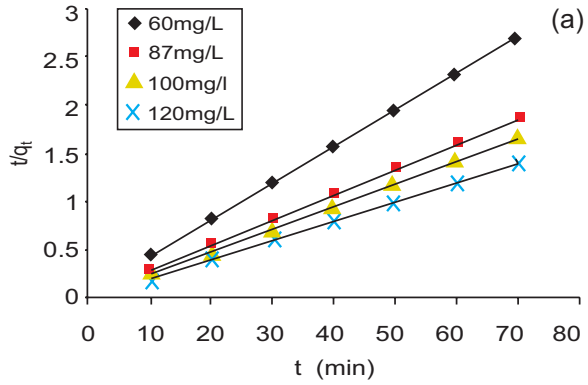

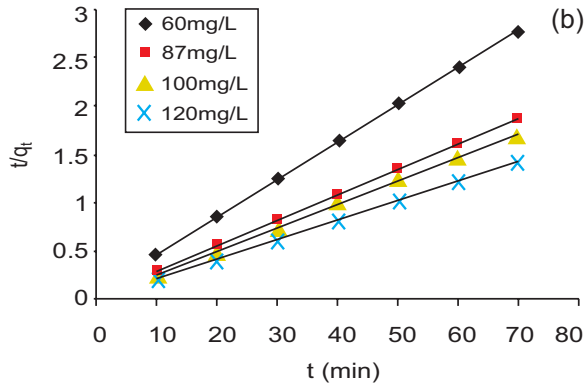

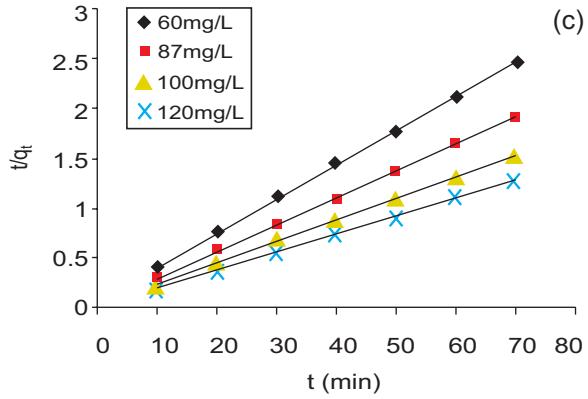

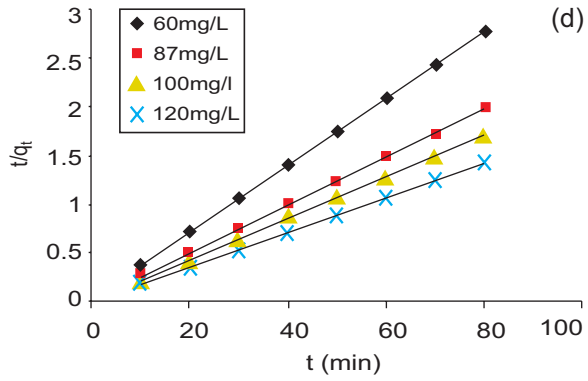

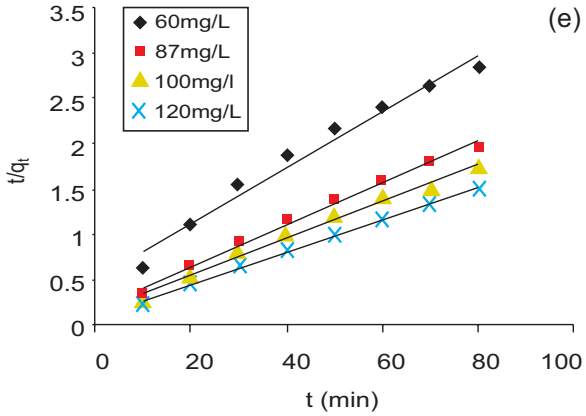

Fig. 6a-e. Relation between t/q_t versus time of the tested dye at different concentrations, (a) 1,4DHAB; (b) 1,3DHAB; (c) 1,4HAAB; (d) 1,2HAAB and (e) 1,3HAAB.

the range between (0.98-1.0) for all of the dyes and at all concentrations. In addition, the values of calculated q_e (q_e calc.) agreed very well with the experimental q_e (q_e exp) data. These results suggest that, the adsorption of the considered dyes on CAC obeys the second order kinetic model for the entire period of adsorptions based on the assumption that, the rate limiting step may involve chemisorptions. The investigation also revealed that, the increase of the initial concentration increases the initial rate of adsorption (h), since it enables the mass transfer of the adsorbate molecules from the solution to the solid surface of adsorbent. The results obtained are similar to data of other studies observed in the literature (EL-Nemr *et al*., 2009; Khaled *et al*., 2009).

Elovich kinetic model. This model (eq. 6) is fitted to the adsorption data of the studied dyes under similar conditions that used when applying the Pseudo first and second order models. The linear relationships between q_t and lnt shown in (Fig. 8) are used to calculate the values of Elovich constant represented by the initial rate of adsorption (α, mg/g/min) and desorption constant (β, g/mg). These constants were determined at various concentrations, from the slope and intercept of the straight lines (Fig. 8), respectively. The estimated values are listed in Table 10.

Increase in the initial rate of adsorption (α) is observed with the increase of initial concentration, accompanied by increase of desorption constant. These results can be interpreted as follow; as mentioned earlier, the increase of initial concentration facilitate the molecular

Table 9. Results of the fitting of the pseudo second order model on adsorption data, pH=7, T= 20 °C and CAC dose = 2 g/L

Dye	C_i (mg/L)	q_e calc (mg/g)	k_2 (g/mg/min)	H (mg/g/min)	q_e exp (mg/g)	R
1,4DHAB	60	26.315	0.0278	19.251	25.847	1
	87	38.167	0.0390	56.812	37.737	1
	100	42.553	0.0472	85.468	42.304	1
	120	51.020	0.0600	156.182	50.720	1
1,3DHAB	60	25.906	0.0188	12.617	25.340	0.9998
	87	37.174	0.0387	53.480	36.786	1
	100	41.493	0.0443	76.270	41.159	1
	120	49.751	0.0546	135.144	49.548	1
1,4HAAB	60	28.818	0.0283	23.503	28.400	1
	87	41.152	0.0451	76.376	40.793	1
	100	46.296	0.0518	111.024	46.116	1
	120	54.945	0.0705	212.836	54.851	1
1,2HAAB	60	29.069	0.0595	50.278	28.835	1
	87	42.016	0.0584	103.096	41.862	1
	100	47.169	0.0671	149.292	47.088	1
	120	56.179	0.0792	249.962	56.010	1
1,3HAAB	60	32.467	0.0013	1.370	28.295	0.9864
	87	46.511	0.0009	1.947	40.828	0.9951
	100	48.309	0.0030	7.001	45.574	0.9969
	120	56.497	0.0033	10.533	53.861	0.9984

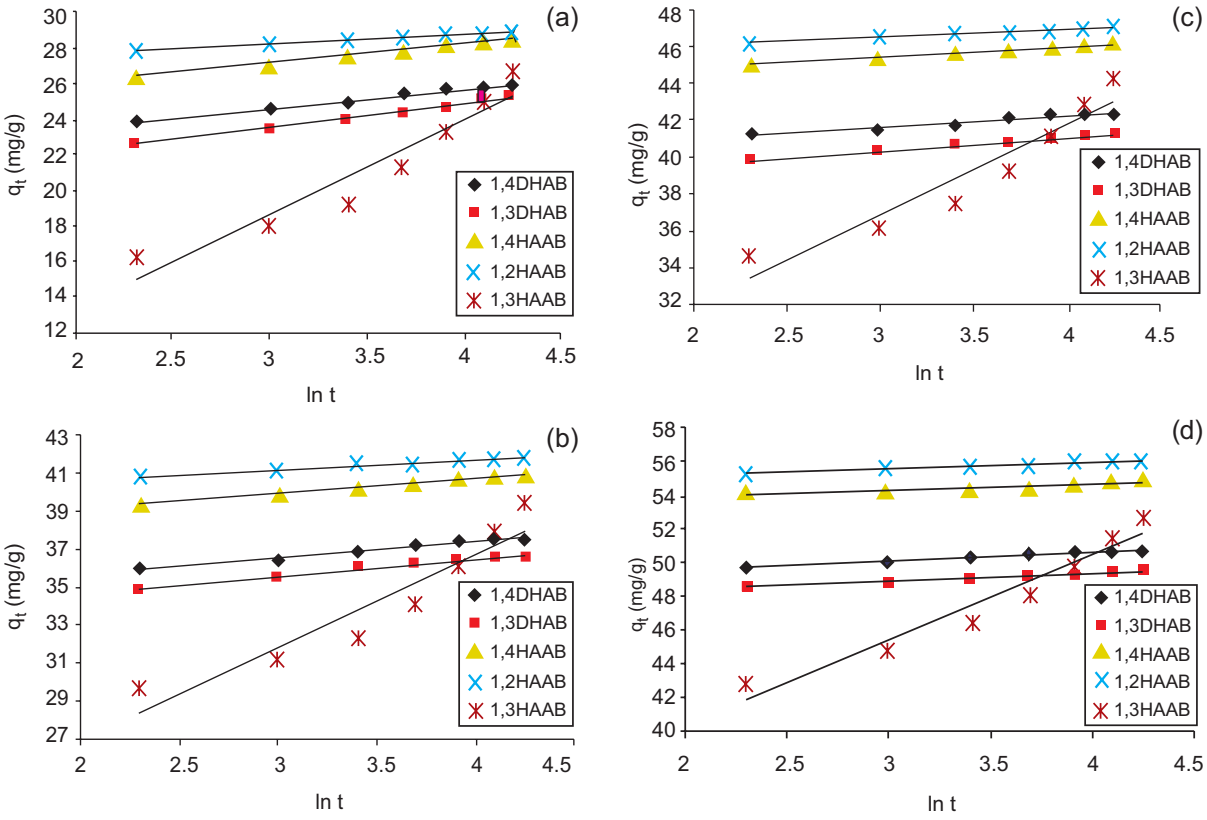

Fig. 7a-d. The relation between q_t versus ln t at different initial concentrations, (a) 60 mg/L; (b) 87 mg/L; (c) 100 mg/L and (d) 120 mg/L.

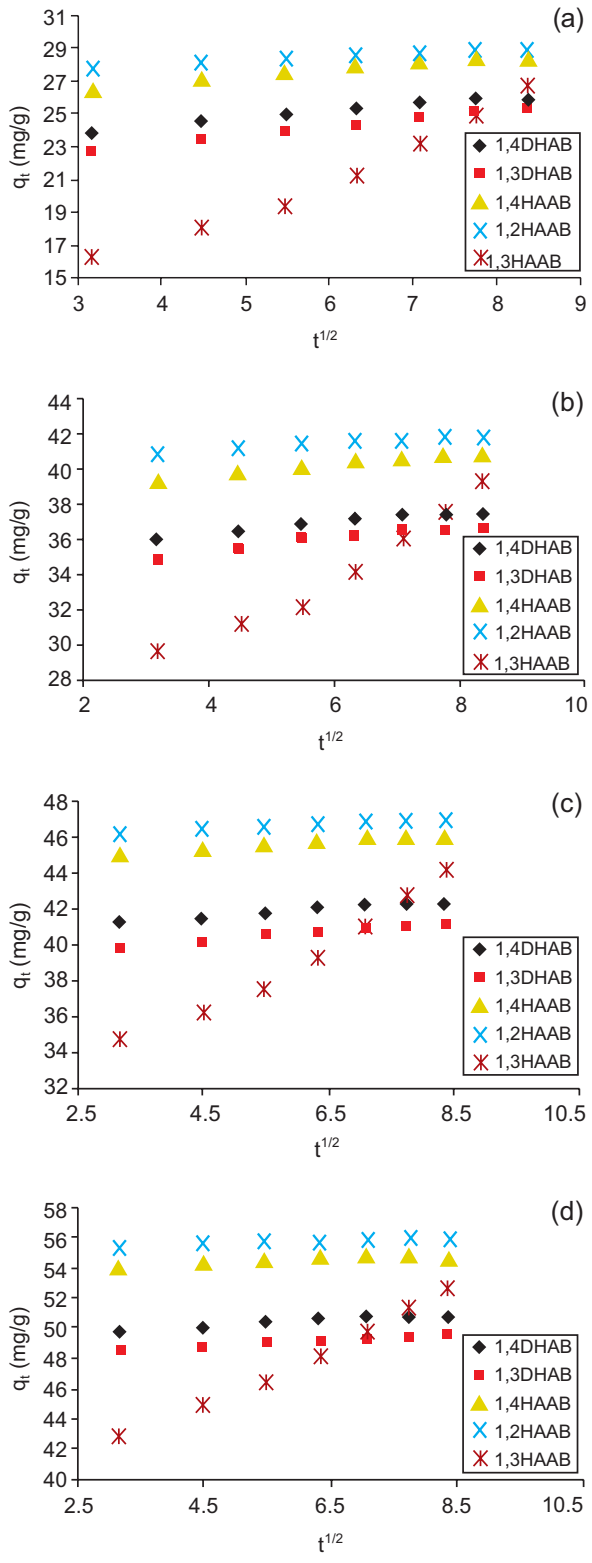

Fig. 8a-d. Relationship between q_t versus $t^{1/2}$ at different initial concentrations, (a) 60 mg/L; (b) 87 mg/L; (c) 100 mg/L and (d) 120 mg/L.

Table 10. Results of the application of Elovich equation on the adsorption data, pH = 7, CAC dose = 2 g/L and T = 20 °C

Dye	C_i (mg/L)	β (g/mg)	α (mg/g/min)	R
1,4DHAB	60	0.927	4.344E08	0.9918
	87	1.211	9.464E17	0.9903
	100	1.402	6.706E23	0.9895
	120	1.793	2.793E37	0.9936
1,3DHAB	60	0.720	1.603E06	0.9952
	87	1.090	4.145E15	0.9866
	100	1.384	6.287E22	0.9968
	120	1.926	1.914E39	0.9933
1,4HAAB	60	0.959	1.053E10	0.9956
	87	1.318	2.723E21	0.9944
	100	1.791	6.007E33	0.9930
	120	2.569	8.182E58	0.9698
1,2HAAB	60	1.857	1.407E21	0.9901
	87	1.968	4.278E33	0.9970
	100	2.318	1.400E45	0.9937
	120	2.881	5.789E67	0.9944
1,3HAAB	60	0.172	1.105E02	0.9536
	87	0.184	1.011E05	0.9497
	100	0.187	6.003E04	0.9553
	120	0.186	7.545E06	0.9722

transfer on to the solid surface which leads to increase in the initial concentration due to the availability of active sites on the carbon surface in the first few minutes. As the coverage of carbon surface increase, the competition among adsorbate molecules to be attached on the limited number of active sites remained on the carbon surface increased, creating a repulsion forces toward the adsorbent surface which weaken the bonding energy and increasing the desorption process. This observation is consistent with other results found in the literature (EL-Nemr *et al*., 2009; Khaled *et al*., 2009).

The intraparticle diffusion model. The possibility of applying this model on the adsorption data of the studied azo dyes on CAC is tested in terms of the graphical relationship (eq. 7) between the amount of dye adsorbed and the square root of time.

The plot between q_t against $t^{1/2}$, shown in (Fig. 8), is found to give two lines. The rate of diffusion constant (K_{diff}, mg/g/min) is directly estimated from the slope of the second regression line and the value of C is represented by the intercept.

The values of correlation coefficients, K_{diff} and C are given in Table 11.

Table 11. Results of the application of the intraparticle diffusion model on adsorption data, pH = 7, T = 20 °C and CAC dose = 2 g/L

Dye	C_i (mg/L)	K_{diff} (mg/g/min)	C (mg/g)	R
1,4DHAB	60	0.3964	22.735	0.9852
	87	0.3020	35.399	0.9785
	100	0.2601	40.296	0.9745
	120	0.2031	49.138	0.9775
1,3DHAB	60	0.5152	21.110	0.9984
	87	0.3298	34.265	0.9585
	100	0.2645	39.074	0.9863
	120	0.1932	47.954	0.9985
1,4HAAB	60	0.3840	25.347	0.9907
	87	0.2761	38.646	0.9773
	100	0.2072	44.453	0.9952
	120	0.1473	53.637	0.9912
1,2HAAB	60	0.1854	27.315	0.9632
	87	0.1774	40.383	0.9842
	100	0.1521	45.793	0.9932
	120	0.1214	55.002	0.9827
1,3HAAB	60	2.1234	8.5916	0.9878
	87	1.9919	22.359	0.9856
	100	1.9500	27.601	0.9888
	120	1.9461	36.207	0.9963

Figure 8 confirms that, the adsorption of the tested dyes on CAC vary in a similar trend. The two intersecting lines obtained in each plot indicate that, the adsorption mechanism includes two steps independent of each other. The first one is fast and representing the attachment of dye onto the external surface of carbon at the beginning of the adsorption process. The second step occurs with a slower rate in which the dye molecules diffuse into the pores exist on the carbon surface. Since the plots of q_t versus $t^{1/2}$ obtained for all of the dyes do not pass through the origin point, the intraparticle diffusion is not the rate limiting step, and the surface adsorption is operating concurrently during the dye-carbon interactions.

The values of the thickness of the boundary layer(C) were found to increase with the increase of initial concentrations, which reflect the decrease of probability of the external mass transfer and increasing the chance of internal transfer. This observation is supported by the values of the intraparticle diffusion constants (K_{diff}) which decrease with the increase of the initial dye concentrations. The main reason for such behaviour is the increase of adsorbate-adsorbate interactions that result from the increase of initial concentration (Kannan and Sundaram, 2001).

The linear relationships between q_t and $t^{1/2}$ based on the correlation coefficient values close to unity is a good indication of the application of this model on the studied systems and may confirm that, the intraparticle diffusion process is the rate determining step.

Conclusion

In this study, a number of di-azo dyes are synthesized. These dyes were of great stability and have properties that making them suitable for industrial application specially textile industry. The results of the investigation dealing with the methodology of treating the water pollution, that may occur as a result of throwing such dyes into water sources as an industrial waste, by adsorption.

The forces controlling the adsorption process and the mechanism by which the adsorption is performed are investigated by employing equilibrium and kinetic studies which are conducted at the optimal conditions of the adsorption system.

References

Ahmed, A.A., Hameed, B.H., Aziz, N. 2007. Adsorption of direct dye on palm ash: kinetic and equilibrium modeling. *Journal of Hazardous Materials*, **141:** 70-76.

Aksu, Z. 2003. Reactive dye bioaccumulation by *Saccharomyces cerevisiae*. *Process Biochemistry*, **38:** 1437-1444.

AL-Abady, R.T.Gh. 2010. Thermodynamic and kinetic study of adsorption of di-azo dyes on activated carbon in aqueous solution. *Ph.D. Thesis*, pp. 57-59, Mosul University, Iraq.

AL-Hyali, E.A., Al-Jarjari, I.A. 2008. Study of the adsorption of some azo dyes on activated carbon. *Journal of Education and Science*, **21:** 31-48.

Annadurai, G., Juang, R.S., Lee, D.J. 2002. Use of cellulose-based wastes for adsorption of dyes from aqueous solutions. *Journal of Hazardous Materials*, **92:** 263-274.

Arami, M., Limaee, N.Y., Mahmoodi, N.M., Tabrizi, N.S. 2005. Removal of dye from colored textile wastewater by orange peel adsorbent: equilibrium and kinetic studies. *Journal of Colloid and Interface Science*, **288:** 371-376.

Chien, S.H., Clayton, W.R. 1980. Application to Elovich equation to the kinetics of phosphate release and

sorption on soils. *Soil Science Society of America Journal*, **44:** 265-268.

Crini, G., Peindy, H.N., Gimbert, F., Robert, C. 2007. Removal of C.I. basic green 4 (Malachite green) from aqueous solutions by adsorption using cyclodextrin based adsorbent: kinetic and equilibrium studies. *Separation and Purification Technology*, **53:** 97-110.

Dushenkov, V., Kumar, P.B.A.N., Motto, H., Raskin, I. 1995. Rhizofiltration: The use of plants to remove heavy metals from aqueous systems. *Environmental Science and Technology*, **29:** 1239-1245.

El-Geundi, M.S. 1991. Homogeneous surface diffusion model for the adsorption of basic dyestuffs onto natural clay in batch adsorbers. *Adsorption Science and Technology*, **8:** 217-225.

EL-Nemr, A., Abdelwahab, O., EL-Sikaily, A. 2009. Removal of direct blue-86 from aqueous solution by new activated carbon developed from orange peel. *Journal of Hazardous Materials*, **161:** 102-110.

EL-Ashtoukhy, el S.Z. 2009. *Luffa aegyptiaca* as a novel adsorbent for removal of direct blue dye from aqueous solution. *Journal of Environment Management*, **90:** 2755-2761.

Eren, Z., Acar, F.N. 2006. Adsorption of reactive black 5 from aqueous solution: equilibrium and kinetic studies. *Desalination*, **194:** 1-10.

Freundlich, H.M. 1906. Uber die adsorption in losungen. *Zeitschrift fur Physikalsche Chemie*, **57A:** 385-470.

Hameed, B.H. 2009. Spent tea leaves: A new non-conventional and low cost adsorbent for removal of basic dye from aqueous solutions. *Journal of Hazardous Materials*, **161:** 753-759.

Ho, Y.S. 2006. Review of second-order models for adsorption system. *Journal of Hazardous Materials*, **136:** 681-689.

Ho, Y.S., Wase, D.A.J., Forster, C.F. 1996. Kinetic studies of competitive heavy metal adsorption by sphagnum moss peat. *Environmental Technology*, **17:** 71-77.

Kannan, N., Sundaram, M.M. 2001. Kinetic and mechanism of removal of methylene blue by adsorption on various carbons: a comparative study. *Dyes and Pigments*, **51:** 25-40.

Khaled, A., EL-Nemr, A., Sikaily, A., Abdelwahab, O. 2009. Removal of direct N blue-106 from artificial textile dye effluent using activated carbon from orange peel: Adsorption isotherm and kinetic studies. *Journal of Hazardous Materials*, **165:** 100-110.

Lagergren, S. 1898. *Zur theorie* der sogenannten (About the theory of so-called adsorption of solubale substances). Kungliga Svenska Vetenskapsakademiens. *Handlingar*, **24:** 1-39.

Lewis, D.M. 1999. Coloration for the next century. *Rewiew of Progress in Coloration and Related Topics*, **29:** 23-28.

Malik, P.K. 2003. Use of activated carbons prepared from sawdust and rice husk for adsorption of acid dyes: A case study of acid yellow 36. *Dyes and Pigments*, **56:** 239-249.

McKay, G., Ho, Y.S. 1999. Pseudo second order model for adsorption process. *Process Biochemistry*, **34:** 451-465.

McKay, G., Blair, H.S., Gardner, J.K. 1982. Adsorption of dyes on chitin: Equilibrium study. *Journal of Applied Polymer Science*, **27:** 3043-3057.

Mohorcic, M., Friedrich, J., Pavko, A. 2004. Decoloration of the di-azo dyes reactive black 5 by immobilized *Bjerkandera adusta* in a stirred tank bioreactor. *Acta Chimica Solvenica*, **51:** 619-628.

Ozacar, M., Sengil, I.A. 2003. Adsorption of reactive dyes of calcined alunite from aqueous solutions. *Journal of Hazardous Materials*, **98:** 211-224.

Reddy, S.S., Kotaiah, B., Reddy, N.S.P., Velu, M. 2006. The removal of composite reactive dye from dyeing unit effluent using sewage sludge derived activated carbon. *Turkish Journal of Engineering and Environmental Sciences*, **30:** 367-373.

Shah, B.A., Shah, A.V., Singh, R.R. 2009. Sorption isotherms and kinetics of chromium uptake from wastewater using natural sorbent material. *International Journal of Environmental Science and Technology*, **6:** 77-90.

Sharma, I., Goyal, D. 2009. Kinetic modeling: Chromium(III) removal from aqueous solution by microbial waste biomass. *Journal of Scientific and Industrial Research*, **68:** 640-646.

Shukla, A., Zhang, Y.H., Dubey, P., Margrave, J.L., Shukla, S.S. 2002. The role of saw dust in removal of unwanted materials from water. *Journal of Hazardous Materials*, **B95:** 137-152.

Slokar, Y.M., Le Marechal, M. 1998. Method of decoloration of textile wastewaters. *Dyes and Pigments*, **37:** 335-357.

Smith, B., Koonce, T., Hudson, S. 1993. Decolorizing dye wastewater using chitosan. *American Dyestuff Reporter*, **82:** 18-36.

Suteu, D., Bilba, D. 2005. Equilibrium and kinetic study of reactive dye brilliant red HE-3B adsorption by

activated charcoal. *Acta Chimica Solvenica*, **52:** 73-79.

Sutherland, J.B. 2004. Degradation of hydrocarbons by yeast and filamentous fungi. In: *Fungal Biotechnology in Agricultural, Food and Environmental Applications*, D. K. Arora, (ed.), pp. 457-469, Marcel Decker Inc., New York, USA.

Thambavani, D.S., Sabitha, M.A. 2012. Kinetic and isotherm studies of biodegradation on sugar mill waste water using *Mangifera indica* leaf powder. *Research Journal of Pharmaceutical, Biological and Chemical Sciences*, **3:** 247-260.

Van der Zee, F.P. 2002. Anaerobic Azo Dye Reduction. *Ph.D. Thesis*, 8 pp., University of Wageningen, The Netherlands.

Vandevivere, P.C., Bianchi, R., Verstraete, W. 1998. Treatment and reuse of wastewater from the textile wet processing industry: Review of emerging technologies. *Journal of Chemical Technology and Biotechnology*, **72:** 289-302.

Volgel, A. 1964. *A Textbook of Practical Organic Chemistry*, pp. 622-623, 3rd edition, Longmans, Green and Co. Ltd., London, UK.

Wallace, T.H. 2001. Biological Treatment of a Synthetic Dye Water and an Industrial Textile Wastewater Containing Azo Dyes Compounds. *M.Sc. Thesis*, pp. 4-13, Blacksburg, Virginia, USA.

Weber, W.J., Morris, J.C. 1963. Kinetics of adsorption on carbon from solution. *Journal of Sanitary Engineering Division, American Society of Civil Engineering*, **89:** 31-59.

Woodard, F. 2001. *Industrial Treatment Handbook*. pp. 376-451, Butterworth-Heinemann, Publisher, UK.

Yasin, Y., Hassein, M.Z., Ahmed, F.H. 2007. Adsorption of methylene blue onto treated activated carbon. *The Malaysian Journal of Analytical Science*, **11:** 400-406.

Yu, L.J., Shukla, S.S., Dorris, K.L., Shukla, A., Margrave, J.L. 2003. Adsorption of chromium from aqueous solutions by maple sawdust. *Journal of Hazardous Materials*, **B100:** 53-63.

Pak. j. sci. ind. res. Ser. A: phys. sci. 2013 **56** (2) 86-92

A Study on the Production of Biodiesel from Used Frying Oil

Mehmood Abbas[a], Farooq Ahmad[a]*, Adnan Skhawat Ali[a], Maqsood Ahmed[a], Muhammad Farhan[a], Syed Ahtisham Shabbir[b], Aqsa Iftikhar[a] and Nazish Mohy-u-Din[a]

[a]Sustainable Development Study Centre, GC University, Lahore, Pakistan

[b]Directorate General of Health, Lahore, Government of Punjab, Pakistan

(received February 28, 2012; revised December 29, 2012; accepted January 4, 2013)

Abstract. The study was carried out to utilize waste frying oil for biodiesel production because it is cheap, easily available and renewable raw material. The used frying oil was analyzed for water contents (0.43 %), iodine value (52), sponification value (205), free fatty acids (8.7 %) and acid value (0.8 mg KOH/g). Esterification and transesterification were conducted to convert free fatty acids and triglycerides to methyl ester (biodiesel), respectively. One-step and two-step transeterification reactions were carried out to measure the efficiency of these processes for biodiesel production. The biodiesel produced from used frying oil was examined for flash point (185 °C), kinematic viscosity (4.86 mm^2/s) and specific gravity (0.884 g/mL) that were meeting the limits of ASTM and Thai standards. Hence, it was proved to be a useful technique for biodiesel production at commercial scale.

Keywords: biodiesel, esterification, transesterification, waste cooking oil, renewable raw material

Introduction

Worldwide oil consumption was 3571.6 million tons, in 2000 but in 2010, the consumption reached 4028.1 million tons, with average annual increase of 3.1%. According to British Petroleum Statistical Review of World Energy (2011), the world oil reserves were estimated 188.8 million tons with a reserve to production ratio of 46.2 years at the end of 2010 (Goldemberg, 2008). The first diesel engine that ran on vegetable oil was built in 1893 by Rudolf Diesel and gave the idea of using vegetable oil as a transportation fuel. Current energy demand is hardly fulfilled by conventional energy resources such as petro-diesel, coal and natural gas. The reserves of petroleum fuel will deplete in near future (Sheehan *et al*., 1998). Petroleum price has not only been increasing but also causing environmental pollution by producing hazardous gases due to incomplete combustion of these fuels (Marchetti *et al*., 2007). Balance between economic, agriculture and environmental development could be made by using alternative fuel which should be economically competitive, technically feasible, readily available and environmentally acceptable. Biodiesel synthesized from renewable raw material has all these properties (Meher *et al*., 2006). In the recent years particular focus has been emphasized on biodiesel production from cheaper sources such as vegetable oil (Balat, 2008) because it is renewable, eco-friendly, biodegradable and non toxic in nature. Moreover, biodiesel is a clean fuel having no sulphur emissions and lower heat of combustion than petro-diesel (Srivastava and Prasad 2000). Biodiesel produced from animal fat and used frying oil is eco-friendly and good alternative to diesel fuel (Demirbas, 2005). Recently scientists all over the world are trying to produce more and more biodiesel because it can be used as substitute for petro-diesel without the modification in diesel engines (Demirbas, 2002). Biomass, vegetable oil, animal fat and used frying oil can be used to produce biodiesel by reacting with alcohol (methanol or ethanol) and strong base catalyst such as potassium or sodium hydroxide (Kalam and Masjuki 2002).

Renewable raw material such as oil could be converted into its corresponding fatty ester (biodiesel) by transesterification reactions. Transesterification process can proceed with or without alkali catalyst by using primary or secondary monohydric aliphatic alcohols. However, for the production of biodiesel, various types of oils (as raw material), homogeneous catalysts (potassium hydroxide, sodium hydroxide, sulphuric acid and supercritical fluids), heterogeneous catalysts and enzyme (lipase) can be used (Marchetti *et al*., 2007).The blend of biodiesel with petro-diesel could also be used in transport sector. The blend of biodiesel

*Author for correspondence; E-mail: fagondal82@yahoo.com

are denoted as Bxx, where xx shows the quantity of biodiesel blended with petro-diesel. For units, B100 is referred to 100% biodiesel and B80 is referred to 80% biodiesel and 20% petro-diesel and so on (Demirbas, 2007).

Used frying oil is the residue which can be collected from restaurants, kitchens and food processing factories for the production of biodiesel. It is not recommended to be used again for cooking or frying purpose. Normally it is disposed in water bodies, where it is not only causing water pollution but also causing harm to aquatic organisms. Used frying oil can be a good option as raw material, because its price is 2 to 3 times lower than fresh vegetable oils which in turn reduce the production cost of biodiesel (Hameed *et al.*, 2009). Although the physical and chemical characteristics of used frying oil are different from fresh edible oil but both oils can be transformed into biodiesel by applying same method i.e. transesterification reaction by alkali catalyst, acid catalyst or using enzymes. The used frying oil can be effectively converted into biodiesel by two-step transesterification reaction. The two-step transesterification reaction consists of alkali catalyzed reaction, and acid catalyzed reaction. The properties of biodiesel produced from used frying oil are certainly similar to those produced from their respective fresh vegetable oil (Loh *et al*., 2006).

The present study was conducted to measure conversion efficiency of used frying oil to biodiesel. Used frying oil was analyzed before its conversion to biodiesel to measure its suitability for biodiesel production. Biodiesel was analyzed after its production from used frying oil and compared with ASTM standards (2002). Comparison of yield of one-step and two-step transesterification reactions was another part of the study.

Materials and Methods

Collection of samples. Used frying oil was purchased from two different chicken frying shops from different locations of Shahdara Town, Lahore that was repeatedly used for frying from early morning to mid night and on closure of the restaurant it was put into a plastic can for sale or thrown in sewage drain. The price of used frying oils was 0.33 US$/L. The oil sample was collected in plastic bottles and transferred to laboratory for further processing. The collected sample was contaminated with suspended carbon particles and water content. Sieving and filtration were done to remove food contents and suspended carbon particles.

Analytical procedures. Before transesterification of the oil to methyl esters all impurities were removed before its conversion to biodiesel. For removing large solid particles a sieving plate with mesh size 170 mm was used and to remove all suspended particles Whattman filter paper was used. Used frying oil sample was heated at 60 °C for 30 min to remove water content. Fatty acid profile was analyzed by gas chromatography mass spectrometry (GC-MS, Shimadzu GC-14-A). Properties of used frying oil sample such as, acid value free fatty acid value, iodine value and saponification value were analyzed by methods of Raie (2008).

Experimental setup. Sodium methoxide was prepared by mixing NaOH and pure methanol. Sodium hydroxide was used 1% wt (dry weight basis) to oil and methanol was used 10% (dry weight basis) to used frying oil with molar ratio 6:1 (Charoenchaitrakool and Thienmethangkoon, 2011). The measured amount of NaOH and pure methanol were mixed in beaker and stirred for 30 min.

Transesterification reaction was carried out by mixing oil with sodium methoxide to convert fatty acids (triglycerides) of used frying oil to methyl esters (Biodiesel). Sodium methoxide was mixed in used sample when its temperature reached to 60 °C and stirred continuously for 30 min. The mixture was then allowed to stand in separating funnel for at least 8 h. Two layers were produced, (a) with glycerol in the bottom and (b) methyl ester at the top. Upper layer was mixed with hexane to dissolve methyl esters, and then hexane was separated by distillation afterwards to get pure biodiesel (Ahmad *et al*., 2009).

Two-step catalyzed process was used i.e. esterification and transesterification. In the esterification process, free fatty acids (FFA) were reduced in the used frying oil using sulphuric acid as a catalyst. The optimum conditions were obtained using molar ratio of methanol to used frying oil 6:1 with 0.68% wt of sulphuric acid and reaction time 1 h at 51 °C. In the transesterification reaction, methanol and alkali (NaOH) the catalyst was used to convert triglyceride portion of the used frying oil to methyl ester and glycerol. The optimum conditions were obtained using molar ratio of methanol to used sample 9:1 with 1 %wt of base catalyst and reaction time 1 h at 55 °C (Charoenchaitrakool and Thienmethangkoon, 2011; Lotero *et al*., 2005).

The final product of methyl ester was identified with the help of thin layer chromatography (TLC) at Applied Chemistry Research Centre, Pakistan Council of

Scientific and Industrial Research (ACRC-PCSIR) Laboratories, Lahore. Thin layer chromatogram was prepared with particular length, width and thickness (20 cm × 20 cm × 0.25 mm) by utilizing water and silica gel. The plate was air dried and activated on heating at 105 °C in the oven for 1 h. Biodiesel was dissolved in pure *n*-hexane as *n*-hexane, and diethyl ether (80:20) were used as solvent system. The 2, 7-dichlorofluorescein as non-destructive locating agent was required to see colour bands (purple-yellow) under ultra violet light of 366 nm wavelength.

Results and Discussion

Water content. Water content of oil sample was removed up to 0.43% by heating for 35 min (Table 1). The water content present in the used oil sample decreased the efficiency of the transesterification process, because it decomposes the esters present in the oil and results in the saponification of oil by base catalyst. Presence of high water content in the oil can be tackled by acid catalyst, which increases the efficiency of transesterification process named as two content step transesterification process. Water in pretreated used frying oil was determined to be 0.1 % by weight (Charoenchaitrakool and Thienmethangkoon, 2011). Minimum water content and free fatty acid content in oil were very important for getting optimal results in the process of transesterification. Basic catalyst can only be utilized in transesterification process, when there is low water and free fatty acid contents. If the water content and fatty acid are high then two-step transesterification process is suitable in which the first-step is carried out with acid catalyst and the second-step with basic catalyst. Reaction rate can be increased by increasing reaction time (Ahmad *et al.,* 2009). In this current study, both processes were used to measure their efficiency.

Iodine value. Iodine value can be used to measure the unsaturation of oils. It is the percentage of iodine in centi-grams which 1 g of sample absorbed. Iodine value of used frying oil sample was calculated to be 52 mg/g (Table 1). Balat and Balat (2010) calculated iodine value 35-61% for palm oil and 110-143 % for sunflower oil. According to Oliveira *et al.* (2010) the oil showed iodine index 7.21g/100g. Low value of iodine indicated lower unsaturated compounds of carbon and the biodiesel produced from that oil was resistant to oxidation process.

Table 1: Analysis of pretreated frying oil sample

Parameters tested	Results
Water content (%)	0.43
Nature of food (fried)	Chicken meat
Iodine value (mg/g)	52
Saponification value (mg/g)	205
Free fatty acid (%)	8.7
Acid value (mg KOH/g)	0.8

Saponification value. The process of saponification of sodium soap obtained from vegetable oil can be described in the following chemical equation:

vegetable oil + NaOH $\rightarrow$ RCOONa + glycerin (Demirbas, 2002).

The saponification value of used frying oil was measured to be 205 mg/g (Table 1). Demirbas (2009b) calculated the sponification value 188.2. High level of saponification required that sample must be esterified with sulphuric acid with methanol. If the free fatty acid level exceeds 0.5% by weight then the saponification reduces the formation and yield of methyl ester (biodiesel) and hindered settling of products obtained (Canakci and Gerpen, 2001).

Acid and free fatty acid values. The free fatty acid (FFA) value is the amount of milligram of KOH needed to neutralize fatty acids in 1g of oil. The FFA value measured in used frying oil of current study was 8.7% (Table 1). Balat and Balat (2010) calculated FFA value 5.6 for frying oil and >20 for waste palm oil while Berrios *et al.* (2010) measured FFA value 2.14 for used frying oil. High free fatty acid content can be esterified using acid catalyst. Good quality methyle esters can be obtained by basic catalyst if free fatty acid content remained lower than 1.0 wt% (Meng *et al*., 2008).

The acid value is the amount in milligram (mg) of aqueous potassium hydroxide (KOH) in 1 g of oil to neutralize the total free fatty acids. The acid value of sample studied was determined to be 0.8 mg KOH/g of oil (Table 1). Berrios *et al*. (2010) measured acid value 0.14 mg for used frying oil. In the process of base catalyzed transesterification the acid value of the oil must be less than 1 mg (Demirbas, 2009c). If the acid value exceeds 1 mg then additional alkali must be used to neutralize the free fatty acids (Canakci and Ozsezen, 2005).

Fatty acid composition and yield of reaction. Fatty acid composition of used frying oil was analyzed by gas chromatography. It was found that the used frying oil contained 0.1 wt% myristic acid, 7.88 wt% palmitic

acid, 0.35 wt% stearic acid, 54.54 wt% oleic acid, 28.96 wt% linoleic acid, 7.546 wt% linolenic acid, 0.18 wt% arachidonic (Table 2). Charoenchaitrakool and Thienmethangkoon (2011) reported the percentage composition of fatty acids in waste frying oil as 1.1 wt% myristic acid, 25.8 wt% palmitic acid, 4.7 wt% stearic acid, 34.6 wt% oleic acid, 29.4 wt% linoleic acid, 2.5 wt% linolenic acid, and 0.2 wt% arachidonic acid. Demirbas (2009a) calculated fatty acid composition of waste cooking oil from sunflower seed oil as 6.8 wt% C16:0 (palmitic acid), 3.7 wt% C18:0 (stearic acid), 22.8 wt% C18:1 (oleic acid), 65.2 wt% C18:2 (linoleic) and 0.1 wt% C18:3 (linolenic).

In one-step transesterification process, the yield of biodiesel was calculated to be 88% with glycerine as a byproduct. In two-step process, the yield of biodiesel was higher (92%) than one step process (Table 3). Formation of soap during one-step reaction was the reason of its low yield. However, in two-step reaction, sulphuric acid caused esterification of FFAs before biodiesel synthesis thus reducing the chances of soap formation. Zhang *et al.* (2003) described that high free fatty acid contents required to have pretreatment process in which the acid catalyst such as sulphuric acid was used to reduce the free fatty acid (FFA) contents.

Table 2. Percentage composition of fatty acids in used frying oil

Fatty acid profile	Result (%)
C14:0 Tetradecanoic (myristic)	Traces (0.1)
C16:0 Hexadecanoic (palmitic)	7.88
C18:0 Octadecanoic (stearic)	0.35
C18:1 Octadecenoic (oleic)	54.54
C18:2 Octadecadienoic (linoleic)	28.96
C18:3 Octadecatrienoic (linolenic)	7.546
C20:0 Eicosanoic (arachidonic)	0.18
Total saturated fatty acids	8.51
Total unsaturated fatty acids	91.046
Others	0.444

Table 3. Measurement of amount and yield of products from 200 mL of used frying oil

Products of the processes	One-step process	Two-step process
Biodiesel produced (mL)	176	184
Glycerin and other byproduct (mL)	24	16
Yield of biodiesel (%)	88	92

Quality assessment of biodiesel. One step and two step transesterification processes were used for the production of biodiesel from used frying oil under reaction conditions shown in Table 4.

In sample 1 (two-step process) the used frying oil was almost completely converted to biodiesel (methyl ester) and was according to ASTM standard (2002) of biodiesel because there were no fatty acids and glycerides found in final product (biodiesel). Biodiesel produced by one-step transesterification process (sample 2) contained fatty acids and glycerides along with methyl ester. Therefore, the biodiesel produced from used frying oil was of good quality by two-step transesterification process using acid and base catalyst than by using one-step transesterification process using base catalyst as the final product contained some amount of fatty acids and glycerides (Fig. 1).

Kinematic viscosity. Kinematic viscosity is the quotient of the dynamic viscosity divided by density (Va/d) at same temperature. The viscosity of biodiesel produced from used samples determined by ASTM D445 method was 4.86 at 40 °C (Table 5). Charoenchaitrakool and Thienmethangkoon (2011) reported the viscosity of biodiesel 4.61. Balat (2008) reported that the biodiesel has viscosity close to diesel fuel. Viscosity effects the injection equipment at the time of operation of fuel and at low temperature the increase in the viscosity effects fluidity of fuel. By increasing the temperature of reaction, viscosity decreased and miscibility of methanol and oil

Table 4. Optimization of reaction conditions for transesterification of used frying oil

Reaction conditions	One-step process transesterification	Two-step process	
		Esterification	Transesterification
Catalyst	NaOH	H_2SO_4	NaOH
Methanol to oil ratio	3:1	6:1	9:1
Temperature (°C)	60	51	55
Reaction time (min)	30	60	60

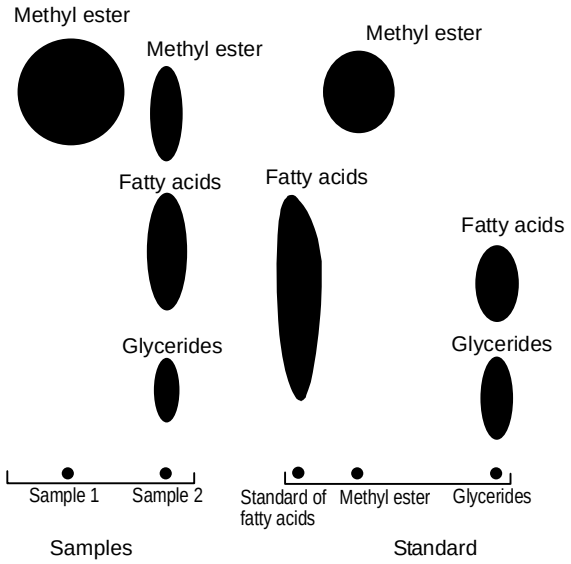

Fig. 1. Separation and identification of biodiesel (methyl ester) production from used frying oil by using solvent system at *n*-hexane to diethylether ratio of 80:20.

increased that ultimately increased the free fatty acid conversions (Park *et al.*, 2010).

Flash point. Flash point is the temperature recorded on thermometer at the time of application that causes a distinct flash in the interior of cup. The flash point of biodiesel produced in this study was determined by ASTM D93 testing method and the value obtained was 185 °C (Table 5). Charoenchaitrakool and Thienmethangkoon (2011) reported the flash point of biodiesel was 160. The ASTM D6751-02 standard for flash point of biodiesel is more than 130 °C. Demirbas (2009c) reported the flash point for biodiesel prepared from waste cooking oil was 469 K (196 °C).

Specific gravity. Specific gravity is the ratio of weight of given volume of material to weight of an equal volume of water. In this method both weights recorded in vacuum condition and the standard reference temperature for both, material and water was 60 F. The specific gravity of biodiesel measured by ASTM D1298 testing method was 0.884 g/mL (Table 5). The minimum values of specific gravity indicate the removal of heavy glycerine and thus completion of reaction (Sharma *et al.*, 2008). Balat and Balat (2010) calculated the specific gravity of biodiesel 0.88 g/mL. Berrios *et al.*, (2010) measured the specific gravity of biodiesel obtained from used frying oil in pressure system was 0.875 g/cm. Demirbas (2009c) measured density of biodiesel from waste cooking oil as 0.897 kg/L at 288K0.

Conclusion

Energy crises and environmental impacts of fossil fuel are forcing world to search its alternatives such as biofuels. Therefore, biodiesel production from cheaper raw material can be a fruitful technology. Used frying oil could be the suitable raw material otherwise it is disposed off in water bodies or soil causing environmental and health problems. Synthesis of biodiesel from this waste oil could be the best use of it. In the present study, biodiesel was produced from used frying oil by two methods and it was found that the biodiesel produced from two-step transesterification method gives good quality in comparison to one-step transesterification process as soap formation took place in one-step process. Properties of biodiesel such as kinematic viscosity, flash point and specific gravity were analyzed and found within ASTM (2002) standards limits for biodiesel.

Recommendations

* Repeated use of frying oil should be banned to avoid health risk and its market value could be

Table 5. Analysis of biodiesel produced from used frying oil and its comparison with international standards

Properties of biodiesel	Testing methods	Biodiesel of this study	ASTM D6751 (2002)	Thai Standard EN 14214 (2004)
Kinematic viscosity at 40 °C (mm^2/s)	ASTM D445	4.86	1.9–6.0	3.5–5.0
Flash point (°C)	ASTM D93	185	> 130	> 101
Specific gravity (g/mL)	ASTM D1298	0.884	-	0.860-0.900

created by using it for biodiesel production.

* Following results of current study for biodiesel production from used frying oil should be launched at commercial scale as it is an efficient, cheaper and feasible raw material.
* Further research is needed on conversion of used frying oil to biodiesel by using various catalysts to enhance its yield.

Acknowledgement

The authors acknowledge Sustainable Development Study Centre at Government College University Lahore for providing funding for this current study and Dr. Muhammad Zeeshan at Applied Chemistry Research Centre (ACRC), PCSIR Laboratories Lahore for guiding and providing testing facilities of oil and biodiesel. Authors are also thankful to Tahir Sattar and Ikram Hussain Arain, Chief Chemist at Southern Electric Power Company Limited, Lahore for their cooperation in biodiesel testing.

References

Ahmad, M., Zafar, M., Khan, M.A., Sultana, S. 2009. Biodiesel from *Pongamia pinnata* L. oil: A promising alternative bioenergy source, Part A: *Energy Sources*, **31:** 1436-1442.

ASTM D6751 2002. Standard Specification for Biodiesel Fuel (B100) Blend Stock for Distillate Fuels. www.astm.org/DATABASE.CART/HISTORICAL D6751-02.htm. DOI: 10.1520/D6751-02.

Balat, M., Balat, H. 2010. Progress in biodiesel processing. *Applied Energy*, **87:** 1815-1835.

Balat, M. 2008. Modeling vegetable oil viscosity. *Energy Source, Part A*: Recovery, *Utilization and Environment Effects*, **30:** 1856-1869.

Berrios, M., Martin, M.A., Chica, A.F., Martin A. 2010. Study of esterification and transesterification in biodiesel production from used frying oils in a closed system. *Chemical Engineering Journal*, **160:** 473-479.

Canakci M., Ozsezen A. N. 2005. Evaluating waste cooking oils as alternative diesel fuel. *Gazi University Journal of Science*, **18:** 81-91.

Canakci, M., Van Gerpen, J. 2001. Biodiesel production from oils and fats with high free fatty acids, *Transactions of the American Society of Agricultural Engineerings*, **44:** 1429-1436.

Charoenchaitrakool, M., Thienmethangkoon, J. 2011. Statistical optimization for biodiesel production from waste frying oil through two-step catalyzed process. *Fuel Processing Technology*, **92:** 112-118.

Demirbas., A. 2009a. Production of biodiesel fuels from linseed oil using methanol and ethanol in non-catalytic SCF conditions. *Biomass Bioenergy*, **33:** 113-118.

Demirbas**.**, A. 2009b. Progress and recent trends in biodiesel fuels. *Energy Conversion and Management*, **50:** 14-34.

Demirbas., A. 2009c. Biodiesel from waste cooking oil via base-catalytic and supercritical methanol transesterification. *Energy Conversion and Management*, **50:** 923-927.

Demirbas., A. 2007. Importance of biodiesel as transportation fuel. *Energy Policy*, **35:** 4661-4670.

Demirbas., A. 2005. Biodiesel production from vegetable oils via catalytic and noncatalytic supercritical methanol transesterification methods. *Progress in Energy Combustion Science*, **31:** 466-487.

Demirbas A. 2002. Diesel fuel from vegetable oil via transesterification and soap pyrolysis. *Energy Source*, **24:** 835-841.

Goldemberg., J. 2008. Environmental and ecological dimensions of biofuels. In: *Conference on the Ecological Dimensions of Biofuels*, Washington, D.C., USA.

Hameed, B. H., Goh C. S., Chin, L.H. 2009. Process optimization for methyl ester production from waste cooking oil using activated carbon supported potassium fluoride. *Fuel Processing Technology*, **90:** 1532-1537.

Kalam M.A., Masjuki, H.H. 2002. Biodiesel from palm oil an analysis of its properties and potential. *Biomass Bioenergy*, **23:** 471-479.

Loh, S.K., Choo, Y. M., Cheng, S.F., Ma, A. N. 2006. Recovery and conversion of palm olein derived used frying oil to methyl esters for Biodiesel. *Journal Oil Palm Research*, **18:** 247-252.

Lotero, E., Liu, Y., Lopez, D.E., Suwannakarn, K., Bruce, D.A., Goodwin, J.G. 2005. Synthesis of Biodiesel via Acid Catalysis. *Industrial & Engineering Chemistry Research*, **44:** 5353-5363.

Marchetti, J.M., Miguel, V.U., Errazu, A.F. 2007. Possible methods for biodiesel production. *Renewable and Sustainable Energy Reviews*, **11:** 1300-1311.

Meher, L.C., Sagar, V.D., Naik, S.N. 2006. Technical aspects of biodiesel production by transesterification; A review. *Renewable and Sustainable Energy Review*, **10:** 248-268.

Menga, X., Chen, G., Wang, Y. 2008. Biodiesel production

from waste cooking oil via alkali catalyst and its engine test. *Fuel Processing Technology,* **89:** 851-857.

Oliveira, J.F.G., Lucena, I.L., Saboya, R.M.A., Rodrigues, M.L., Torres, A.E.B., Fernandes, F.A.N., Cavalcante Jr, C.L., ParenteJr, E.J.S. 2010. Biodiesel production from waste coconut oil by esterification with ethanol: The effect of water removal by adsorption. *Renewable Energy*, **35:** 2581-2584.

Park, Y.M., Lee, J.Y., Chung, S.H., Park, I.S., Lee, S.Y., Kim, D.K., Lee, J.S., Lee, K.Y. 2010. Esterification of used vegetable oils using the heterogeneous WO_3/ZrO_2 catalyst for production of biodiesel. *Bioresource Technology,* **101:** 59-61.

Raie, M.Y. 2008. *Oil, Fats and Waxes,* 1st edition, National Book Foundation, Islamabad, Pakistan.

Sharma, Y.C., Singh, B., Upadhyay, S.N. 2008. Advancements in development and characterization of biodiesel: A review. *Fuel*, **87:** 2355-2373.

Sheehan, J., Cambreco, V., Duffield, J., Garboski, M., Shapouri, H. 1998. An overview of biodiesel and petroleum diesel life cycles. *A Report by US Department of Agriculture and Energy*, pp. 1-35, Washington, D.C., USA.

Srivastava, A., Prasad, R. 2000. Triglycerides-based diesel fuels. *Renewable and Sustainable Energy Reviews,* **4:** 111-133.

Thai standard EN 14214. 2004. Biofuels Standard & Regulations in Thailand. Thailand Institute of Scientific and Technological Research (TISTR). http://www.tistr.or.th.

Zhang, Y., Dube, M.A., McLean, D.D., Kates, M. 2003. Biodiesel production from waste cooking oil: Process design and technological assessment. *Bioresource Technology*, **89:** 1-16.

Pak. j. sci. ind. res. Ser. A: phys. sci. 2013 **56** (2) 93-99

Thermo-Kinetics Studies of Dye Removal with Kaolin from *Tectona grandis* and Indigo Dye Effluents

Abayomi Olagundoye Adetuyi*, Abdul-Akeem Alaba Mojibola and Jamiu Mosebolatan Jabar
Department of Industrial Chemistry, Federal University of Technology, P.M.B 704, Akure, Ondo State, Nigeria

(received May 15, 2012; revised August 28, 2012; accepted September 12, 2012))

Abstract. The kinetics and thermodynamic behaviour of dye molecules removed from *Tectona grandis* and indigo dye effluents using kaolin as the coagulant were studied and the results obtained were compared with the commercial alum (as standard). Comparison of data obtained from Langmuir and Freundlich isotherms indicated that the coagulation process was chemisorptions. The isotherm parameters of Langmuir isotherm such as coagulation capacity Q_o; coagulation energy intensity b; and correlation coefficient R^2, in this study were greater than that of Freundlich. The correlation coefficient of the pseudo-second-order kinetics was almost equal to unity and the values of $q_{e(Cal.)}$ were of insignificant difference from the corresponding $q_{e(exp.)}$ and these made the pseudo-second-order kinetics fitted well with the coagulation process. The thermodynamic parameters (ΔH and ΔS) obtained indicated that the coagulation process was endothermic and spontaneous, respectively. The negative values of ΔG shows the irreversible nature of the coagulation process and the correlation coefficients (R^2) closed to unity indicates the fitness of the coagulation thermodynamics with the experimental data.

Keywords. coagulant, effluents, kinetics, endothermic, thermodynamics

Introduction

Waste water generated at various stages in textile industry differ in composition, strength and volume. When not properly treated before discharged into rivers, it pollutes the receiving water body by causing injury to the aquatic plants, animals and making the water unfit for human consumption (Dae-Hee *et al.,* 1999).

According to Chakrabarti *et al.* (1988) most of the available dyes and pigments consisting of over 7,000 different chemical structures used in textile industry are completely resistant to biodegradation processes and for this reason, physical process for their removal from the effluent is recommended. Chemical process may increase the harmful effect of the effluent on the receiving water body (Pitter and Chudoba, 1990). The conventional physical methods of treating effluent are sorption with the aid of chitin called ozonization method (Safarik, 1995), organic carbon (Murphy *et al.,* 1992; Gupta *et al.,* 1990), and electrochemical oxidation (Lin and Peng, 1994). The high cost of the above mentioned methods led researchers to look for cost effective method (called coagulation) with equal or more removal efficiency than the conventional treatment methods. Coagulation method has been found easy to operate and energy saving treatment alternatives (Hassani *et al.,* 2008). It can be expressed as the conversion of colloidal and dispersal particles into small visible floc upon addition of a simple coagulant. It brings about compression of the electrical double layer surrounding each suspended particle, as a result of decrease in the magnitude of the repulsive interactions between particles and destabilization of the particles. The most common coagulants used in wastewater treatment are alum $Al_2(SO_4)_3.12H_2O$, poly aluminium chloride (PAC) and sometimes kaolin. Poly aluminium chloride is more effective than alum in wastewater treatment but highly expensive and more toxic than alum with demerit of skin infection (like eczema) on consumer of the treated wastewater. As a result of these, kaolin is mostly preferred due to its abundance, environmental friendly and availability at low cost (Ma and Wang, 2006; Exall and Vanloon, 2003).

Kaolin has been reported by Ma and Wang (2006) to be used in treatment of oil polluted water with about 99 % removal of chemical oxygen demand, biological oxygen demand, total dissolve solids and hardness. Other areas where it is utilized are pharmaceutical industry, for production of drug used in treatment of various gastrointestinal problems; cosmetics for

*Author for correspondence; E-mail: yomiadetuyi2002@yahoo.com

production of talc; production of glossy paper for magazine and newspaper; paints production for gloss level control, and insecticides to control arthropods (Barker *et al.,* 2007; Belloto *et al.,* 1995). The active chemical component responsible for wastewater treatment in kaolin is aluminium silicate hydroxide ($Al_2Si_2O_5(OH)_4$) popularly called kaolinite. It is a fine, white layered silicate mineral with one tetrahedral sheet linked through oxygen atom to one octahedral sheet of alumina octahedral (Deer *et al.,* 1992).

Thus, this research was primarily designed to focus on the kinetic and thermodynamic studies of the coagulation of *T. grandis* and indigo dyes' effluents using kaolin as coagulant.

Materials and Methods

The tender leaves of teak plant (*Tectona grandis)* and kaolin ($Al_2Si_2O_5(OH)_4$) were obtained from forestry plantation and Industrial Design Department of Federal University of Technology, Akure, Nigeria, respectively. Alum ($Al_2(SO_4)_3.12H_2O$) was purchased from Pasca Chemicals Store, Akure, Nigeria. Indigo dye and pre-bleached white cotton fabric were purchased from a dyestuff market in Akure, Nigeria. All the chemicals and equipment used were of analytical grade and obtained from Chemistry Department of Federal University of Technology, Akure, Nigeria.

Coagulation process. The effluents used in this study were procured from pilot dyeing of cellulosic fabric with indigo and the extracted *T. grandis* dye. These dye effluents then were subjected to coagulation/ flocculation process via jar experiment.

The effect of coagulant dosage, contact time and temperature on colour removal was studied by coagulation of *T. grandis* and indigo dye effluent with kaolin. The coagulant dosage was varied from 0.2 to 1.0 g with contact time 1.5 h, temperature of 303 K and agitation speed of 100 rpm using Gallenkamp orbital shaker. At the end of the contact time, the solutions were centrifuged at 500 rpm for 1.00 h using uniscope centrifuge machine and the absorbance of the supernatants read at 530 nm and 410 nm were used to extrapolate concentrations of the treated *T. grandis* and indigo dye effluent, respectively from prepared working curve using camspec spectrophotometer.

The effect of contact time on dye removal from the effluent was carried out by varying contact time from 0.5-3.5 h with coagulant dosages of 0.5 g, temperature of 303 K and agitation speed of 100 rpm. At the end of each pre-determined contact time, the solutions were treated as done in effect of coagulant dosage to obtain correspond concentration of dye removed from the effluent.

The effect of temperature on dye removal efficiency of the coagulant from generated dyeing effluents was studied by batch technique using Roaches dyeing machine. The coagulation temperature was varied from 303 K - 343 K with coagulant dosage of 0.5 g, contact time of 1.5 h and agitation speed of 100 rpm. The dyeing cups were removed from the dyeing machine at the end of 1.5 h contact time and the solutions therein were treated as done for previous removal technique to obtain percentage dye removal from the treated effluents (Rakhi and Vankar, 2007; Manaskorn *et al.,* 2004).

The data obtained from effect of coagulant dosage, contact time and temperature were used to obtain useful information for the isotherm, kinetics and thermo-dynamics studies.

Coagulation isotherm. Data obtained from effect of coagulant dosage were used for Langmuir and Freundlich isotherm studies using linearized equations $1/q_e = Q_o + 1/bQ_oC_e$ and $\log q_e = \log K_f + 1/n \log C_e$, respectively.

Where, q_e = amount of dye coagulated per unit weight of coagulant (mg/g), C_e = equilibrium concentration of the coagulant (mg/L), Q_o = Langmuir maximum monolayer coagulation capacity (or total number of binding sites) (mg/g), b = coagulation energy (L /mg), K_f and n are Freundlich constants, associated with coagulation capacity and intensity respectively (Himanshu and Vashi, 2010).

Coagulation kinetics. The data obtained from kinetic parameters for the coagulation process were analyzed with Lagergren pseudo-first-order and pseudo-second-order kinetic models expressed by the equations:

$$\text{Log}(q_e - q_t) = \log q_e - \frac{K_1 t}{2.303}$$ (Lagergren pseudo-first-order linearized equation)

$$t/q_t = 1/K_2 q^2_e + t/q_e$$ (Lagergren pseudo-second-order linearized equation)

Where, q_e and q_t refer to the quantity of dye coagulated (mg/g) at equilibrium and at any time, t (h), respectively, K_1 is the equilibrium rate constant of pseudo-first-order coagulation kinetic (h^{-1}) and K_2 is equilibrium rate constant of pseudo-second-order coagulation (g/mg h) (Adetuyi and Jabar, 2011).

Coagulation thermodynamics. Model of coagulation thermodynamic was investigated by using second law of thermodynamic equations expressed as:

$\Delta G = \Delta H - T\Delta S$
$\Delta G = - RT \ln K_\theta$

Equating the above equations, gave Van't Hoff equation below:

$$\text{Log } K_\theta = \frac{-\Delta H^\theta}{2.303\ RT} + \frac{\Delta S^\theta}{2.303\ R}$$

Where, K = thermodynamic equilibrium constant (C_{solid}/C_{liquid}), C_{solid} = solid phase dye concentration at equilibrium (mg/ L), C_{liquid} = liquid phase dye concentration at equilibrium (mg/ L), T = temperature in Kelvin, R = universal gas constant (8.314J/molK), ΔH^θ = standard enthalpy change (KJ/Mol), ΔS^θ = standard entropy change (KJ/Molk) and ΔG = free energy change (KJ/Mol) (Chan-Li *et al.,* 2007; Atkins and de Paula, 2006).

Results and Discussion

The calibration curves of *T. grandis* and indigo dye were prepared at wavelength of maximum absorption (λ_{max}) 530 nm and 410 nm, corresponding to the absorption of reddish-brown and greenish-yellow (leuco-dye), respectively (Adetuyi and Jabar, 2011; Adetuyi *et al.,* 2002). They were reproducible and linear over the calibration range used in this study.

Dye removal efficiency. The quantity of dye removed increased from 90.47 to 99.36 % as coagulant dosage increased from 0.2 g to 1 g in *T. grandis* while that of effluent from indigo dye was increased from 89.97 to 99.23 % using kaolin as coagulant, as against treatment using alum as standard coagulant with percentage removal of 88.98 to 98.73 % of *T. grandis* dye from the effluent and 88.43 % to 98.72 % indigo dye was removed from the effluent as coagulant dosage increased from 0.2 g to 1 g (Table 1). The data in this Table shows that kaolin has higher dye/ colour removal efficiency than the standard (alum). Hence, kaolin could be a good substitute of alum in industrial effluent treatment because it is cheaper and abundant.

Increase in contact time and temperature of coagulation process increased the percentage of colour removal in the effluents (Table 1-2). It was equally noticed that kaolin performed better than the chosen standard and it was more effective in treatment of *T. grandis* effluent than that of indigo.

Coagulation isotherm. ***Langmuir isotherm.*** Linearized Langmuir equation $1/q_e = Q_o + 1/bQ_oC_e$ was used to obtain isotherm data by plotting a graph of $1/q_e$ against $1/C_e$ as shown in Fig. 1, where intercept of the graph equal to Langmuir maximum monolayer coagulation capacity, Q_o and Langmuir constant b, called energy of coagulation process was gotten from the slope of the

Table 1. Effect of coagulant dosage and temperature on *Tectona grandis* and indigo dye effluents

Coagulant	Coagulant dosage (g)					Temperature (K)				
	0.2	0.4	0.6	0.8	1.0	303	313	323	333	343
	(colour removed %)					(colour removed %)				
KT	90.47	92.16	95.98	98.73	99.36	93.43	95.13	97.25	98.73	99.15
AT	88.98	91.10	95.76	98.09	98.73	92.37	93.43	95.76	98.09	98.52
KI	89.97	92.03	96.40	98.72	99.23	92.55	93.83	97.17	98.72	98.97
AI	88.43	91.52	95.89	98.20	98.72	92.03	93.57	96.14	98.20	98.46

Table 2. Effect of contact time on *Tectona grandis* and indigo dye effluents

Coagulant	Time (h)						
	0.50	1.00	1.50	2.00	2.50	3.00	3.50
	Colour removed (%)						
KT	91.53	94.28	96.40	97.67	98.73	98.94	98.94
AT	90.25	93.01	95.55	97.55	97.88	98.31	98.52
KI	90.23	91.77	95.37	96.92	98.20	98.46	98.46
AI	89.20	90.23	95.37	96.92	98.20	98.46	98.46

KT = Kaolin treated *T. grandis* dye effluent; AT = Alum treated *T. grandis* dye effluent; KI = Kaolin treated indigo dye effluent; AI = Alum treated indigo dye effluent.

graph and it was used to calculate Langmuir dimensionless separation factor, r. Table 3 shows intercept, slope and Langmuir constants for coagulation of *T. grandis* and indigo dyes, the maximum monolayer coagulation capacity Q_o of the coagulation for dye from the effluents, dimensionless factor r and correlation coefficient R^2 were found to be in order AT > KT and AI > KI. In contrary, the values of Langmuir constant b were found to be in order KT > AT and KI > AI, while the values of r < 1 show that the coagulation process is favourable.

Freundlich isotherm. Figure 2 shows graph of log q_e against log C_e from which, the slope and intercept are obtained (Table 3) and used to determine the adsorption capacity and intensity of coagulation process, respectively. Adsorption capacity K_f was in order KT > KI and AT > AI and adsorption intensity was in order KT > KI and AT = AI. Table 3 equally shows that kaolin has greater coagulation capacity and intensity than alum (standard), this observation further support the possibility of kaolin replacing alum for coagulation/ treatment of waste water. The values of coagulation intensity n > 1 in all treated effluent, is an indication of good coagulation process.

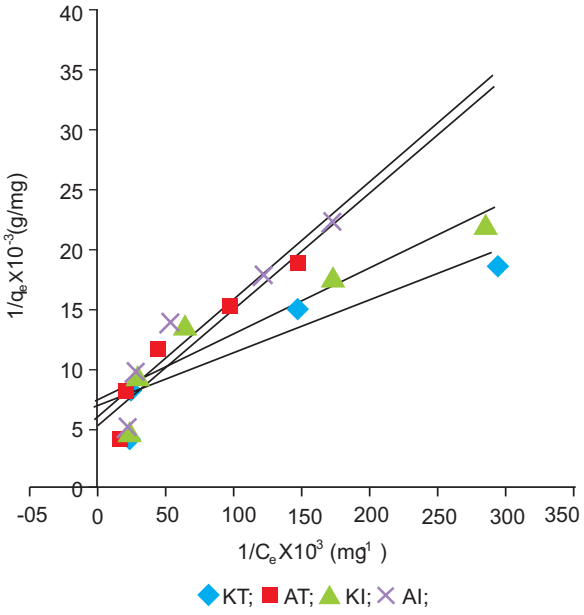

Fig. 1. Linearized Langmuir isotherm of *T.grandis* and indigo dye.

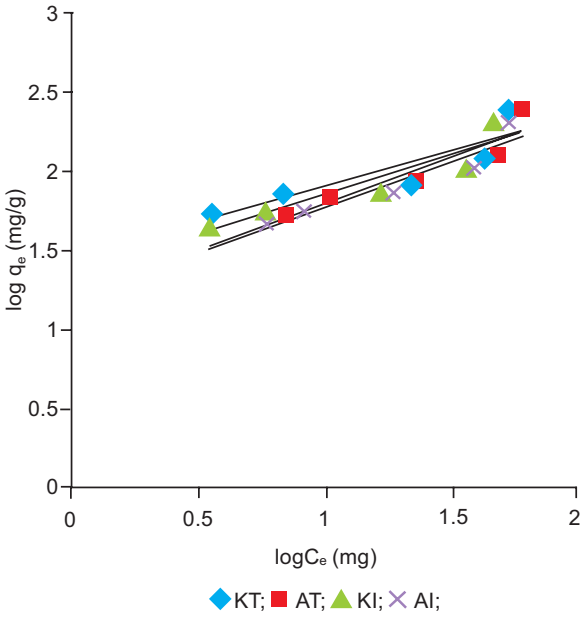

Fig. 2. Linearized Freundlich isotherm for *T. grandis* and indigo dye.

Comparison of data obtained from Langmuir and Freundlich isotherm indicated that the coagulation process was chemisorption since Langmuir coagulation capacities Q_o was greater than that of Freundlich K_f, Langmuir coagulation energy/ intensity b and correlation coefficient R^2 were also greater than that of Freundlich.

Coagulation kinetics. The data obtained from the plot in Fig. 3 (Lagergren first-order-kinetic) did not fit well

Table 3. Coagulation isotherm and thermodynamics parameters for *Tectona grandis* and indigo dye effluents

	Langmuir						Freundlich					Thermodynamics (Van't Hoff)					
Coag.	C × 10^{-3} (mg/g)	Slope (g)	Q_o (mg/g)	b (L/mg)	r	R^2	C (mg/g)	Slope (g^{-1})	k_f (mg/g)	n (g^{-1})	R^2	C	Slope (K)	ΔH(KJ/ Mol)	ΔS(KJ/ MolK)	ΔG(KJ/ Mol)	R^2
KT	6.78	0.04	147.56	0.15	0.01	0.81	1.44	0.46	27.67	2.19	0.81	9.41	- 2.52	48.27	0.18	- 6.33	0.98
AT	5.18	0.10	193.13	0.05	0.03	0.90	1.21	0.59	16.18	1.71	0.87	7.97	- 2.11	40.40	0.15	- 5.8	0.94
KI	7.28	0.06	137.40	0.13	0.02	0.87	1.36	0.49	22.75	2.04	0.85	9.54	- 2.58	49.30	0.18	- 5.95	0.96
AI	6.00	0.10	167.25	0.06	0.04	0.91	1.18	0.59	15.24	1.71	0.90	8.07	- 2.14	40.96	0.15	- 5.86	0.96

Key: Coag. = Coagulation; C = Intercept.

Table 4. Coagulation kinetics parameters for *Tectona grandis* and indigo dye effluents

Coagulants	Linearized Lagergren pseudo-first-order						Linearized Lagergren pseudo-second-order				
	$C \times 10^{-3}$ (mg/g)	Slope (mg/gh)	K_1 (h^{-1})	$q_{e\ Cal}$ (mg/g)	R^2	$q_{e\ Exp}$ (mg/g)	$C \times 10^{-3}$ (hg/mg)	Slope $\times 10^{-3}$ (g/mg)	K_2 (g/mgh)	$q_{e\ Cal}$ (mg/g)	R^2
KT	1.73	- 0.91	2.09	54.08	0.92	107.36	0.32	9.24	0.265	108.26	1.00
AT	1.68	- 0.78	1.79	47.75	0.94	106.90	0.37	9.28	0.233	107.79	1.00
KI	1.71	- 0.90	2.07	51.64	0.94	90.25	0.50	10.95	0.242	91.32	1.00
AI	1.74	- 0.90	2.06	54.95	0.94	90.01	0.56	10.96	0.213	91.24	1.00

with the experimental data since the quantity of dye calculated was by far lesser than the quantity of dye coagulated per unit weight of the coagulant obtained in the experiment ($q_{e(cal)} << q_{e(exp)}$) but Largergren pseudo-second-order coagulation kinetic (Fig. 4) did. Equally, pseudo-second-order kinetic fitted well in all the coagulation process since the correlation coefficient $R^2 \sim 1$ (Table 4), while $R^2 << 1$ in pseudo-first-order kinetic (Table 4). The rate constant K_2 was highest in KT (0.265 g/ mgh), while that of the AI (0.213 g/ mgh) was the lowest, this showed that the coagulation process was fastest in KT and slowest in AI (Minguan, 2009; Hameed *et al.,* 2007; Rakhi and Vankar, 2007).

Coagulation thermodynamics. The plot of log K_o against 1/T gave a straight line graph (Fig. 5) with the intercept and slope used to calculate entropy ΔS and enthalpy ΔH and subsequently the free energy ΔG of the coagulation thermodynamic (Table 3). The value

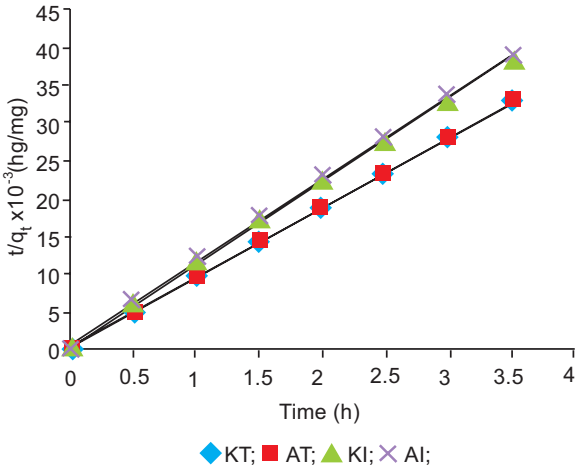

Fig. 4. Linearized Lagergren pseudo-second-order kinetics for the coagulation of *T. grandis* and indigo dye effluents by kaolin and alum.

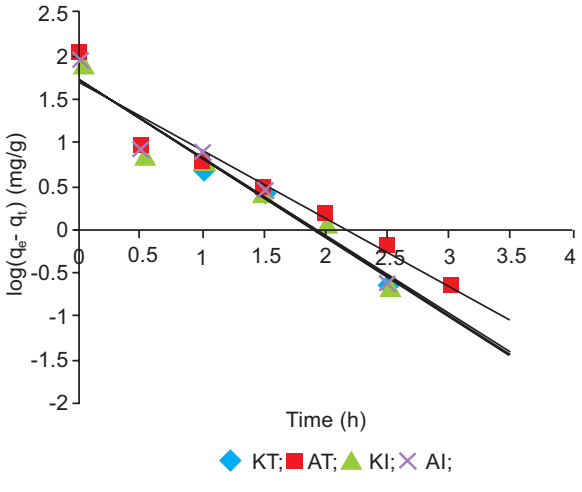

Fig. 3. Linearized Lagergren pseudo-first-order kinetics for the coagulation of *T. grandis* and indigo dye by kaolin and alum.

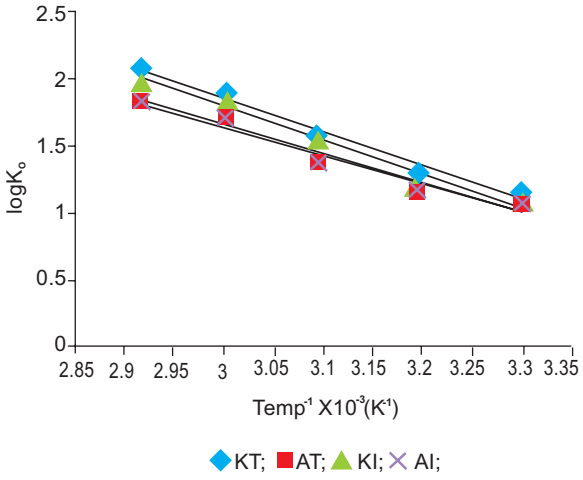

Fig. 5. Van't Hoff plot for the coagulation of *T. grandis* and indigo dye by kaolin and alum.

of ΔH greater than 40 KJ/mol in all the coagulation process indicated that the process is endothermic and chemisorption, while the positive and negative values of ΔS and ΔG are the indication of spontaneity and irreversibility of the process. The correlation coefficients (R^2) were almost equal to unity in all the coagulation processes, evidence that the thermodynamic process fitted quite well with the experimental data.

Conclusion

The study showed that kaolin in place of alum can be used effectively in the removal of both *T. grandis* and indigo dyes from their respective dyeing effluents. The thermo - kinetics parameters for the coagulation process favoured chemisorption and obeyed the Lagergren pseudo-second-order model. Also, the positive values of ΔH and ΔS as well as the negative values of ΔG obtained showed that the interactions of the coagulants with the dye effluents were endothermic, spontaneous and favourable.

References

Adetuyi, A.O., Jabar, J.M. 2011. Kinetic and thermodynamic studies of indigo adsorption of some activated bio-solids. *Journal of Chemical Society of Pakistan,* **33:** 158 - 165.

Adetuyi, A.O., Popoola A.V., Lajide, L. 2002. Isolation and colouring potentials of leave extract of teak plant (*Tectona grandis*). *Journal of Chemical Society of Nigeria,* **28:** 34-39.

Atkins, P.W., de Paula, J. 2006. Thermodynamics and kinetics. In: *Physical Chemistry,* vol. **1**, 212 pp., 8th edition, W.H., Freeman and Company, USA.

Barker, J.E., Holaschke, M., Fulton, A., Evans, K.A., Powell, G. 2007. Effects of kaolin particle film on *Myzus persicae* (Hemiptera: Aphididae) behaviour and performance. *Bulletin of Entomological Research,* **97:** 455-460.

Bellotto, M., Gualtieri, A., Artioli, G., Clark, S.M. 1995. Kinetic study of the Kaolinite-Mullite reaction sequence. Part I: Kaolinite dehydroxylation. *Physics and Chemistry of Minerals,* **22:** 207-217.

Chakrabarti, T., Subrahmanyan, P.V.R., Sundaresan, B.B. 1988. Biodegradation of recalcitrant industrial wastes. In: *Biotreatment Systems,* vol. **2**, pp. 171-234. CRC Press, Inc., Boca Raton, Florida, USA.

Chan-Li, H., Yuwen, L.Y., Chil-Chang, H., Yao-Hui, H., Chuch-Yung, C. 2007. Adsorption kinetics, thermodynamics and desorption studies of C.I. reactive black 5 on a novel photo assisted Fento catalyst. *Dyes and Pigments,* **75:** 130-135.

Dae-Hee, A., Won-Seok, C., Tai-Il, Y. 1999. Dyestuff wastewater treatment using chemical oxidation, physical adsorption and fixed bed biofilm process. *Process Biochemistry,* **34:** 429-439.

Deer, W.A., Howie, R.A., Zussman, J. 1992. An Introduction to the Rock-Forming Minerals, 2nd edition, 696 pp., Harlow, Longman Scientific and Technical, London, UK and New York, USA.

Exall, N.K., Vanloon, W.G. 2003. Effects of raw water conditions on solution-state aluminum speciation during coagulant dilution. *Water Research,* **37:** 3341-3380.

Gupta, G.S., Prasad, G., Singh, V.N. 1990. Removal of chrome dye from aqueous solutions by mixed adsorbents: fly ash and coal. *Water Research,* **24:** 45-50.

Hameed, B.H., Almad, A.L., Latiff, K.N.A. 2007. Adsorption of basic dye (methylene blue) onto activated carbon prepared from rattan sawdust. *Dyes and Pigments,* **75:** 143- 149.

Hassani, A.H., Seif, S., Javid, A.H., Borghei, M. 2008. Comparison of adsorption process by GAC with novel formulation of coagulation-flocculation for colour removal of textile wastewater. *International Journal of Environmental Research,* **2:** 239-248.

Himanshu, P., Vashi, R.T. 2010. Treatment of textile wastewater by adsorption and coagulation. *E-Journal of Chemistry,* **7:** 1468-1476.

Lin, S. H., Peng, C.F. 1994. Treatment of textile wastewater by electrochemical method. *Water Research,* **28:** 277 - 282.

Manaskorn, R., Sirawan, R., Summate, T. 2004. Removal of reactive dyes from aqueous solution using bagasse fly ash. *Songklanakarin Journal of Science Technology,* **26:** 13-24.

Ma, H.Z., Wang, B. 2006. Multifunctional microsized modified kaolin and its application in wastewater treatment. *Journal of Hazardous Materials,* **136:** 365-370.

Minguan, R. 2009. Natural organic matter removal by coagulation: Effect of kinetics and hydraulic power, pp. 135-136, I WA Publishing, Beijin China

Murphy, O.J., Hitchens, G.D., Kaba, L., Verostko, C. 1992. Direct electrochemical oxidation of organic for wastewater treatment. *Water Research,* **26:** 443-445.

Pitter, P., Chudoba, J. 1990. *Biodegrability of Organic Substances in the Aquatic Environment,* pp. 7-83, CRS-Press, Boca Raton, Florida, USA.

Rakhi, S., Vankar, P.S. 2007. Dyeing cotton, wool and silk with *Hibiscus mutabilis* (Gulzuba). *Dyes and Pigments,* **74:** 464-469.

Safarik, I. 1995. Removal of organic polycyclic compounds from water solutions with a magnetic chitosan based sorbent bearing copper phthalocyanine dye. *Water Research,* **29:** 101-105.

Pak. j. sci. ind. res. Ser. A: phys. sci. 2013 **56** (2) 100-106

Effect of Mining on Heavy Metal Concentration in Soils from the Vicinity of Itakpe Iron Ore Mine in Kogi State, Nigeria

Christiana Omono Matthews-Amune* and Samuel Kakulu

Department of Chemistry, University of Abuja, Abuja, Nigeria

(received June 6, 2012; revised August 31, 2012; accepted September 12, 2012)

Abstract. The effects of mining on soils from Itakpe iron ore mining area in Kogi State, Nigeria were studied through the determination of the heavy metals (Cd, Cu, Mg, Ni, Pb and Zn) using flame atomic absorption spectroscopy. Soil samples were collected during the dry and rainy seasons. Significant levels of heavy metals were found. Median topsoil concentrations (0-15 cm) for Cd, Cu, Mg, Ni, Pb and Zn were 0.16±0.02, 0.15±0.03, 0.04±0.03, 0.1±0.02, 0.07±0.01, 0.04±0.04 μg/g, respectively. The heavy metal concentrations of control soil were relatively lower than those in the Itakpe mining environment soil and within levels of total metal contamination in the normal soil content intervals and maximum allowable limits of heavy metals in soils. Correlations analysis shows that heavy metals were closely correlated with each other except for Pb, indicating the studied metals are from the same pollutant resource. This shows, mining as contributing to the metallic levels in the Itakpe mining site.

Keywords: mining, heavy metals, soil, pollution

Introduction

The need for a country's economic, agricultural and industrial development acts as a challenge to safe and pure environment. These activities affect the natural and biological redistribution of metals through altering their chemical forms and introducing contaminants into the environment. (Ezeh and Chukwu, 2011; Aremua *et al.,* 2010; Wu *et al.,* 2010, Prathumratana *et al.,* 2008). The result is that metal pollutants are distributed in the atmosphere, water, soil and vegetation and could have long term hazardous impact on ecosystems. (Aremua *et al.,* 2010; Jung, 2008; Arogunjo, 2007). The greatest concerns are the heavy metals which are those with potential human and environmental toxicity accumulate in soils and induce pollution of food chain endangering the ecosystems safety and human health (Arogunjo, 2007; Ullrich *et al.,* 1999).

Heavy metals are persistent and have ability to bio-accumulate, transform to more toxic form, can neither be degraded nor destroyed and have average long-life (Arogunjo, 2007; Ukpebor and Unuigbe, 2003; Wong *et al.,* 2002). Some metals are essential trace element needed by organisms but the main threats to human health are associated with exposure to Pb, Hg, Cd and As; whose biotoxicity and occurrences require the knowledge of their sources, leaching processes, chemical conversions and modes of deposition to pollute the environment. (Ezeh and Chukwu, 2011; Yahaya *et al.,* 2009).

Chronic concentration or deficiency of these metals can have serious health effects varying from irritant to acute or chronic diseases, such as cancer, reproductive and nervous diseases, and so on. (Gutiérrez-Ginés, 2010; Arogunjo, 2007; Lin *et al.,* 2005).

Mining is needed to develop economic growth for many countries and it caused pollutant questions. Mining and metal processes activities which are major sources of anthropogenic pollution result in metals being released from their stable form into the environment. (Jung, 2008; Arogunjo, 2007). The Itakpe iron ore deposit in Nigeria is reported to release Ti, Cr, Mn, Cd, Ta, Ca, Zn, Cu into the environment while ore from Ipoti, Nigeria is reported to release Cd, (Arogunjo, 2007). Pollutants present in tailings and mine waste leads to metals scattering in the mine surroundings with their continuous disperse by soil erosion, wind action and effluent draining the waste into arable land, rivers and ground waters with change in climate leading to seasonal variations in their metallic levels. (Ameh and Akpah, 2011; Jung, 2008; Jian-Min *et al.,* 2007; Lin *et al.,* 2005).

With increase of industrialization and agricultural activities heavy metals are increasing in environment. Monitoring of bio available metals in polluted soils is

*Author for correspondence; E-mail: omonomathews@yahoo.com

threatening due to the presence of heavy metals in our environment, food crops and most edibles. Hence, there is an increasing need to study heavy metal distribution and accumulation in soils. The aim of this study was to determine the effect of iron mining on Itakpe mining soil, Nigeria by exploring the difference in the concentration of heavy metals from farm land, located in mining area and control sites. This study will help to target strategies for quality soil management.

Materials and Methods

The study area was Nigeria Iron Ore Mining Company, Itakpe in Okehi LGA of Kogi State in the North Central part of Nigeria. It lies within longitude 6° 16'E and latitude 7° 36'N. The residents are peasant farmers.

Figure 1 shows map of Itakpe with sampling points. A total of 75 soil samples were collected using a stainless steel knife from the upper 15cm layer during the dry season (DS) in January and rainy season (RS) in July 2010 in the Itakpe mining environment farms. Control soil samples were collected from Osara Dam Area 12 km away from Itakpe. Soil samples were collected in nylon bags previously soaked in 10% HNO_3 solution for 24 h, rinsed with deionized water and air dried. The collected soil samples were air-dried for 72 h, ground in a mortar and passed through 0.005 mm sieve and stored in clean polythene bags. All reagents used were of analytical grade (BDH, Poole, England). All glassware were washed with detergent, rinsed with distilled water, soaked in 10% HNO_3 for 24 h and rinsed.

Fig. 1a. Map of Nigeria showing Kogi State b, Map of Itakpe mining environment showing sampling areas.

Soil pH was determined using a soil-water ratio 1: 2.5 (w/v). Soil organic matter was determined using the Walkey-Black wet oxidation method. (Udovic *et al.,* 2009). Soil particle size distribution was done using Hydrometer method and soil carbonate was determined by the concentrated HCl acid method (Udovic *et al.,* 2009).

Tessier *et al.* (1979) total metal analysis method was used in the extraction of heavy metals from soil. Extraction was done by digesting 1 g (<0.005 mm) of soil sample with a mixture of 10 mL HF and 2 mL $HClO_4$ to near dryness; a second addition of 10 mL HF and 1 mL $HClO_4$ was made and again the mixture was evaporated to near dryness. Finally 1 mL $HClO_4$ alone was added and the soil sample evaporated until the appearance of white fumes. The residue was dissolved in concentrated HCl and diluted to 25 mL. The resulting solution was filtered into a plastic bottle ready for AAS. Atomic Absorption Spectrophotometer (AAS) model 210VGP, Buck Scientific Incorporated USA with air-acetylene flame was used for the determination of heavy metals in this work. Assessment of accuracy and precision was done through using three replicate samples, precision, spiking and quality control system (International standard reference material-Soil Reference Material 989, Wageningen Evaluating Programs for Analytical Laboratories (WEPAL), Netherland), spiking of plant samples and reagent blanks.

Results and Discussion

The physico-chemical properties of the studied soil are shown in Table 1 while Table 2 shows the concentration of heavy metals in dry and rainy season soil. Table 3 indicates Pearson correlations analysis for the studied metals. Analysis of soil Reference Material 989 from Netherland gave Cu 144.5±11.6 and Pb 253.8±13.8 µg/g against the standard values of 153±3.9 and 282±3.6 µg/g for Cu and Pb, respectively. Total soil concentration of Cd ranged from 0.12-0.18, Cu 0.08-0.18, Mg 0.04-0.04, Ni 0.05-0.17, Pb, 0.05-0.07 and Zn 0.03-0.04 µg/g. The metallic levels in the mining site and control sites were generally low. The mining site soil is mainly sandy, neutral, moderately high in carbonate and low in organic matter. Cd level during the RS was observed to be highest metallic level in all the studied metals followed by Cu during the DS. Zn and Pb levels were relatively low (Zn 0.03-0.04 and Pb 0.05-0.07 µg/g). Total soil metal level for Mg was same for both seasons. Total metal levels in the control farm were relatively lower than mining environment soil. The metallic levels observed were lower than the normal soil content intervals and maximum allowable limits of heavy metals in soils (Pendias and Dubka, 1992; Bero and Reaves, 1984).

Soil contains various functional groups which are effective agents for heavy metal sorption with soil properties such as the level of Fe, Al, and Mn oxides, hydroxides, clay content, texture and organic matter acting as controlling factors (Amen and Akpan, 2011; Hesterberg, 1998). Soil matrix constituting elements required for plant growth and those potentially toxic are important (Hesterberg, 1998). Their interaction affects the properties and processes in the soil which are determined by rainfall distribution, erosion and soil properties (pH, soil drainage, redox potential, organic matter and clay content) with the dominant process at any specific time determining the retention capacity of heavy metals. (Lee *et al.,* 2001; Hesterberg, 1998).

All the studied metals were present in the mining site soil which indicates that there are variations of metals in the topsoil of the mining site. Such variations could be due to aerial deposition from mining. According to Ullrich *et al.* (1999) such variation of metals in the topsoil could be attributed to historical mining and smelting. Generally the metal levels were low in both sites with metallic levels of mining site soil slightly higher than that of the control soil in both seasons. The lower concentration levels recorded on the control soil could be due to lower intensive activities, which induce the pollution of heavy metals.

The heavy metals present in the tailings, parent materials and agrochemicals provide the source for the degree of contamination observed in the mining site soil. There are reports that, in mining environments dust laden metals spread as a layer of dust on every surface in the area due to blasting of the rocks during mining (Jung, 2008; Jian-Min *et al.,* 2007; Zhou *et al.,* 2007).

Table 1. Physico-chemical properties of the studied soils

Parameter (%)	Mining site	Control
Sand	72.24	78.24
Silt	7.28	7.28
CO_3^{2-}	4.61	4.72
Clay	20.48	14.48
Tom	2.17	3.17
pH	7.3	8.3

Table 2. Concentration of heavy metals in dry and rainy season soils ± SD (μg/g)

Metal	Dry season	Rainy season	Mean conc.	Control
Cd	0.14 ± 0.01	0.18±0.02	0.16±0.02	0.10±0.01
	(0.17-0.18)[a]	(0.12-0.15)[a]	(0.14-0.18)[a]	(0.09-0.11)[a]
Cu	0.16±0.03	0.13±0.03	0.15±0.03	0.07±0.01
	(0.08-0.18)[a]	(0.14-0.17)[a]	(0.12-0.18)[a]	(0.06-0.08)[a]
Mg	0.04±0.002	0.04±0.002	0.04±0.02	0.03±0.003
	(0.04-0.04)[a]	(0.04-0.04)[a]	(0.01-0.05)[a]	(0.027-0.033)[a]
Ni	0.07±0.01	0.15±0.03	0.11±0.02	0.01±0.01
	(0.05-0.09)[a]	(0.13-0.17)[a]	(0.08-0.12)[a]	(0.00-0.02)[a]
Pb	0.06±0.02	0.07±0.004	0.07±0.01	0.02±0.001
	(0.05-0.07)[a]	(0.06-0.07)[a]	(0.06-0.08)[a]	(0.017-0.021)[a]
Zn	0.04±0.05	0.04±0.03	0.04±0.03	0.03±0.01
	(0.03-0.04)[a]	(0.03-0.04)[a]	(0.00-0.08)[a]	(0.02-04)[a]

a = range.

Table 3. Pearson correlations for the studied metals

Metals	Cd	Cu	Mg	Ni	Pb	Zn
Cd	1	-	-	-	-	-
Cu	1.000	1	-	-	-	-
Mg	-1.000	-1.000	1	-	-	-
Ni	0.916	0.920	-0.914	1	-	-
Pb	-0.309	-0.319	0.303	-0.664	1	-
Zn	0.838	0.844	-0.834	0.986	-0.778	1

Zhou *et al.* (2007) reported, that tailings as contributing 567, 1140, 2.48 and 191 μg/g of Cu, Zn, Cd and Pb, respectively to the soil around the Dabaoshan Mine in China. Weathering also leads to oxidation of sulphide bearing minerals which causes acid mine drainage (AMD) characterized by release of metals leading to high concentration of heavy metals, acidity and salinity of soil in agricultural lands in mining sites (Jian-Min *et al.,* 2007; Lin *et al.,* 2005).

Mining activities have various impacts such as oxidation of metal sulphides induces soil acidification and imped natural colonization of vegetation causing soil erosion (Jian-Min *et al.,* 2007; Lin *et al.,* 2005) and heavy metals, derived from mining activities, may be carried on to agricultural land by erosion. Thus the variations in metallic level observed during the RS could be due to erosion which results in uneven distribution of metals in certain part of the soil due to the topography of the land. Such reports have been given by earlier authors (Cebula and Ciba, 2005; Lin *et al.*, 2005; Lee *et al,.* 2001, Hesterberg, 1998), Cebula and Ciba (2005) reported very high levels of Pb (10 915 mg/kg), Cd (6.2 mg/kg) and Zn (1650 mg/kg) after erosion. This results in uneven distribution of heavy metals on the same plot i.e. above permissible levels and within permissible levels which made the area to be excluded from farmland.

The percentage of organic matter in the mining soil was relatively lower than the control site. The low metallic levels in the mining site topsoil could be due to low percentage of organic matter which indicates lower retention of metals than in the control soil. This explains the nearness observed in metallic level of the mining site soil to the control soil. Such effects have been reported previously by Jung (2008). Organic matter plays an important role in soil structure, water retention, cation exchange and in the formation of complexes (Yahaya *et al.,* 2009; Okoronkwo *et al.,* 2006). The organic matter content in soil for example makes metal such as Cu to be bound and made unavailable through formation of complexes. (Li *et al.,* 2005). The Cu is an essential micronutrient for physiological processes in plants such as photosynthesis and respiration, carbohydrate distribution, nitrogen and cell wall metabolism, seed production and disease resistance (Lin *et al.,* 2005). According to Clemente *et al.* (2008), organic matter level influences migration of metals to deeper soil fractions and causes difficulty in the dissolution of metals during extraction. Such soils have been reported to have low sorption capacity for metal ions (Jung, 2008). The percentage clay fraction in the mining site soil is observed to be low. Soils with high percentage sand and low percentage clay content have high pollutant leaching potentials which makes such

soil risky to underground water (Okoronkwo *et al.,* 2006).

The mining site soil pH was observed to be neutral while the control site was alkaline. Cd adsorption to soil particles is reported to be greater in alkaline or neutral soils than acidic soil (Jung, 2008; Lisbeth *et al.,* 2008; Ullrich *et al.,* 1999). Soil pH is especially important in soil processes, such as determining the availability and solubility of heavy metals in soil and their transportation (Lisbeth *et al.,* 2008; Ullrich *et al.,* 1999; Hesterberg, 1998). At low pH, metals are more soluble in the soil solution thus increasing soil metal toxicity and uptake by plants (Yahaya *et al.,* 2009). Other soil properties could influence such effects. Lisbeth *et al.* (2008) reported that 10% Pb desorption was observed at pH 2.5 in a particular soil, whereas in another soil 60 % Pb was desorbed at the same pH. The mining site soil was observed to be moderately high in carbonate. According to Michaud *et al.* (2007), metals antagonize themselves in calcareous soils and plant Cu phytotoxicity in is reported to be greater in calcareous soils than non-calcareous soils. Calcareous and non-calcareous soils have been reported to occur within fields and this result in possible occurrence of toxicity in some parts of the soil and non toxic situation in another part within the same vicinity (Michanud *et al.,* 2007). When such situation exists in agricultural soils it is important to identify them and target strategies of managing such soils. The presence of sulphur in the mining site soil could cause the introduction of acid mine drainage most often associated with mines and waste left untreated (Zhou *et al.,* 2007). Acid mine drainage could cause removal of vegetation in the mine site resulting in soil erosion and pollution of the soil with heavy metals (Lin *et al.,* 2005). Elevated levels of Cd, Cu, Pb and Zn were found in plants grown on tailings of a Korean mine (Lee *et al.,* 2001).

There was no specific variation pattern between the rainy and dry season metal levels. This is in agreement with Jung and Thornton (1997) findings but disagrees with Yahaya *et al.,* (2009) and Lee *et al.* (2001), who reported higher levels during the DS. However, there were variations which could be due to changes in physico-chemical properties of soils during both seasons. Possible reason in the mining site could be related to distance from the mine, topographic features and wind dispersal patterns of metals. Such finding has been reported by previous authors. (Jung, 2008; Lin *et al.,* 2005; Lee *et al.,* 2001; Ullrich, 1999) According to Jung (2008) variations in metallic levels could be due to differences in soil mineralogy and origin. Lee *et al.* (2001) reported variation in metallic levels to be due to the precipitation of hydride, carbonate, sulfide and iron compounds. Other possible causes, such as non-equilibrium distribution of water, microbial mediated processes and variation in soil properties within a short distance due to changes in metal solubility have been reported (Hesterberg, 1998). However, anomalies in metallic levels could occur as a result of heavy metal deposition on soil surface from various sources such as emissions of metal-carrying dusts, gases and smoke from industrial undertakings or land filled industrial waste through atmospheric transportation (Galiulin *et al.,* 2002; Wong *et al.,* 2002).

Other researchers have reported variations during the RS to be due to the differences in the individual metal solubilities and dissolution of carbonates and oxides by acidic rain (Jung, 2008; Cebula and Ciba, 2005; Ukpebor and Unuigbe, 2003; Wong *et al.,* 2002).

The ANOVA analysis showed that the concentrations of individual heavy metals in the mining site soil were significantly higher ($p<0.05$) than the control soils, indicating that the mining site soil increased the heavymetal concentrations in soils.

These metallic levels are lower than that reported by Ezeh and Chukwu (2011) and Iorfa *et al.,* (2011) and within the range reported by Aremua *et al.* (2010) in mining environments in Nigeria. In furtherance the observed metallic levels were lower than the range reported in mining environment by Wu *et al.* (2010) in China, Ullrich *et al.* (1999) in Poland, Gutiérrez-Ginés *et al.* (2010) in Spain and Prathumratana *et al.* (2008) in Europe.

Pearson correlations for the studied metals (Table 3) show that the metals were closely correlated Cd/Cd, Cu/Cd, Mg/Cd, Ni/Cd, Zn/Cd, Cu/Cu, Cu/Mg, Cu/Ni, Cu/Zn, Mg/Mg, Mg/Ni, Mg/Zn, Ni/Zn, Zn/Zn except for Pb which correlated with only Ni. This shows that the studied metals except Pb are from the same origin. The presence of Pb in the soil can be attributed to the fuel used in the various machinery for the mining process. Such has been reported by previous authors (Stephanic, 1998). There was no significance at the 0.05 level and at the 0.01 level.

Conclusion

The exploitation of an iron ore mine in Itakpe, Nigeria, has made the soil metal polluted. Correlations studies

show the studied metals except Pb to be closely correlated indicating that they are from the same origin. The results show that the soil is slightly polluted and with gradual buildup could become highly polluted. There is need for regular monitoring to target strategies for quality soil management.

References

Ameh, E.G., Akpah, F.A. 2011. Heavy metal pollution indexing and multivariate statistical evaluation of hydrogeochemistry of River PovPov in Itakpe Iron-Ore mining area, Kogi Sate, Nigeria. *Advances in Applied Science Research,* **2:** 33-46.

Aremua, M.O., Sangarib, D.U., Adeyeyec, E.I., Ishalekua, Y.Y. 2010. Metal concentration in soils, ponds and associated food crops in Azara derelict barytes mining area in Nigeria. *Electronic Journal of Environmental Agricultural and Food Chemistry,* **9:** 10-18.

Arogunjo, A.M. 2007. Heavy metal composition of some solid minerals in Nigeria: Any health implication to inhabitants around the mining sites. *International Journal of Applied Environmental Science,* **2:** 143-153.

Bero, M.I, Reaves, G.A. 1984. Background levels of trace elements in soils. In: *Proceeding of 1st International Conference on Environmental Contamination.* pp. 333-340, CEP Consultants, Edinburgh, Scotland, UK.

Cebula, E., Ciba, J. 2005. Effects of flooding in southern Poland on heavy metal concentrations in soils. *Soil Use and Management,* **21:** 348-351.

Clemente, R., Dickinson, N.M., Lepp, N.W. 2008. Mobility of metals and metalloids in a multi-element contaminated soil 20 years after cessation of the pollution source activity. *Environmental Pollution,* **155:** 254-261.

Ezeh, H.N., Chukwu, E. 2011. Small scale mining and heavy metals pollution of agricultural soils: The case of Ishiagu Mining District, South Eastern Nigeria. *Journal of Geology and Mining Research,* **3:** 87-104.

Galiulin, R.V., Bashkin, V.N., Galiulina, R.A., Kucharski, R. 2002. Airborne soil contamination by heavy metals in Russia and Poland, and its remediation. *Land Contamination & Reclamation,* **10:** 179-187.

Gutiérrez-Ginés, M.J., Pastor, J., Hernández, A.J. 2010. Effect of heavy metals from mine soils on *Avena sativa* L. and education strategies. *Fresenius Environmental Bulletin,* **19:** 2083-2086.

Hesterberg, D.1998. Biogeochemical cycles and processes leading to changes in mobility of chemicals in soil. *Journal of Agriculture Ecosystems and Environment,* **67:** 121-133.

Iorfa, A.C, Ntonzi, N.T, Ukwang, E.E., Abara, I.B.E.K., Neji, P. 2011. A study of the distribution pattern of heavy metals in surface soils around Arufu Pb-Zn mine, Northeastern Nigeria, using factor analysis. *Research Journal of Chemical Sciences,* **1:** 70-80.

Jian-Min, Z., Zhi, D., Mei-Fang, C.A.I., Cong-Qiang, L.I.U. 2007. Soil heavy metal pollution around the Dabaoshan Mine, Guangdong Province, China. *Pedosphere,* **17:** 588-594.

Jung, M.C. 2008. Heavy metal concentrations in soils and factors affecting metal uptake by plants in the vicinity of a Korean Cu-W mine. *Sensors,* **8:** 2413-2423.

Jung, M.C., Thornton, I. 1997. Environmental contamination and seasonal variation of metals in soils, plants and waters in the paddy fields around a Pb-Zn mine in Korea. *The Science of the Total Environment,* **198:** 105-121.

Lee, C.G., Chon, H.T., Jung, M.C. 2001. Heavy metal contamination in the vicinity of the Daduk Au-Ag-Pb-Zn mine, Korea. *Applied Geochemistry,* **16:** 1377-1386.

Li, W., Zhang, M., Shu, H. 2005. Distribution and fractionation of copper in soils of apple orchards. *Environmental Science and Pollution Research International,* **12:** 168-172.

Lin, C., Tong, X., Lu, W., Yan, L., Wu, Y., Nie, C., Chu, C., Long, J. 2005. Environmental impacts of surface mining on mind lands in the Dabaoshan mine region, Southern China. *Land Degradation and Development,* **16:** 463-474.

Michaud, A.M., Bravin, M.N., Galleguillos, M., Hinsinger, P. 2007. Copper uptake and phytotoxicity as assessed in situ for durum wheat (*Triticum turgidum durum* L) cultivated in Cu-contaminated, former vineyard soils. *Plant and Soil,* **298:** 99-111.

Okoronkwo, N.E., Odemelam, S.A., Ano, O.A. 2006. Levels of toxic elements in soils of abandoned waste dump site. *African Journal of Biotechnology,* **5:** 1241-1244.

Ottosen, L.M., Hansen, H.K., Jensen, P.E. 2008. Relation between pH and desorption of Cu, Cr, Zn, and Pb from industrially polluted soils. *Water, Air and Soil Pollution,* **201:** 295-304.

Pendias, P.W, Dubka, C.M. 1992. Background levels and environmental influence on trace metals. In:

Soils of Temperate Humid Zone of Europe: Biogeochemistry of Trace Metals, Adriano, (ed.), pp. 61-64, CRS Press, Boca Raton, Florida, USA.

Prathumratana, L., Kim, R., Kim, K.W. 2008. Heavy metal contamination of the mining and smelting district in Mitrovica, Kosovo. In: *Proceedings of the International Symposia on Geoscience Resources and Environments of Asian Terranes (GREAT 2008),* 4th IGCP 516, and 5th APSEG. Bangkok, Thailand.

Stephanic, J. 1998. Major issues in miner health. *Environmental Health Perspectives,* **106:** 538-543.

Tessier, A., Campell, P.G.C., Bisson, M. 1979. Sequential extraction procedure for the speciation of particulate trace metals. *Analytical Chemistry,* **51:** 844-851.

Udovic, M., Drobne, D., Lestan, D. 2009. Bioaccumulation in *Porcellio scaber* (Crustacea Isopoda) as a measure of the EDTA remediation efficiency of metal-polluted soil. *Environmental Pollution,* **157:** 2822-2829.

Ukpebor, E.E., Unuigbe, C.A. 2003. Heavy metal concentration in the subsoil of refuse dumpsite in Benin City, Nigeria. *Ghana Journal of Science,* **43:** 9-15.

Ullrich, S.M., Ramsey, M.H., Helios-Rybicka, E. 1999.Total and exchangeable concentrations of heavy metals in soils near Bytom, an area of Pb/Zn mining and smelting in Upper Silesia, Poland. *Applied Geochemistry,* **14:** 187-196.

Wong, S.C., Li, X.D., Zhang, G., Qi, S.H., Min, Y.S. 2002. Heavy metals in agricultural soils of the Pearl River Delta, South China. *Environmental Pollution Journal,* **119:** 33-44.

Wu, X., Hu, X.F., Zhang, G.., Cao, X., Jiang, Q., Li, S., Li, Y. 2010. Impact of Mn-ore mining on heavy metal accumulation in the soils and vegetables nearby in Hunan Province, China. In: *19th World Congress of Soil Science, Soil Solutions for a Changing World.* Brisbane, Australia.

Yahaya, M.I, Mohammad, S., Abdullahi, B. K. J. 2009. Seasonal variations of heavy metals concentration in Abattoir dumping site soil in Nigeria. *Journal of the Applied Science Environmental Management,* **13:** 9-13.

Zhou, J., Dang, Z., Cai, M., Liu, C., 2007. Soil heavy metal pollution around the Dabaoshan Mine, Guangdong Province, China. *Pedosphere,* **17:** 588-594.

Pak. j. sci. ind. res. Ser. A: phys. sci. 2013 **56** (2) 107-121

Hydrochemical Characterization and Quality Evaluation of Groundwater in Parts of the Basement Complex Area of Ekiti, Southwestern Nigeria

Talabi Abel Ojo[a]* and Tijani Moshood Niyi[b]
[a]Department of Geology, Ekiti State University, Ado-Ekiti, Nigeria
[b]Department of Geology, University of Ibadan, Ibadan, Nigeria

(received August 8, 2011; revised March 29, 2012; accepted April 25, 2012)

Abstract. Well water (88 samples) were collected across various bedrock units in the basement terrain of Ekiti area, Southwestern Nigeria. They were subjected to *in-situ* physico-chemical measurement and hydrochemical analyses using ICP-OES and ion-chromatography methods for cations and anions, respectively. To understand the water quality and utilisation aspects of groundwater, chemical indices like sodium %, sodium adsorption ratio (SAR), Wilcox diagram and salinity diagram were constructed based on the analytical results. The results show pH values ranging between 6.0-7.8 and total hardness (TH) 3.2-508.7 mg/L. Major cations concentrations were in the order of $Ca^{2+} > K^{+} > Na^{+} > Mg^{2+}$ with average values of 28.5, 26.8, 24.2 and 7.9 mg/L, respectively while that of the anions were $HCO_3^{-} > Cl^{-} > SO_4^{2-} > NO_3^{-}$ with average values of 118.7, 54.2, 23.8 and 0.92 mg/L. The main hydrochemical facies being Ca-HCO_3 waters. The ionic orders of abundance varied in different rocks of the study area. These concentration trends show a low total dissolved solids (130-1544 µS/cm) indicating a low water-rock interaction due to low residence time which is an indication of CO_2 dominated infiltration recharge with limited migratory history typical of the shallow basement terrain in the study area. Quality assessment revealed a potable groundwater system with chemical parameters within the acceptable limits of the WHO and SON drinking water standards with exception of Fe, Mn and Pb in a couple of locations. Also, the estimated SAR alongside TDS revealed a shallow groundwater system suitable for irrigation purposes.

Keywords: basement, sodium adsorption ratio, salinity, water-rock interaction, irrigation

Introduction

Water quality assessment is an integral part of groundwater management. Water quality is a term used to describe the chemical, physical and biological characteristics of water, usually with respect to its suitability for a particular purpose. Assessment of the occurrence of chemicals that can harm water quality such as nutrients and pesticides in water sources, require recognition of complicated interconnections among surface water and ground water, atmospheric contributions, natural landscape features, human activities, and aquatic health.

Olayinka *et al*. (1999) suggested that water quality is subjective and as such depends on its use. Therefore, water quality standards differ depending on various uses including domestic (drinking), agriculture/irrigation and industrial applications. The water quality may yield information about the environments through which the water has circulated (Raju, 2007).

Groundwater usage in the crystalline basement terrain of Ekiti area, Southwestern Nigeria is increasing as a result of population growth and agricultural activities. Going by the 1991 census, the population of the area was 1.65 million while in 2001 it was 2.05 million. This represents about 2.44% growth rate per annum with a current projected population of about 2.55 million that has led to the expansion of large areas of unplanned sub-standard housing especially in the major towns of the study area. In most of these areas public water supply by government is not available and as such residents of these areas usually use groundwater as a source of inexpensive high quality domestic water supply. The uncontrolled expansion of this kind of housing, together with increasing sewage and effluent leakage, indiscriminate waste disposal and uncontrolled commercial activities has led to increasing pollution and deterioration of groundwater quality which may probably result in public health problems. The uncontrolled application of fertilizer and pesticides to sustain agriculture that employs over 80% of the workforce in the study area could contribute to groundwater contamination in addition to possible contamination arising from domestic waste, sanitary sewage as well as a wide

*Author for correspondence; E-mail: soar_abel@yahoo.com

variety of dissolved and suspended contaminants. This trend warrants an understanding of the hydrogeochemistry of the groundwater system, providing the fact that both agriculture and domestic water supply rely on the shallow groundwater system of the study area.

Groundwater has particular importance in the crystalline basement terrain of Ekiti area where most people rely on a combination of hand-dug wells and public boreholes for their drinking water supply. Although, groundwater use is generally less visible than surface water supplies, but surface water is more prone to contamination from anthropogenic activity and in many situations could not be extended to the rural populace where potable water is inadequate due to high cost distribution network. On the other hand, groundwater could be made available in residential areas apart from the fact that it increasingly provides the main source of agricultural irrigation in the study area as well as vital safety net for the dry season food security when most of the streams and rivers have dried off.

Water quality analysis is one of the most important aspects in groundwater studies. The hydrochemical study reveals the quality of water that is suitable for domestic, agriculture and industrial purposes. Also, changes in groundwater quality due to water-rock interaction or any type of anthropogenic influence can be understood through such type of study (Sadashivaiah *et al*., 2008). The definition of water quality depends much on the desired use of water. Therefore, different uses require different criteria of water quality as well as standard methods for reporting and comparing results of water analysis (Babiker *et al*., 2007). Additionally, the chemical composition of groundwater is dictated by a combination of factors such as lithogenic input of metals through water-rock interaction, anthropogenic activities and more recently the impacts of climatic variability (Berner and Berner, 1987).

Apart from the above highlighted issues, in previous research was carried out in Southwestern Nigeria on groundwater potential zonation, chemical quality and geophysical and geo-electrical characteristics of shallow groundwater by Talabi and Tijani (2011), Tijani *et al*. (2010), Omotoyinbo and Okafor (2008), Oyinloye and Ademilua (2005), Bolarinwa and Elueze (2005), Elueze *et al*. (2004) and Ehinola (2002).

Location and geological setting of the study area. The study area (Ekiti area) is located between latitudes 7° 25'-7° 52'N North of the Equator and longitudes 4°48'-5° 30'E east of Greenwich Meridian covering an area of about 4,344 km^2 (Fig.1). The area is characterized by alternating wet and dry season. The wet season usually lasts from April to October and is dominated by heavy rainfall (1500 mm) while the dry season covers the period from November to March every year with temperature ranging from 25-30 °C. The topography is generally undulating with most area lying above 250 m above sea level. The landscape is characterized by old plains, broken by steep sided outcrop dome rocks (Inselbergs) that may occur singularly or in crops of ridges. Such outcrops exist mainly in form of rugged hills at Ado-Ekiti (central part of the study area) and Ikere-Ekiti in the southern part. The study area is underlain by Precambrian crystalline rocks mostly of igneous-metamorphic origin with ages greater than 300 Ma to 450 Ma (Matheis, 1987). Prominent rock units include granite gneiss, migmatites, schist/quartz schist, porphyritic granite, fine-medium grained granite and charnockite.

The migmatites are predominant in the study area covering over 50% (Fig. 2).

The rock exposures occur as highly denuded hills of essentially fine-medium textures with closely spaced alternating bands of leucocratic and melanocratic minerals. They are characteristically low lying, fine textured, and conspicuously foliated with abundance of platy biotite minerals sandwiched into zones that are markedly distinguishable from the light coloured quartzo-feldspartic portions. The granite and the charnockite occur as intrusive bodies into the pre-existing migmatite rocks. Their textures range from fine to medium grain and in some cases coarse-porphyritic. Quartzite occurs as ridge of steeply dipping, massively bedded, fine-medium grained bodies while in some cases as quartz rubbles.

Hydrogeological setting of the study area. The hydrogeology of the area is controlled by climatic factors in addition to geology and structural features. The geological formations underlying an area and the structures determine the types of aquifer and their recharge process while climatic factors determines the amount and rate of recharge of the aquifer (Ademilua and Olorunfemi, 2000). The major surface waters in the study area are the rivers Ogbesse, Elemi, Obiba, Ureje, Ero, Osun, Ose and Oni with their tributaries forming a somewhat dendritic drainage pattern (Fig. 1).

The volume of water in the rivers depends to a greater extent on the period of the seasons. During the rainy season, there is a great increase in flow volume in the rivers while there is complete absence of water in some of the rivers during dry season. In any basement rock area, groundwater occurs in the weathered mantle or in the joints and fractured systems of the unweathered rocks and in buried stream channels (Ako and Olorunfemi, 1989).

Surface water percolates down through the fractures starting the chemical weathering processes. However, it has been reported that the highest groundwater yield in the study area are located where thick overburden overlies fractured rocks. Groundwater supply in the study area is mainly from shallow hand dug wells and shallow few boreholes. Two major aquifer units have been identified: the weathered and fractured bedrock units (Ademilua and Olorunfemi, 2000).

Generally, records of dug wells in the area indicate depths from 23.4 to 92.0 m, static water levels from 1.0 to 21.0 m and yields in the range of 8.64-354.24 m^3/day (Talabi and Tijani, 2011). However, based on rock types, the depth of the dug wells vary from 23.4 to 80.0 m in the migmatite rocks, 26.0 to 92.0 m in the granites/granite

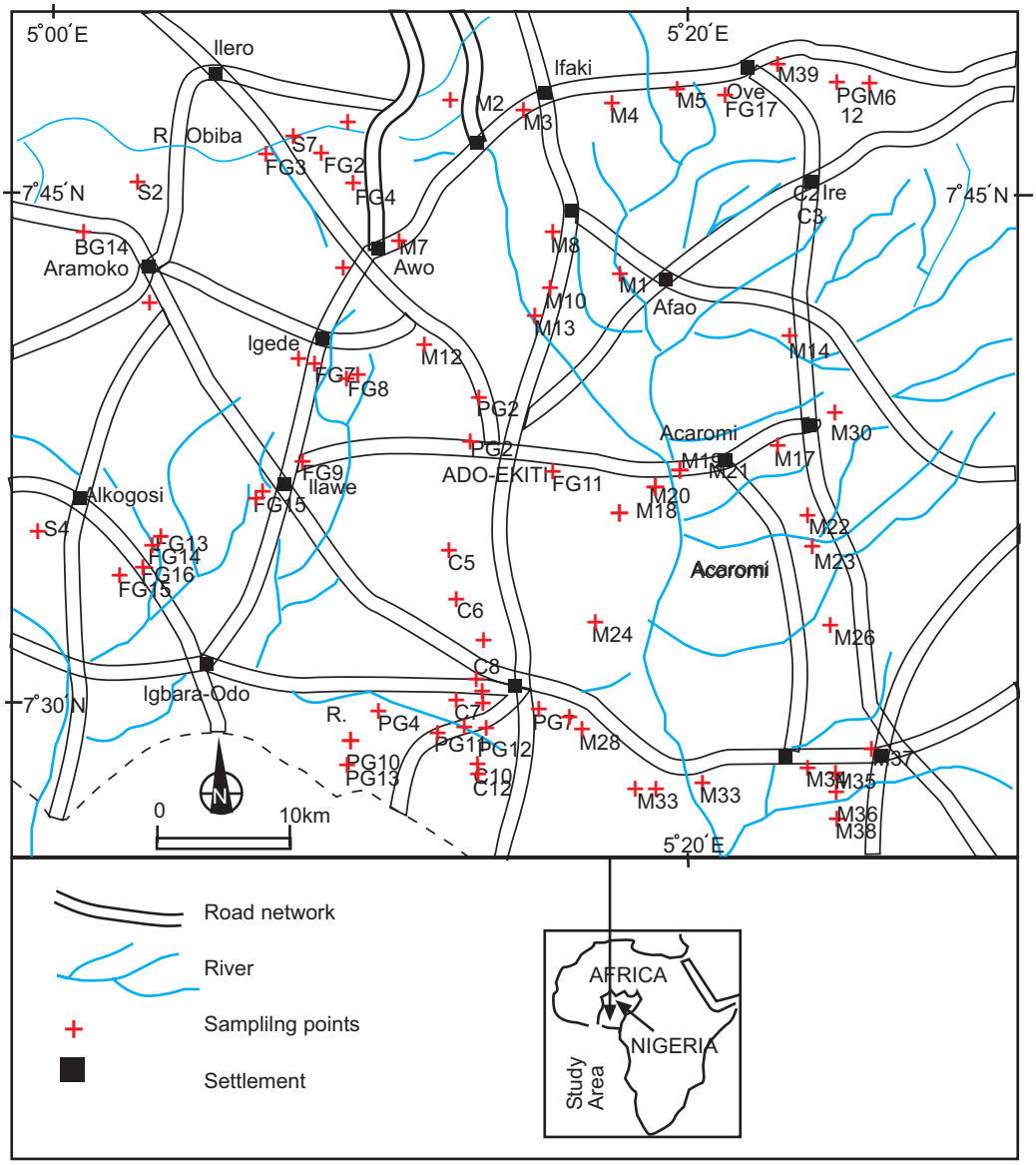

Fig. 1. Location map of the study area.

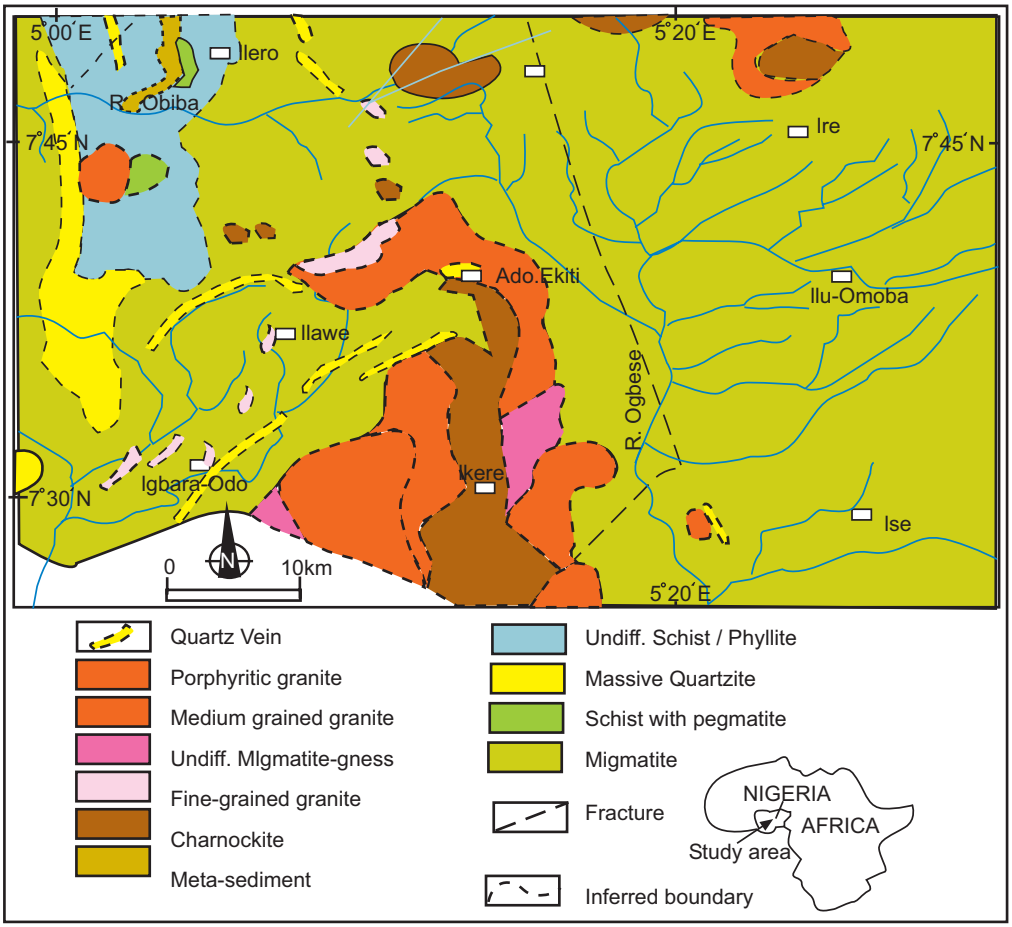

Fig. 2. Geological map of the study area.

gneisses and from 23.4 to 80 m in the quartzite/quartz-schist rocks. The static water level ranges from 1.3 to 21.0 m, 1.0 to 18.0 m and 2.0 to 14.4 m in the migmatites, granites/granite-gneisses and quartzite/quartz-schist rocks, respectively. Dug wells yields are highly variable and lie in the range of 8.64-354.24 m^3/d in the migmatites. In the granites/granite-gneisses and the quartzite/quartz-schist, wells yields are within 8.64-175.39 m^3/d and 43.2-304.99 m^3/d, respectively. Thus, the groundwater in the study area is tapped at shallow depths for domestic and agricultural purposes through hand-dug wells that terminate in the weathered crystalline rocks and if deep enough could sustain the dry season.

The objective of the present study was to assess groundwater chemical composition based on rock types and its suitability for different uses (i.e. domestic, irrigation and drinking purposes) in the crystalline Basement area of Ekiti, Southwestern Nigeria.

Materials and Methods

Groundwater samples were obtained from 88 water wells spatially distributed over the study area in July, 2008 (Fig.1). The samples were collected in clean polythene bottles. Prior to collection, the polythene bottles were pre-cleaned by rinsing them in 10% nitric acid and subsequently cleaned with de-ionized water. Two sets of samples were taken from each well. The first set for cations/metals determination were acidified with concentrated nitric acid while the other set for anion analyses were left unacidified. Cation concentrations were analysed by ICP-OES method while anion analysis was by the ion-chromatography method. *In situ* measurements of temperature (°C), EC (µS/cm) and pH were carried out using multiparameter portable meter (Testr^{Tm} 35 series). Field measurements of EC reflect the amount of total dissolved solids (TDS) in natural waters. The relationship between TDS and EC

can be described by an equation; TDS (mg/L) ≈ EC (μS/cm) × 0.75 was employed in the present study. Measurement precision was checked by taking two replicates of the groundwater sample from each bedrock type including a blank in each batch. As part of data evaluation, the results were compared with local and international standards for drinking water (Standard Organisation of Nigeria (SON, 2007), World Health Organisation (WHO, 2004). Furthermore, statistical evaluation of the overall data was performed using Rockwork, 2004 v. 4.8.19, while chemical indices like percent sodium, sodium adsorption ratio (SAR) were calculated based on the analytical results.

Results and Discussion

Groundwater chemistry. Knowledge regarding the groundwater quality is important, as it is the main factor determining its suitability for drinking, domestic, agricultural and industrial utilization (Subramani *et al*., 2005). Table 1 shows summaries of the water chemistry while summaries based on different rock units in the study area compared with WHO (2004) and SON (2007) drinking water standards are presented in Table 2. The results revealed that the analyzed groundwater samples were characterized by slight acidity to moderate alkalinity with pH values from 6.0 to 7.8. Electrical conductivity (EC) ranges from 30 to 1,544 μS/cm while TDS and TH range from 22.5 to 1158 mg/L and 3.2 to 508.7 mg/L (Table 1), respectively suggesting a low mineralized soft groundwater system with limited residence time and low water-rock interactions which could be responsible for the observed generally low concentration trends in different bedrock types (Table 2). However, 7 out of the total 88 groundwater samples within migmatite bedrock have their EC >1000 μS/cm. The relatively high TDS especially in the few sampling points close to dumpsite is an indication of contamination by leachates as one would have expected a low TDS of <500 mg/L characteristic of uncontaminated freshwater in a typical basement complex setting.

In general, the concentration of the major cations was in the order $Ca^{2+} > K^{+} > Na^{+} > Mg^{2+}$ with average value of 28.5 mg/L, 26.5 mg/L, 24.5 mg/L and 7.9 mg/L, respectively, while the order of major anions concentration was $HCO_3^{-} > SO_4^{2-} > Cl^{-} > NO_3^{-}$ with average value of 118.7 mg/L, 54.3 mg/L, 23.8 mg/L and 0.9 mg/L, respectively. With respect to trace metals, the concentrations of Co (0.002-0.049 mg/L); Cu (0.002-0.19 mg/L); Fe (0.02-4.33 mg/L); Mn (0.01-0.61 mg/L); Pb (0.01-0.10 mg/L) and Zn (0.005-1.72 mg/L) were within the permissible limits of SON (2007) and WHO (2004) standards except in a few locations where Fe, Mn and Pb exceeded the standard values.

Iron and manganese often occur naturally together though the most common source of iron and manganese in groundwater of an area is man made, including sources from corrosion of metal in well casing, piping, pump parts, storage tanks or other objects of cast iron or steel that may be in contact with groundwater. Industrial effluent, acid-mine drainage, sewage and landfill leachates may also contribute iron and manganese to the groundwater of an area. However, in the study area, the sources of the iron and manganese can be attributed to weathering of iron and manganese bearing minerals and rocks, such as amphiboles, ferromagnesian micas and magnetite. Manganese or iron at concentrations above the drinking water guidelines may affect the taste or colour of well water. Although iron and manganese do not pose a health risk at levels normally found in drinking water, their presence indicate deteriorating groundwater quality and could necessitate well rehabilitation to forest all possible health problems that may arise from the deteriorating groundwater.

Table 1. Overall summary of chemical parameters in the study area

Parameters	Min.	Max	Mean	Median	Std.Dev.
Temp.	23.9	29.9	26.69	26.7	0.96
pH	6	7.8	6.16	6.1	0.63
EC μ/cm	30	1544	433.7	291	349.9
TDS (mg/L)	22.5	1158	325.27	218.25	262.42
TH	3.22	508.74	193.78	77.55	86.62
Ca mg/L	0.3	107	28.54	22.45	22.74
Mg mg/L	0.3	58.8	7.92	5	8.74
Na mg/L	1.1	169	24.48	14.15	27.18
K mg/L	0.3	143	26.54	9.8	33.72
Fe μg/L	20	4330	370.45	105	716.61
Mn μg/L	10	610	58.75	20	98.38
Cu μg/L	2	186	8.55	2	22.08
Pb μg/L	10	100	11.4	10	9.89
Zn μg/L	5	1720	73.74	20	201
Co μg/L	2	49	3.27	2	5.88
HCO_3 mg/L	7.32	439.34	118.69	86.95	100.09
SO_4 mg/L	3.24	219.76	54.28	31.35	50.6
Cl mg/L	1.75	124.6	23.8	17.85	21.85
NO_3 mg/L	0.01	5.2	0.92	0.3	1.2
SAR	0.15	4.98	1.04	0.69	0.87
MH	2.34	49.59	21.31	20.28	9.72

SAR = sodium adsorption ratio; MH = total hardness

Table 2. Summary showing range of chemical parameters based on bedrock types compared with WHO and SON standard values

Parameters	Migmatite N=37	Porphyritic granite N=14	F-M. grained granite N=17	Schist/ quartz-schist N=7	Charnockite N=13	WHO standards (2004)	SON standards (2007)
Temp. °C	24.6-28.5	25.8-29.9	23.9-27.1	25.5-27.8	25.4-29.1	-	-
pH	6.0-7.8	6.1-6.7	6.3-7.5	6.2-7.2	6.4-7.0	6-9	6.5-8.5
EC(µS/cm)	30.0-1544.0	90.0-775.0	54.0-906.0	133.0-1175.0	31.2-215.1	1500	-
TDS(mg/L)	22.5-1158.0	67.5-581.3	40.5-679.5	99.8-881.3	46.5-510.8	1000	500
TH(mg/L)	10.2-508.7	9.4-164.6	8.4-229.2	25.9-257.7	62.0-681.0	500	150
Ca(mg/L)	2.6-107.0	2.6-52.3	2.2-73.4	5.3-75.6	0.3-54.9	200	-
Mg(mg/L)	0.5-58.8	0.7-8.6	0.7-15.6	2.3-16.8	0.3-19.0	-	-
Na(mg/L)	1.1-169.0	2.1-64.5	1.7-48.1	1.9-72.4	2.7-37.8	200	200
K(mg/L)	0.3-143.0	3.4-37.4	1.8-76.9	5.2-90.8	0.9-53.3	200	-
Fe(µg/L)	30.0-3050.0	20.0-4330.0	40.0-2640.0	40.0-3100.0	40.0-620.0	300	300
Mn(µg/L)	10.0-610.0	10.0-370.0	10.0-260.0	10.0-210.0	10.0-100.0	400	200
Cu(µg/L)	2.0-186.0	2.0-54.0	2.0-57.0	2.0-30.0	2.0-20.0	1000	1000
Pb(µg/L)	10.0-100.0	10.0-20.0	10.0-20.0	10.0-10-0	10.0-10.0	10	10
Zn(µg/L)	5.0-1720	5.0-462.0	5.0-210.0	5.0-353.0	6.0-508.0	3000	3000
Co(µg/L)	2.0-49.0	2.0-4.0	2.0-7.0	2.0-6.0	2.0-5.0	-	-
HCO_3(mg/L)	10.4-439.3	17.7-194.7	7.3-243.5	12.2-94.2	36.61-277.6	240	-
SO_4(mg/L)	3.2-219.8	14.6-94.6	6.5-155.4	8.2-167.4	8.2-167.4	250	200
Cl(mg/L)	1.8-124.6	4.9-42.0	2.8-52.5	21.3-197.4	6.3-87.5	250	250
NO_3(mg/L)	0.01-4.4	0.01-1.6	0.02-5.2	0.2-1.5	0.2-1.0	50	50

The values of Pb in excess of approved WHO standard value in the study area occur in few locations close to mechanic workshops and market waste dumps. The leaching of waste materials in a few locations into the subsurface may probably be the source of lead in groundwater.

Further evaluation of analytical results based on rock types indicate that among major cations, K^+ was dominant in migmatite and quartzite/quartz-schist rocks constituting 34.11% and 35.0% of the total cation concentrations, respectively. Ca^{2+} was dominant in fine-medium grained granites constituting 40.0% while Na^+ was dominant in the porphyritic granites constituting 41.68% of the total cations concentrations. Mg^{2+} was of secondary importance in the groundwater of the study area as it represents less than 8.5% of the cations concentrations in the various rock types with the exception of migmatite where it constitute 10.21% (Fig. 3). Furthermore, cations concentrations show the lowest values in charnockitic rocks (Fig. 3). The order of cations abundance vary considerably based on rock types. However, the order of their abundance follow similar trend of $K^+ > Ca^{2+} > Na^+ > Mg^{2+}$ in migmatite and quartzite/quartz-schist, $Ca^{2+} > K^+ > Na^+ > Mg^{2+}$ in fine - medium grained granite and charnockite while the trend of $Na^+ > Ca^{2+} > K^+ > Mg^{2+}$ in porphyritic granite was distinct from other rock types. The distinct order of cations abundance in porphyritic granite might be the result of its chemical composition of this rock type that is rich in sodic feldspar.

Among the major anions, HCO_3^- was dominant in all rocks except schist/quartz-schist where Cl^- was dominant

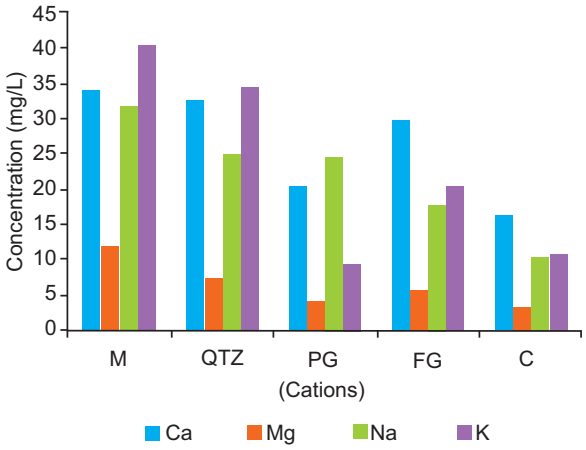

Fig. 3. Mean concentration of major cations based on rock types. M = migmatite; QTZ = quartzite/quartz-schist; PG = porphyritic granite; FG = fine-medium grained granite; C = charnockite.

(Fig. 4). Similar concentrations trend of HCO_3^->Cl^- >SO_4^{2-} >NO_3^- was observed in migmatite and charnockitic rocks while the concentrations trend of HCO_3^- >SO_4^{2-}>Cl^->NO_3^- was observed in porphyritic granite and fine-medium grained granite. Distinct concentrations trend of Cl^->SO_4^{2-}>HCO_3^->NO_3^- was observed in schist/quartz-schist. This variability is expected considering the heterogeneity of the basement rocks that respond to weathering differently and the localized nature of the basement aquifers. The dominance of HCO_3^- ion may be attributed to CO_2 charged meteoric water that produce weak carbonic acid that later dissociates into hydrogen ions and bicarbonate ions as expressed in the equation below:

$$CO_2(g) + H_2O(l) \rightarrow H_2CO_3(aq)$$
$$H_2CO_3(aq) \rightarrow H^+(aq) + HCO_3(aq)$$

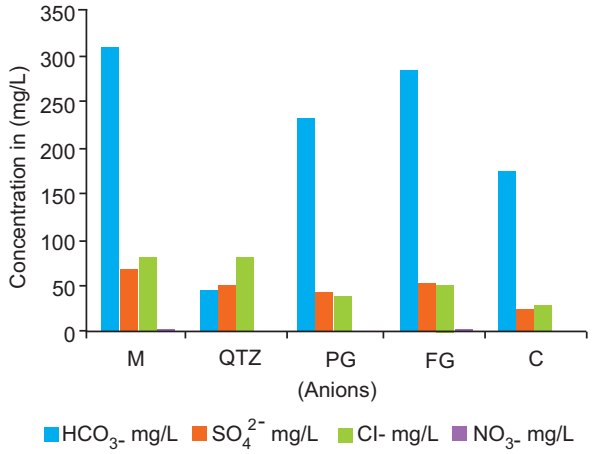

Fig. 4. Mean concentration of major anions based on rock types. M = migmatite; QTZ = quartzite/quartz-schist; PG= porphyritic granite; FG = fine-medium grained granite; C = charnockite.

Furthermore, correlation analysis between various attributes of shallow groundwater in the study area has been done and is presented in Table 3. The EC is strongly correlated with TH, Ca, Mg and Na. Among the anions, with the exception of NO_3, HCO_3, SO_4 and Cl show high correlation with EC. The results show that the dissolved ions in the groundwater are responsible for EC. The hardness is strongly correlated with the major ions, with the exception of NO_3, indicating that the hardness result from geogenic input of the dissolved ions rather than from anthropogenic activity. In addition, the relatively strong correlation of the major ions is an indication that the ions are guided by the same geochemical factors and were found within the same geochemical environment. However, the poor correlation of NO_3^- with other measured parameters indicates that it comes from a different source i.e. anthropogenic source rather than geogenic. Similarly, the major exchangeable ions Na and Ca, Na and Mg correlate positively. The fact that groundwater electrical conductivity is a reflection of the total ions is supported by the observed relatively high positive correlation (0.98) between these parameters (Fig. 5). In view of the above highlighted observations, the concurrent variations in the composition of ions in the groundwater of the study area is probably predominantly due to the result of dissolution/precipitation reaction and ions concentration effects.

Mechanism controlling groundwater chemistry of the study area. Knowledge of processes that control groundwater composition is required for a rational management of water quality. The concentration of dissolved ions in groundwater samples are generally governed by lithology, nature of geochemical reactions and solubility of the aquifers rocks (Nosrat and Asghar,

Table 3. Correlation analysis of physico-chemical parameters of the groundwater samples

Parameters	Ca	Mg	Na	K	HCO_3	SO_4	Cl	NO_3	TH	pH	EC
Ca	1.000	–	–	–	–	–	–	–	–	–	–
Mg	0.733	1.000	–	–	–	–	–	–	–	–	–
Na	0.525	0.556	1.000	–	–	–	–	–	–	–	–
K	0.674	0.472	0.543	1.000	–	–	–	–	–	–	–
HCO_3	0.879	0.810	0.781	0.754	1.000	–	–	–	–	–	–
SO_4	0.599	0.658	0.553	0.613	0.682	1.000	–	–	–	–	–
Cl	0.753	0.662	0.819	0.698	0.837	0.570	1.000	–	–	–	–
NO_3	0.242	0.078	0.002	0.320	0.186	0.260	0.120	1.000	–	–	–
TH	0.959	0.895	0.574	0.638	0.912	0.665	0.768	0.191	1.000	–	–
pH	0.649	0.330	0.343	0.562	0.557	0.363	0.577	0.064	0.562	1.000	–
EC	0.897	0.800	0.754	0.762	0.953	0.670	0.830	0.215	0.920	0.522	1.000

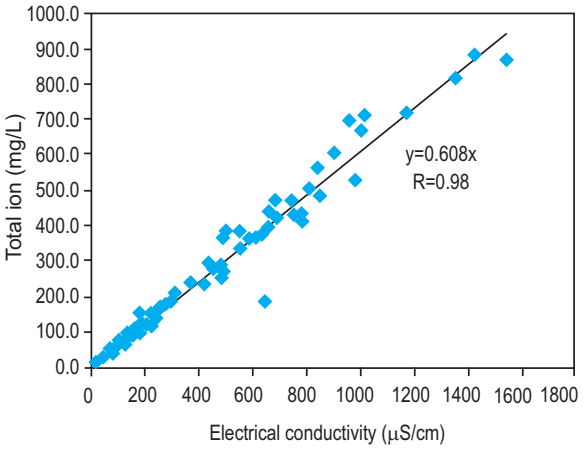

Fig. 5. A correlation plot between total ions and specific electrical conductivity.

2010). Gibbs (1970) had pointed out that the rate of evaporation, chemical composition of rocks and chemical composition of rainwater generally control the chemistry of water.

In order to evaluate the sources of various ions in the groundwater of the study area, a plot of the TDS against $Na^+/(Na^+ + Ca^{2+})$ ratio (Fig. 8), indicate that the groundwaters may have modified their chemistry from the weathered materials derived from the underlying bedrocks. The diagram of (Gibbs, 1970) indicate that 47.72% of the groundwater samples representing 42 out of total 88 samples are in the rock dominant category while the rest fall in the dilution field. The dilution effect is pronounced due to the period of sampling i.e. peak of the rainy season (July, 2008). Rock dominance of almost half of the samples is caused by the interaction between the aquifer rocks and groundwater.

Drinking water quality assessment. The main objective of hydrogeochemical assessment is to determine groundwater suitability for different uses based on different chemical indices. In this study, assessment of the suitability for drinking and domestic uses was evaluated by comparing the hydrochemical parameters of groundwater in the study area with the prescribed specification of World Health Organization (WHO, 2004) and Standard Organisation of Nigeria (SON, 2007) (Table 2).

The pH values of the groundwater vary between 6.0-7.8, indicating slight acidity to moderate alkaline nature of the groundwater. According to the WHO, the range of desirable pH values of water prescribed for drinking purposes is 6-9 (WHO, 2004) while that of SON (2007) is between 6.5-8.5. Water samples in few locations fall outside the desirable pH values. This slight increase in H^+ ions probably resulted from the generation of carbonic acid from intensive rainfall that characterized the sampling period. Table 2 shows that few of the parameters exceed the maximum permissible limits of WHO (2004). The EC and concentration of TDS is more than the maximum permissible limits of 1500 µS/cm and 1000 mg/L, in 1.0% and 3.0% of the total groundwater samples, respectively. The recommended limit for sodium concentration in drinking water is 200 mg/L. A higher sodium intake may cause hypertension, congenial heart diseases and kidney problems (Singh *et al*., 2008). Sodium concentrations was within the prescribed limit of 200 mg/L in all analyzed groundwater samples of the study area. The overall drinking water quality assessment revealed that the chemical profiles, with very few exceptions, are within the permissible limits of WHO (2004) and SON (2007) standards and as such suitable for drinking purpose.

Suitability for irrigation purpose. Knowledge of irrigation water quality can influence crop productivity more than soil fertility, hybrid, weed control and other strategies and is critical to understanding agricultural management for long-term productivity. The water quality evaluation in this study was carried out to determine its suitability for agricultural purposes. The suitability of groundwater for agricultural purpose is based on the effects of the total salt content, sodium and specific ion toxicities of the water on both the plant and the soil. In fact, salts can be highly harmful, and can limit plants growth physically by restricting the water uptake through modification of osmotic processes. Also salts may damage plant growth chemically by the effects of toxic substances upon metabolic processes. For this study salinity, alkali and magnesium hazards are considered for evaluation of the suitable quality of groundwater for irrigation as highlighted below.

Salinity hazard. The most influential water quality guideline on crop productivity is the water salinity hazard as measured by electrical conductivity (EC). The primary effect of high EC water on crop productivity is the inability of the plant to compete with ions in the soil solution for water (physiological drought). The higher the EC, the less water is available to plants, even though the soil may appear wet, this is due to the fact that usable plant water in the soil solution decreases dramatically as EC increases. The total soluble salt

content of irrigation water generally is measured either by determining its electrical conductivity (EC), reported as micro Siemens per centimeter, or by determining the actual salt content in parts per million (ppm). In this study, the EC was determined based on the US Salinity Laboratory (1954) classification, the salinity hazard for groundwater samples in the study area is classified into three classes; low (C1), medium (C2) and high (C3) as presented in Fig. 6. Results show that 47 groundwater samples with EC<500 µS/cm, representing 53.42% of the total groundwater samples of the study area fall in the low salinity hazard category (C1), 26 groundwater samples representing 29.54% with 500<EC<1000 µS/cm are in the medium category (C2) while 15 of the total groundwater samples representing 17.04% with EC>1000 µS/cm belong to the high salinity hazard category (C3). Normally, irrigation water with an EC of <700 µS/cm causes little or no threat to most crops while EC >3000 µS/cm may limit their growth (Tijani, 1994). Thus groundwater in the low salinity hazard category can be used as irrigation water on all soils while those in the medium salinity hazard can be used in most cases as irrigation water without any special practices for salinity control. However, water samples that fall in the high salinity hazard class (C3) may have detrimental effects on salt sensitive crops and, in certain cases, it may adversely affect many plants. Irrigation

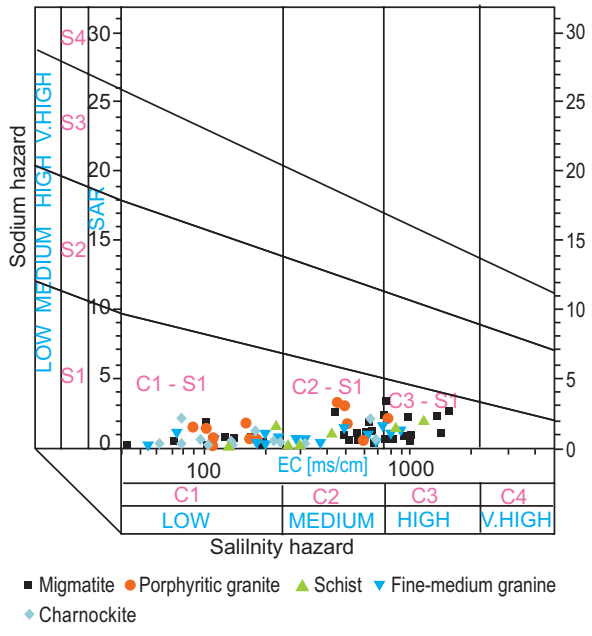

Fig. 6. Salinity diagram for classification of irrigation waters (Based on Richards, 1954).

in such areas require careful management practices. Low to high salinity hazards cut across migmatite, quartzite/quartz-schist and fine-medium grained granite settings while groundwater samples from porphyritic granite and charnockite are restricted to low to medium salinity hazards. The high salinity hazard in some of the groundwater samples could probably have resulted from soluble mineral materials along the flow path of groundwater and also from dissolution of the chemical fertilizers by irrigation water and municipal waste disposal.

Alkali hazard. Although plant growth is primarily effected by the salinity (EC) level of the irrigation water, the application of water with a sodium imbalance can further reduce yield under certain soil texture conditions. Reductions in water infiltration can occur when irrigation water contains higher sodium than calcium and magnesium contents. A high salt content (high EC) in water leads to formation of saline soil while high sodium content (SAR) leads to development of an alkaline soil (Khodapanah *et al*., 2009). The alkali hazard is typically expressed as the sodium adsorption ratio (SAR). This index quantifies the proportion of sodium (Na) to calcium (Ca) and magnesium (Mg) ions in a sample. The SAR assesses the potential for infiltration problems due to a sodium imbalance in irrigation water. The SAR is mathematically computed using the following formula given by Richards (1954).

$$SAR = \frac{Na^{+}}{\sqrt{\frac{(Ca^{2+}) + (Mg^{2+})}{2}}}$$

Ions in the equation are expressed in milliequivalent per litre. The SAR values plotted on the US salinity diagram as alkalinity hazard shows that all groundwater samples in the study area have SAR<10 i.e. SAR range between 0.15-4.98 and consequently fall in the low sodium hazard category. As per alkali hazard classification by Richard (1954), water with EC<250 µS/cm and SAR<10 are in the excellent irrigation water category while those with 250<EC<750 µS/cm and 10=SAR<18 are in good irrigation water quality. Based on this classification, 26 out of 37 groundwater samples from migmatite rock unit are in the excellent to good irrigation water category. In addition, 13 out of 14 samples, 6 out of 7 samples, 14 out of 17 samples and the whole 13 samples in porphyritic granite, quartz-schist, fine-medium grained granite and charnockite, respectively fall in this same class of irrigation water. In all, 72 out

of 88 groundwater samples are in excellent to good category implying the suitability of greater proportion of the groundwater system in the study area for irrigation purpose. As for the doubtful water category, with 750 EC≤ 2250 µS/cm, groundwater samples from migmatite bedrock settings has the greatest value of 12 out of 37 groundwater samples. The high EC values on migmatite is not unexpected; migmatite being a composite silicate metamorphic rock, pervasively heterogeneous on a meso to macroscopic scale with variable mineral dissolutions in groundwater and in few locations, domestic waste dumps contribute to the high EC values.

Magnesium hazard. Calcium and magnesium exist as positively charged ions in water and they counteract the deleterious effect of sodium through cation exchange process. For plant growth Ca and Mg are essential but at times, they may associate with soil aggregation and friability by destroying soil structure. A state of equilibrium is maintained by Ca^{2+} and Mg^{2+} in groundwater (Hem, 1985). However, during equilibrium, an increase in Mg^{2+} will adversely affect the soil quality rendering it alkaline which could result in decrease of crop yield (Kumar *et al*., 2007). Paliwal (1972) developed an index for calculating the magnesium hazard (MH). The MH is calculated using the formula:

$$MH=Mg^{2+}/(Ca^{2+} + Mg^{2+}) \times 100$$

In the study area, evaluated chemical data revealed that the MH values range from 3.80 to 76.42 with average value of 31.11. Furthermore, 93% of groundwater samples i.e. 82 out of 88 samples fall within permissible limit of 50 while only 6 samples (3 in migmatite, 1 in fine-medium grained granite, 1 in quartz-schist, 1 in charnockite) fall outside the limit (Paliwal, 1972).

Water classification for irrigation utility. In order to classify the groundwater samples from the study area for irrigation uses Na % = (Na^+) *100/$(Ca^{2+} + Mg^{2+} + Na^+ + K^+)$ was estimated for each sample where, the quantities of all cations are expressed in milliequivalents per litre (epm). Sodium percentage (Na%) in the study area generally ranges between 5.97-53.14% with exception of few higher values (78.96 in charnockite, 66.95 in migmatite, 63.58 and 61.36 in porphyritic granite bedrock settings). These high values derive from waste dumps' leachates in few highlighted locations that add to geogenic solutes from weathering and dissolution of rocks and minerals. Based on Sadashivaiah *et al*. (2008) the classification of groundwater for irrigation purposes was grouped as excellent (< 20%), good (20-40%), permissible (40-60%), doubtful (60-80%) and Unsuitable (>80%) based on sodium percentage. From the estimated Na% of the study area, 66 out of the 88 groundwater samples with 28, 7, 5, 16 and 10 samples from migmatite, porphyritic granite, quartz-schist, fine-medium grained granite and charnockite bedrock settings, respectively have excellent to good irrigation water quality. Also, 15 out of the 88 samples with 7, 4, 1, 1 and 2 samples from migmatite, porphyritic granite, quartz-schist, fine-medium grained granite and charnockite rock units, respectively have permissible irrigation water quality. None of the samples have unsuitable irrigation water quality but 8 of them with 3 samples from migmatite, 3 samples from porphyritic granite and 1 sample each from quartz-schist and charnockite bedrock settings, respectively have doubtful irrigation water quality. Furthermore, the US Salinity Laboratory Diagram (USDA, 1954) in which salinity hazard was plotted against sodium hazard (Fig. 6), indicates that all the groundwater samples from the study area fall in low sodium hazard with estimated SAR range values of 0.15-4.98 while their salinity hazard range from low to high i.e. low salinity has EC< 500µS/cm, medium salinity has 500<EC<1000 µS/cm while high salinity has EC >1000 µS/cm. Nine (9) out of the 13 samples in high salinity hazard are in the migmatite bedrock. The high salinity in migmatite bedrock may be from geogenic dissolution of minerals and probably from anthropogenic source due to refuse dumps close to sampling points.

In addition, Wilcox (1955) irrigation classification diagram (Fig. 7), classified the groundwater in the study area into two classes; (1) excellent to good irrigation water with EC< 750 µS/cm and (2) doubtful to permissible irrigation water category with 750< EC< 2000 µS/cm. Groundwater samples from migmatite still dominate the doubtful to permissible irrigation class which support the earlier observation from US Salinity Laboratory diagram (USDA, 1954). The highlighted irrigation quality profiles revealed that, the groundwater in the study area is suitable for irrigation in most cases, except in a few locations with high salinities.

Characterization of the groundwater system of the study area. Groundwater characterisation constitute one of the vital tools for sustainable development and provides important information for water management. It entails fishing out groundwater bodies that are at risk of failing to meet the approved water standards for domestic, industrial and agricultural utilization.

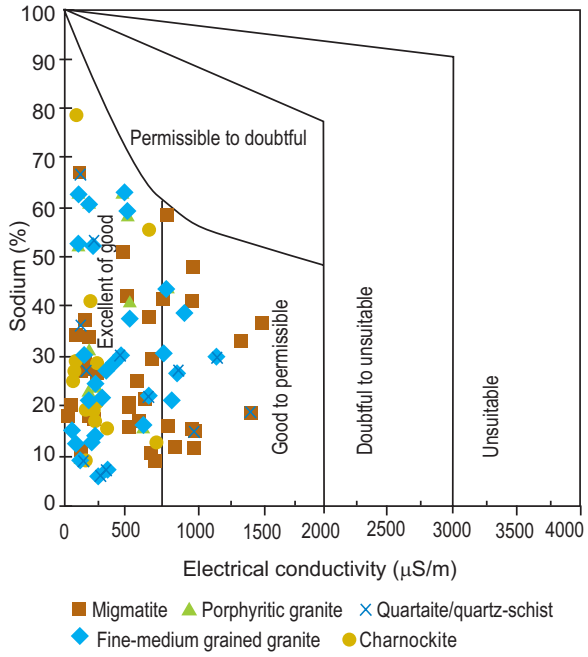

Fig. 7. Plot of sodium percentage and electrical conductivity (Based on Wilcox, 1955) for classification of Groundwater for irrigation uses.

In the study area, 85 out of 88 groundwater samples representing 96.59% (Table 4) have TDS<1000 mg/L and is classified as freshwater based on water classification after Freeze and Cherry (1979). The remaining three (3) samples representing 3.41% exceeded TDS value of 1000 mg/L possibly as a consequence of contamination from waste dumps close to these few wells located on migmatite bedrock.

Furthermore, the total hardness (TH) of the groundwater samples in the study area was calculated using the formula of Sawyer *et al*. (2003), as given below:

$$TH\ (as\ CaCO_3)\ mg/L = (Ca^{2+} + Mg^{2+})\ meq/L * 50.$$

Table 4. Classification of groundwaters (Freeze and Cherry, 1979)

Water (Types)	No. of samples	(%) Samples	Total dissolved solids (mg/L)
Fresh water type	85	96.59	<1000
Brackish water type	3	3.41	1000-10000
Saline water type	-	-	10000-100000
Brine water type	-	-	>100,000
Total	88	100	

The hardness values range from 10.2 to 289.1 mg/L with an average value of 102.40 mg/L except in locations C12, FG15, PG3 and M22 with hardness values of 3.2, 8.4, 9.4 and 508.7 mg/L, respectively. Water hardness is primarily the amount of calcium and magnesium and to a lesser extent, iron in the water is commonly expressed as milligrams of calcium carbonate equivalent per litre. Water containing calcium carbonate at concentrations below 60 mg/L is generally considered as soft; 60-120 mg/L, moderately hard; 120-180 mg/L, hard; and more than 180 mg/L, very hard (McGowan, 2000). The classification of groundwater of the study area (Table 5) based on total hardness (TH) shows that 33 of the groundwater samples fall in the soft water category with the highest proportion from charnockitic bedrock setting i.e. 9 out of the 13 groundwater samples in that bedrock setting. This trend might be as a result of chemical composition of charnockitic rocks as many of the minerals of these rocks are schillerized, as they contain minute platy or rod-shaped inclusions and as such the mineral components when weathered are probably retained in the clay and may not easily dissolved into groundwater aquifers. Also, 24, 15 and 16 of the groundwater samples are in the moderately hard, hard and very hard categories, respectively. Groundwater in the very hard category are more represented in migmatite bedrock i.e. 11 out of 37 samples compared to 3 out of

Table 5. Groundwater classification based on hardness (McGowan, 2000)

TH as $CaCO_3$ (mg/L)	Water (Types)	No. of samples on bedrock settings					Total	Samples (%)
		M	PG	FG	QS	C		
<60	Soft	9	7	6	2	9	33	37.50
60-120	Moderately hard	9	5	5	2	3	24	27.27
120-180	Hard	8	2	3	2	-	15	17.05
>180	Very hard	11	-	3	1	1	16	18.18
Total		37	14	17	7	13	88	100.00

M = migmatite; PG = porphyritic granite; FG = fine to medium grained granite; QS = quartz-schist; C: Charnockite

17 samples in fine to medium grained granite, 1 out of 7 samples in quartz-schist, 1 out of 13 samples in charnockite and none at all in porphyritic granite. This observation is consistent with the observed high values of TDS in few locations on migmatite bedrock close to refuse dumps.

Hydrochemical facies are water masses that have different geochemical attributes and are helpful for comparing the origins and distribution of groundwater system (Lloyd and Heathcote *et al*., 1985). Over the years, the Trilinear Piper diagrams are useful in bringing out chemical relationships among groundwater samples in more definite terms compared to other convectional plotting methods. The concept of hydrochemical facies was developed in order to understand and identify the water composition in different classes. Hydrochemical facies are distinct zones that possess cation and anion concentration categories (Rajendra *et al*., 2009). In case of a clear domination of a particular cation or anion (>50% of total cations or anions), the facies can be identified based on dominant constituents. In case of no clear-cut domination, 1/3 or 33% is taken as cut-off value (Saha *et al*., 2008). Piper (1944) independently developed a diagram called Piper Trilinear diagram to explain the concept of hydrochemical facies. This concept was developed in order to understand and identify the water composition in different classes. The plots include two triangles, one for plotting cations and the other for plotting anions. The cations and anions fields are combined to show a single point in a diamond-shaped field, from which inference is drawn on the basis of hydro-geochemical facies concept. In addition, Piper (1953) further developed an essentially similar diagram modifying the position of the triangles and the diamond shaped field (quadrilateral field) portion. Piper also gave a detailed description of the procedures and examples of application of this diagram to the geochemical interpretation of water analyses. The central diamond-shaped field (quadrilateral field) is used to show the overall chemical character of the water. Back *et al*. (1965) defined the subdivisions of the diamond field that represent water-type categories that form the basis for one common classification scheme for natural waters. The modified Piper diagram, with some changes as to the classification of the different water types was adopted for the interpretation of water facies in this study. To identify the various water facies in the study area, the groundwater samples were plotted in the Ppier Trilinear diagram (Fig. 9). Based on the relative dominance of major cations and anions, different hydrochemical facies with their relative percentages identified in the study area are presented in Table 6.

The hydrochemical water facies of the study area include $CaHCO_3$ (31 samples), NaCl (10 samples), mixed/exchange water type $CaNaHCO_3$ (19 samples), mixed/exchange water type CaMgCl (25 samples) and CaCl (3 samples). The Piper diagram shows that most of the groundwater samples analyzed fall in the field of

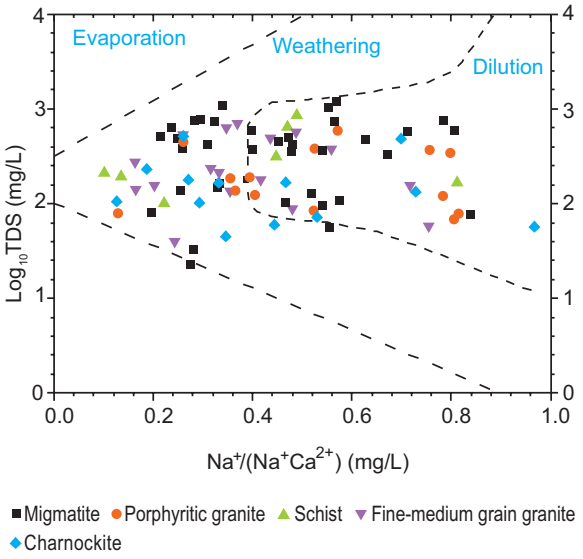

Fig. 8. Plot of Log (TDS) against the Na/Na+Ca (after Gibbs, 1970).

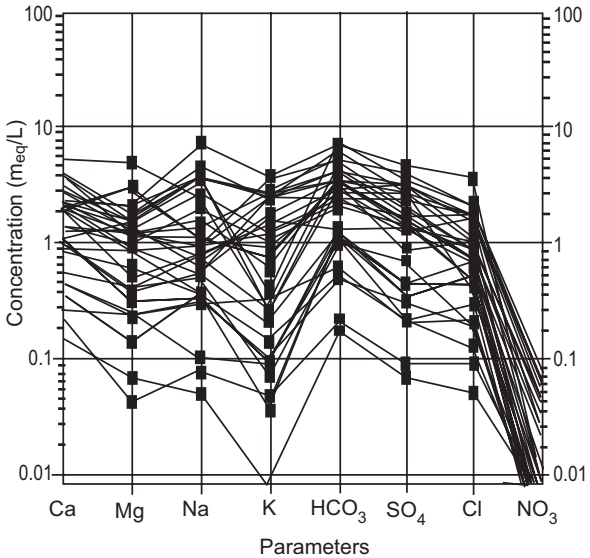

Fig. 9. Schoeller diagram for the groundwater samples.

Table 6. Hydrochemical facies of groundwater in the study area

Facies	No. of samples	Samples (%)
$CaHCO_3$	31	35.23
NaCl	10	11.36
Mixed CaNa HCO_3	18	20.45
Mixed CaMgCl	25	28.41
CaCl	3	3.41
$NaHCO_3$	1	1.14
Total	88	100.00

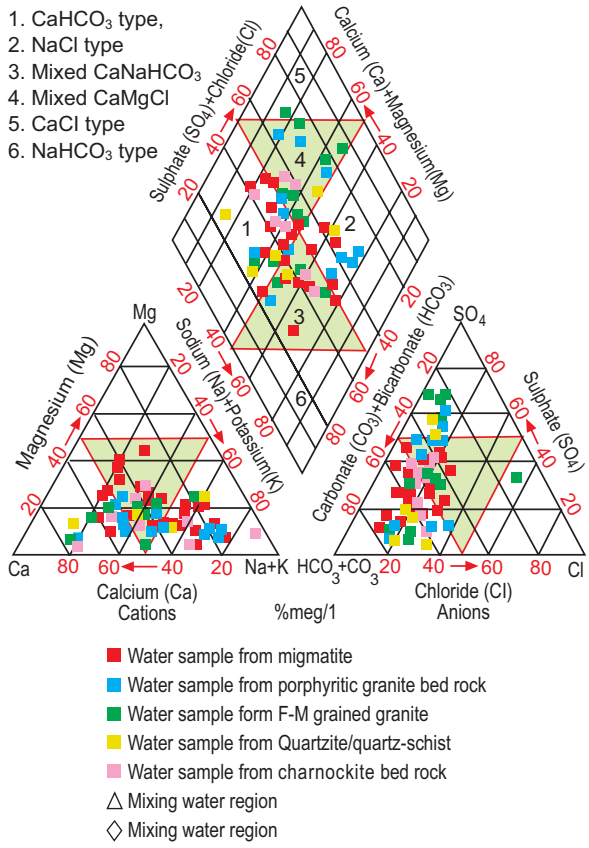

Fig. 10. Groundwater characterization; Piper diagram.

mixed/exchange water type that is, CaMgCl and $CaNaHCO_3$ (43 samples) representing 48.86% of the analysed samples in the study area. Furthermore, alkali metals (Na and K) exceed alkaline earth metals (Ca and Mg) and strong acids exceed weak acids, which implies that the water chemistry of the study area is dominated by alkali and strong acids. In addition, the observed hydrochemical facies, signify that the dissolved ions are mainly geogenic with dominance of water-rock interactions.

Conclusion

The shallow groundwaters in the crystalline basement area of Ekiti, Southwestern Nigeria have been evaluated for their chemical composition and suitability for drinking and irrigation uses. The investigation indicates that the order of major cations abundance is $Ca^{2+}>K^{+}>Na^{+}>Mg^{2+}$ while that of the anions is $HCO_3^{-}>SO_4^{2-}>Cl^{-}>NO_3^{-}$. However, the order of ions abundance is variable based on rock types with similar order of cations abundance of $K^{+}>Ca^{2+}>Na^{+}>Mg^{2+}$ in migmatite and quartzite/quartz-schist, $Ca^{2+}>K^{+}>Na^{+}>Mg^{2+}$ in fine-medium grained granite and charnockite while the trend is $Na^{+}>Ca^{2+}>K^{+}>Mg^{2+}$ in porphyritic granite distinct from other rock types in view of its chemical composition that is rich in sodic feldspar. As regards the major ions, HCO_3^{-} was dominant in all the rocks except schist/quartz-schist where Cl^{-} was dominant. Similar concentrations trend of $HCO_3^{-}>Cl^{-}>SO_4^{2-}>NO_3^{-}$ was observed in migmatite and charnockitic rocks while the concentrations trend of $HCO_3^{-}>SO_4^{2-}>Cl^{-}>NO_3^{-}$ was observed in porphyritic granite and fine-medium grained granite. Distinct concentrations trend of $Cl^{-}>SO_4^{2-}>HCO_3^{-}>NO_3^{-}$ was observed in schist/quartz-schist. Furthermore, with over 90% of the groundwater having TDS <1000, TH <500 and low chemical concentration trends in different rock types imply low mineralized soft groundwater system with limited residence time and limited water-rock interaction.

The overall drinking quality assessment indicates that most of the hydrochemical parameters satisfy WHO (2004) and SON (2007) standard values for drinking water except in few locations where Pb, Fe and Mn exceeded the standard values. Wilcox and US Laboratory Salinity Staff diagrams revealed that most of the groundwater samples are suitable for irrigation purposes under normal condition. The salinity hazard for shallow groundwater system in the study area is classified as low (EC< 500 µS/cm), medium (500< EC< 1000 µS/cm) and high salinity (EC >1000 µS/cm) classes with 47, 26 and 15 samples in the respective classes. Alkali hazard, with values ranging from 0.15 to 4.98, is classified as low in the study area with only 12 out of 88 groundwater samples showing high salinity hazard. Moreover, the estimated SAR values of less than 10 for all groundwater samples in the study area is indicative of good irrigation water, suitable on all agricultural soils. The chemistry of groundwater evolution depends on chemical inputs from precipitation (CO_2 - charged rainwater), chemical

weathering and dissolution of the parent bedrocks. Hence, the resulting groundwater is largely characterised as $CaHCO_3$ water type with relatively low TDS. In addition, mixed/exchange water types ($CaNaHCO_3$ and CaMgCl) as well as scoops of NaCl water type exist in the groundwater system of the study area. Finally, this study has revealed the hydrochemical profiles of groundwater in the study area. However, the relatively high values of lead, iron and manganese contents in the groundwater of the study area demand for further investigation.

References

Ademilua, L.O., Olorunfemi, M.O. 2000. A geoelectric/geology estimation of the groundwater potential of the basement complex area of Ekiti and Ondo States, Nigeria. *Journal of Technoscience*, **4:** 4-18.

Ako, B.D., Olorunfemi, M.O. 1989. Geoelectric survey for groundwater in the Newer Basalts of Vom, Plateau State. *Nigerian Journal of Mining and Geology*, **25:** 247-450.

Babiker, I.S., Mohamed, A.A., Hiyama, T. 2007. Assessing groundwater quality using GIS. *Water Resources Management*, **21:** 699-715.

Berner, E.K., Berner, R.A. 1987. *The Global Water Cycle*: *Geochemistry and Environment*, 397 pp., Prentice Hall, Eaglewood Cliffs, New Jersey, USA.

Bolarinwa, A.T., Elueze, A.A. 2005. Geochemical trends in weathered profiles above granite gneiss and schists of Abeokuta area, Southwestern Nigeria. *Journal of Mining and Geology*, **41:** 19-31.

Ehinola, O.A. 2002. Hydrochemical characteristics of ground water in parts of the basement complex of Southwestern Nigeria. *Journal of Mining and Geology*, **38:** 125-133.

Elueze, A.A., Omidiran, J.O., Nton, M.E. 2004. Hydrochemical investigation of surface water and groundwater around Ibokun, Ilesha area, Southwestern Nigeria. *Journal of Mining and Geology*, **40:** 57-64.

Freeze, R.A., Cherry, J.A. 1979. *Groundwater*, 604 pp., Prentice-Hall, Inc. Englewood Cliffs, New Jersey, USA.

Gibbs, R.J. 1970. Mechanisms controlling world water chemistry. *Science*, **170:** 1088-1090.

Hem, J.D. 1985. Study and interpretation of chemical characteristics of natural waters. *US Geological Survey Water Supply Paper* 2254, pp. 120-157, 3rd edition, US Govet. Printing Office, Alexandria, VA 22304, USA.

Khodapanah, L., Sulaiman, W.N.A., Khodapanah, N. 2009. Groundwater quality assessment for different purposes in Eshtehard District, Tehran, Iran. *European Journal of Scientific Research*, **36:** 543-553.

Kumar, M., Kumari, K., Ramanathan, A.L., Saxena, R. 2007. A comparative evaluation of groundwater suitability for irrigation and drinking purposes in two intensively cultivated districts of Punjab, India. *Environmental Geology*, **53:** 553-574.

Lloyd, J.W., Heathcote, J.A. 1985. *Natural Inorganic Hydrochemistry in Relation to Groundwater*. 294 pp., Oxford University Press and Claredon Press, New York, USA.

Matheis, G. 1987. Nigeria rare metal pegmatites and their lithologic framework. *Geological Journal*, **22:** 271-291.

McGowan, W. 2000. *Water Processing, Residential, Commercial, Light-industrial*, J. F. Harrison (ed.), 309 pp., 3rd edition, Water Quality Association, Lisle, Illinois, USA.

Nosrat, A., Asghar, A.M. 2010. Assessment of groundwater quality and its suitability for drinking and agricultural uses in the Oshnavieh area, Northwest of Iran. *Journal of Environmental Protection*, **1:** 30-40.

Olayinka, A.I., Abimbola, A.F., Isibor, R.A., Rafiu, A.R. 1999. A geoelectrical hydrogeochemical investigation of shallow groundwater occurrence in Ibadan, southwestern Nigeria. *Environmental Geology*, **37:** 31-39.

Omotoyinbo, O.S., Okafor, F.C. 2008. Influence of rock mineralogy on subsurface water in Ado-Ekiti, Nigeria. *African Research Review*, **2:** 175-186.

Oyinloye, A.O., Ademilua, O.L. 2005. The nature of aquifer in the crystalline basement rocks of Ado-Ekiti, Igede-Ekiti and Igbara Odo areas, Southwestern Nigeria. *Pakistan Journal of Scientific and Industrial Research*, **48:** 154-161.

Paliwal, K.V. 1972. *Irrigation with Saline Water*, Monogram-2 (New series), 198 pp., New Delhi, IAR1, India.

Piper, A.M. 1953. A graphic procedure in the geochemical interpretation of water analysis, 14 pp., *US Geological Survey Ground-water Notes Geochemistry No. 12*.

Piper, A.M. 1944. A graphic procedure in the geochemical interpretation of water analyses. *American Geophysical Union Transaction*, **25:** 914-923.

Rajendra Prasad, D.S., Sadashivaiah, C., Rangnna, G.

2009. Hydrochemical characteristics and evaluation of groundwater quality of Tumkur Amanikere lake watershed, karnataka, India. *E-Journal of Chemistry*, **6:** 211-218. http://www.e-journals. net

Raju, N.J. 2007. Hydrogeochemical parameters for assessment of groundwater quality in the upper Gunjanaeru River basin, Cuddapah District, Andhra Pradesh, South India. *Environmental Geology*, **52:** 1067-1074.

Richards, L.A. 1954. *Diagnosis and Improvement of Saline Alkali Soils*, 160 pp., United State Salinity Staff. Agriculture, Handbook 60, US Department of Agriculture, Washington DC, USA.

Sadashivaiah, C., Ramakrishnaiah, C.R., Ranganna, G. 2008. Hydrochemical analysis and evaluation of groundwater quality in Tumkur Taluk, Karnataka State, India. *International Journal of Environmental Research and Public Health*, **5:** 158-174.

Saha, D., Dhar, Y.R., Sikdar, P.K. 2008. Geochemical evolution of groundwater in the Pleistocene aquifers of South Ganga plain, Bihar. *Journal of the Geological Society of India*, **71:** 473-482.

Sawyer, G.N., McMcartly, D.L., Parkin, G.F. 2003. *Chemistry for Environmental Engineering and Science*, 752 pp., 5th edition, McGraw Hill, New York, USA.

Singh, A.K., Mondal, G.C., Suresh, K., Singh, T.B., Tewary, B.K., Sinha, A. 2008. Major ion chemistry, weathering processes and water quality assessment in upper catchment of Damodar River basin, India. *Environmental Geology*, **54:** 745-758.

SON. 2007. *Nigerian Standards for Drinking Water Quality*, 30 pp., Approved by Standard Organization of Nigeria (SON) Publ. NIS. 554.

Subramani, T., Elango, L., Damodarasamy, S.R. 2005. Groundwater quality and its suitability for drinking and agricultural use in Chithar River basin, Tamil Nadu, India. *Environmental Geology*, **47:** 1099-1110.

Talabi, A.O., Tijani, M.N. 2011. Integrated remote sensing and GIS approach to groundwater potential assessment in the basement terrain of Ekiti area southwestern Nigeria. *RMZ-Materials and Geo-environment*, **58:** 303-328.

Tijani, M.N., Nton, M.E., Kitagawa, R. 2010. Textural and geochemical characteristics of Ajali Sandstone, Anambra Basin, SE Nigeria: Implication for its provenance. *Comptes Rendus Geosciences*, **342:** 136-150.

Tijani, M.N. 1994. Hydrogeochemical assessment of groundwater in Moro area, Kwara State, Nigeria. *Environmental Geology*, **24:** 194-202.

USDA 1954. *Diagnosis and Improvement of Saline and Alkali Soils*, *Agricultural Handbook No. 60*. pp. 1-160, Salinity Laboratory, US Department of Agriculture, USA.

WHO. 2004. *Guidelines for Drinking Water Quality.* 515 pp., Recommendations, vol. **1,** 3rd edition. WHO, Geneva, Switzerland.

Wilcox, L.V. 1955. *Classification and Use of Irrigation Waters*. Circular No. 696, 16 pp., United States Department of Agriculture, Washington DC, USA.

Pak. j. sci. ind. res. Ser. A: phys. sci. 2013 **56** (1) 122-124

Short Communication

Cationic Interference in Mercury Analysis by Cold Vapour Atomic Absorption Spectroscopy

Rajkumar Dewani*[a], Shaikh Mohiuddin[b], Iftikhar Imam Naqvi[b] and Syeda Shadiah Masood[b]
[a]Leather Research Center, PCSIR, D-102, SITE, South Avenue, Karachi-75700, Pakistan
[b]Department of Chemistry, University of Karachi, Karachi-75270, Pakistan

(received March 5, 2012; revised August 1, 2012; accepted August 5, 2012)

Abstract. The cationic interference in the analysis of mercury at trace level by cold vapour atomic absorption spectroscopy (CVAAS) has been investigated. Different cations (Na^+, K^+, Fe^{2+}, Zn^{2+}, Cr^{3+}, Co^{2+}, Ni^{2+} and Cu^{2+}) of varying concentrations are examined as possible interferents in the analysis of mercury. Na^+, Fe^{2+}, Zn^{2+} and K^+ did not show any affect due to their presence in the detection of mercury while Co^{2+}, Ni^{2+}, Cu^{2+} and Cr^{3+} had a marked influence on mercury recovery and can be suggested as possible interfering agents for this method of Hg analysis.

Keywords: mercury analysis, cold vapour technique, cationic interference

Mercury is a proven toxic element, even at trace levels and can cause serious human health disorders (Kagaya *et al*. 2004; Hatje *et al*., 1998; Bidone *et al*., 1997a; 1997b). Interference in an analysis is as important as the analysis itself. Several analytical techniques exist to determine mercury at trace levels, among which cold vapour atomic absorption spectroscopy is widely used (Silva *et al*., 2005; Bermejo-Barrera *et al*., 1996; Katiuska *et al*., 1996).

A method has been devised for the indirect determination of iodide based on its interference with the determination of mercury (Afkhami and Khalafi, 2005; Haase and Broekaert, 2002; Sun and Julshamn, 1987; Kuldvere, 1982).

Presence of sulphate ions do not interfere in the analysis (Kolthoff and Sandell, 1952). Copper interference has been reported by Csuros and Csuros (2002), while cobalt interference has been reported by Paklepa *et al*. (2001). Similarly, under ambient conditions, silver, gold, copper, zinc, and aluminum readily form amalgams with liquid or gaseous elemental mercury (Ebadian, 2001; Andren and Nriagu, 1979).

This study is confined to cationic interference confronting in the analysis of mercury by cold vapour atomic absorption spectroscopy (CVAAS). All measurements were recorded on a double beam atomic absorption spectrophotometer (Perkin-Elmer Analyst 700) equipped with cold vapour atomizer (Perkin Elmer MHS-15 mercury hydride system). All the chemicals used were 'AR' grade. A 1000 ppm mercury standard solution of AAS reagent was used (i.e. 4.98 mmol / L Mercuric nitrate in 5 M HNO_3). Other chemicals used were HCl (11.5 M.), $KMnO_4$, H_2SO_4 (98%), HNO_3 (65%) and NaOH.

*Author for correspondence: E-mail: rajdewaan@yahoo.com

Mercury stock solution (1000 ppm) was diluted to 1.0 ppm with deionized water, when required. Stock solutions of 1000 ppm strength of different metal ions such as Na, K, Fe, Zn, Cr, Co, Ni, Cu were prepared from NaCl, KCl, $(NH_4)_2SO_4.FeSO_4.6H_2O$, $Zn_3(PO_4)_2.4H_2O$, $CrCl_3.6H_2O$, $CoSO_4.7H_2O$, $NiSO_4.6H_2O$, and $CuSO_4.5H_2O$ salts, respectively. In order to avoid hydrolysis in metal stock solutions, 5 mL of concentrated 37% HCl solution was added.

Dilutions of 200 ppm, 400 ppm, 600 ppm and 800 ppm were prepared in 100 mL volumetric flasks from the 1000 ppm stock solution, with the addition of one drop of 5% $KMnO_4$ solution and 1 mL of 1.0 ppm standard Hg solution using a micropipette, to give a final solution of 10 ppb Hg concentration. Potassium permanganate was added to reduce possible interference due to sulphide ions (Csuros and Csuros, 2002). Standard solution 10 ppb Hg was also prepared in a similar way without addition of any metal ion. The solutions were analyzed with AAS using MHS 15 system. The lamp current was set at 6 mA, with an integration time of 25 sec. The linear calibration mode was selected, while peak area was used for all calculations. The slit bandwidth was kept at 0.7 nm, at low slit height. Argon gas was purged at 3.0 bar pressure and plunger was held for 5-10 sec in each run.

All over 10 mL aliquot of 10 ppb Hg (II) calibration standard was used. A 3% $NaBH_4$ was prepared in 1% NaOH solution. One drop of 5% $KMnO_4$ solution was added as stabilizing agent in each analysis run. 10 mL of acid mixture (prepared by adding 5 mL of concentrated H_2SO_4 and 2.5 mL of concentrated HNO_3 and 92.5 mL of distilled water) was also added prior to the reduction step.

All the metal ions were scanned up to 1000 ppm with 10 ppb of added Hg (II) and the results are presented in Table 1 and Figs. 1-2.

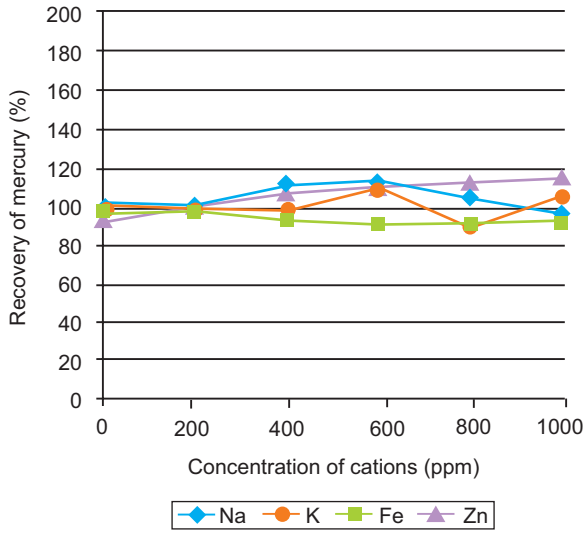

Fig. 1. Profile for cations that do not affect mercury recovery.

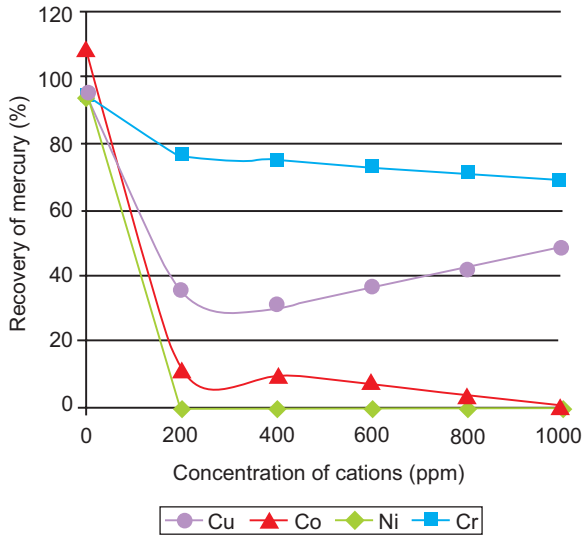

Fig. 2. Interfering affect of cations on recovery of mercury.

Table 1. Recoveries of 10 ppb Hg(II) at different concentrations of cations

Cationic conc.(ppm)	% Recovery of Hg(II) in presence of							
	Na	K	Fe	Zn	Cr	Co	Ni	Cu
0	101.0	95.3	99.0	93.0	95.0	109.0	94.8	96.0
200	100.5	98.0	97.0	100.0	77.0	12.0	ND	36.0
400	111.0	98.3	93.0	107.0	75.0	10.0	ND	31.0
600	112.0	109.2	90.0	109.5	73.0	7.7	ND	37.0
800	104.0	89.8	91.0	112.0	71.0	4.0	ND	43.0
1000	96.0	105.1	92.0	114.0	68.8	0.8	ND	49.0

ND: not detected

Among the investigated cations, Na^+, K^+, Fe^{2+}, and Zn^{2+}, did not show any interference in mercury analysis by cold vapour atomic absorption spectroscopy, while Cr^{3+}, Co^{2+}, Ni^{2+}, and Cu^{2+} significantly reduced the mercury signal, forming characteristic patterns. The Pearson correlation coefficients corroborate that Co (II) and Cr (III), are preferentially reduced prior to the Hg (II) ions because of being present in a greater concentration (Johnson and Kuby, 2008). However, the interference due to presence of Ni (II) and Cu (II) could be due to amalgamation or competitive inhibition or both. The obtained information can help to identify the presence of possible interferents in the sample matrix. This study does not recommend the use of cold vapour technique for mercury analysis if the samples contain more than trace amounts of Cr^{3+}, Co^{2+}, Ni^{2+} and Cu^{2+} ions.

References

Afkhami, A., Khalafi, L. 2005. Indirect determination of sulfide by cold vapour atomic absorption spectrometry. *Microchimica Acta*, **150:** 43-46.

Andren, A.W., Nriagu, J.O. 1979. The global cycling of mercury. In: *The Biogeochemistry of Mercury in the Environment*, J. O. Nriagu (ed.), 3rd edition, pp. 1-21, Elsevier/North-Holland Biomedical Press, Amsterdam, The Netherlands.

Bermejo-Barrera, P., Moreda-Pineiro, J., Moreda-Pineiro, A., Bernejo-Barrera, A. 1996. Use of flow injection cold vapor generation and preconcentration on coated graphite tubes for the determination of mercury in polluted seawaters by electrothermal atomic absorption spectrometry. *Journal of Analytical Atomic Spectrometry*, **11**, 1081-1086.

Bidone, E.D., Castilhos, Z.C., Santos, T.J.S., Cid de Souza, T.M., Lacerda, L.D. 1997a. Fish contamination and human exposure to mercury in Tartarugalzinho River, Amapa State, Northern Amazon, Brazil: A

screening approach. *Water, Air and Soil Pollution*, **97:** 9-15.

Bidone, E.D., Castilhos, Z.C., Santos, T.J.S., Cid de Souza, T.M., Lacerda, L.D. 1997b. Fish contamination and human exposure to mercury in the Tapajos River basin, Para State, Amazon, Brazil: A screening approach. *Bulletin of Environmental Contamination and Toxicology*, **59:** 194-201.

Csuros, M., Csuros, C. 2002. *Environmental Sampling and Analysis for Metals*, pp. 143-151, CRC Press, LLC, USA.

Ebadian, M.A. 2001. Mercury contaminated material decontamination methods: *Investigation and Assessment*, pp. 1-61, Hemispheric Centre for Environmental Technology, Florida International University, Miami, Florida, USA.

Haase, O., Broekaert, J.A.C. 2002. Development of an *on-line* procedure for the indirect determination of iodide by flow-injection cold-vapor atomic absorption spectrometry. *Spectrochimica Acta Part B: Atomic Spectroscopy*, **57:** 157-165.

Hatje, V., Bidone, E.D., Maddok, J.L. 1998. Estimation of the natural and anthropogenic components of heavy metal fluxes in fresh water Sinos river, Rio Grande do Sul State, South Brazil. *Environmental Technology*, **19:** 483-487.

Johnson, R., Kuby, P.J. 2008. *Elementary Statistics*, pp. 163-164, 10th edition, Thomson Brooks/Cole, Belmont, CA, USA.

Kagaya, S., Kuroda, Y., Serikawa, Y., Hasegawa, K. 2004. Rapid determination of total mercury in treated waste water by cold vapor atomic absorption spectrometry in alkaline medium with sodium hypochlorite solution. *Talanta*, **64:** 554-557.

Katiuska, A., Marinela, C., Roman, M., Jose, D., Hilda, L., Elizabeth, G., Lenin, Fresenius, H. 1996. Mercury determination by CV-AAS in wastewater and sewage sludge from a stabilization pond system. *Fresenius Journal of Analytical Chemistry*, **355:** 319-320.

Kolthoff, I.M., Sandell, E.B. 1952. *Textbook of Quantitative Inorganic Analysis*, pp. 560. The Macmillan Company, New York, USA.

Kuldvere, A. 1982. Indirect determination of iodine by cold vapor atomic-absorption spectrophotometry utilizing the interfering effect of iodine against mercury. Part-I. General study and application to the determination of iodine in seaweed. *Analyst*, **107:** 1343-1349.

Paklepa, P., Woroniecki, J., Wrona, P.K. 2001. Transformations in cobalt amalgam - from a homogeneous Co amalgam to nanocrystallites. *Journal of Electroanalytical Chemistry*, **498:** 181-191.

Silva, F.A., de Alcantara, I.L., Roldan, P.S., Padilha, C.C.F., de Araujo, A.B., Valente, J.P.S., Florentino, A.O., Padilha, P.M. 2005. Determination of Hg in water by CVAAS using 2-aminothiazole modified silica. *Ecletica Quimica*, **30:** 47-55.

Sun, F.S., Julshamn, K. 1987. An indirect determination of iodine using HgIn complexes and cold vapor atomic absorption determination of mercury. *Spectrochimica Acta Part B: Atomic Spectroscopy*, **42:** 889-894.